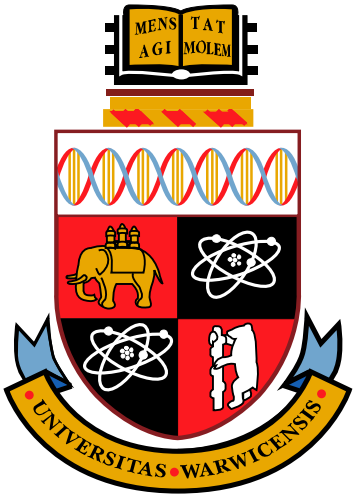

A computational investigation of seasonally forced disease dynamics

James I. MacDonald 9801594

July 6, 2007

A thesis submitted in partial fulfilment of the requirements for the degree of Doctor of Philosophy

Mathematics Institute, Univeristy of Warwick

Contents

List of Figures

List of Tables

Nomenclature

α	Average incubation period
β	Transmission rate
ϵ	Magnitude of imports of infectious individuals
Φ_τ	The annual map of the SIR system with pulsed births
ρ	Smoothing parameter for top hat birth function
τ	Period of birth pulse function, normally 365—the number of days in a year.
a	Rate of loss of infection due to both recovery and mortality, shorthand for $g + d$
a	Scale factor for sinusoidal forcing
B	Birth rate
$B(t)$	Birth rate function
d	Death rate
E	Density of exposed individuals
g	Recovery rate
I	Density of infected
L_t	Discrete time rescaled log if infecteds I.
m	Number of exposed classes
N	Population size

n	Number of infected classes
Q_t	Discrete time rescaled value of susceptibles S.
R	Density of recovered
R_0	The basic reproductive ratio
S	Density of susceptibles
t	Time
w	Duration of top hat function birth pulse.
x	Magnitude of birth pulse

Acknowledgements

First and foremost I would like to thank my supervisor Prof. Matt Keeling for his infinite patience, his constant stream of ideas has kept me inspired throughout. Also my examiners, Dr. Rachel Norman and Prof. Andrew Stuart, whose comments have allowed me to greatly improve this thesis.

I'd like to mention some of my fellow PhD. students here at the University of Warwick who have helped me during the past four years—Dr. Paul Wheeler, Dr. Yvo Pokern, and more recently Mr. Kostas Zygalakis and Mr. Dave White—with whom I have shared room B2.39. Special mentions go to Dave, Paul and Yvo for their proof reading, and again to Yvo for holding my hand when the maths got a bit scary! Also, to Dr. Oliver Tearne, for his help as far back as my undergraduate days, and who allowed me not only to start my career as a movie star while at Warwick (Haven't you seen G103 yet?), but also turn my mathematics into art during the 'banner' project. Paul also deserves another mention for providing many welcome geeky distractions.

Someone else who deserves a mention is Dr. Dave Wood who supervised my forth year project, that lead me to start on this PhD. More recently he has allowed me to earn a few crusts working in various capacities around the department, most notably on MathStuff.

Finally, I would like to thank Dr. Rachel Marrington for her support, and for putting up with me, especially in the final few months, during which I've probably been quite unpleasant to live with, for which I apologise.

This work was funded by a grant from the engineering and physical sciences research council (EPSRC).

Thank you to you all, this PhD would not have happened without you!

Declarations

The author declares that, to the best of his knowledge, the work contained within this thesis is original and his own work under the supervision of his supervisor, Prof. Matt Keeling.

The material in this thesis is submitted for the degree of PhD. to the University of Warwick only and has not been submitted to any other university.

Abstract

In recent years there has been a great increase in work on epidemiological modelling, driven partly by the increase in the availability and power of computers, but also by the desire to improve standards of public and animal health. Through modelling, understanding of the mechanisms of previous epidemics can be gained, and the lessons learnt applied to make predictions about future epidemics, or emerging diseases.

The standard SIR model is in some sense quite a simplistic model, and can lack realism. One solution to this problem is to increase the complexity of the model, or to perform full scale simulation—an experiment *in silico*. This thesis, however, takes a different approach and makes an in depth analysis of one small improvement to the model: the replacement of a constant birth rate with a birth pulse. This more accurately describes the seasonal birth patterns observed in many animal populations. The combination of the nonlinearities of the SIR model and the strong seasonal forcing provided by the birth pulse necessitate the use of numerical methods. The model shows complex multi annual cycles of epidemics and even chaos for shorter infectious periods.

The robustness of these results are proven with respect to a wide range or perturbations: in phase space, in the shape and temporal extent of the birth pulse and in the underlying model to which the pulsing is applied.

To complement the numerics, analytic methods are used to gain further understanding of the dynamics in particular areas of the chosen parameter space where the numerics can be challenging. Three approximations are presented, one to investigate very small levels of forcing, and two covering short infectious periods.

Chapter 1

Introduction

1.1 Motivation

Mathematics has been used to gain insight into the effects of infectious diseases on populations—both human and animal—since as early as the 18^{th} century. One of the earliest papers in the field is that of Bernoulli [1766]. He examines smallpox, now extinct in the wild[1] [Fenner et al., 1988], but which was endemic at the time, and analyses the effect of variolation [Barquet and Domingo, 1997]. Variolation is the act of deliberately infecting someone with small pox, through either a small cut in the skin, or by blowing dried smallpox scabs up the nose, inducing a mild case of the disease, with the intention of providing the individual with immunity. Bernoulli did not consider the dynamics of the infection, but considered a static model where the force of infection (the risk of becoming infected) was constant. His objective was to calculate a life table[2] adjusted as if smallpox where eliminated as a cause of death. This was probably the first example of a compartmental model. Bernoulli's work is revisited by Dietz and Heesterbeek [2000, 2002] One of the amazing things about Bernoulli's work is that it had immediate significance for those in the annuities market, because those who had undergone variolation had a significantly higher life expectancy. So from the start this field of mathematics has been driven by need, rather than simply for the intellectual challenge.

More recently epidemiological models have been used to great effect in

[1] Though some samples still exist in laboratories.

[2] A life table shows the probability that a person of a given age will die before their next birthday.

the prediction and understanding of disease dynamics. Several examples are now considered.

Childhood diseases have long been studied by epidemiologists. The early work of Hamer [1906a,b,c] helped lay the foundation of modern epidemiological modelling. Measles, along with other childhood diseases: chickenpox, mumps, rubella, whooping cough, etc, have possibly seen more work from epidemiologists than other diseases, even though they do not currently cause a major threat to public health, as they are well controlled by vaccination programs [Babad et al., 1995]. The reason for this is simple: there is, for the United Kingdom amongst other countries, extremely good data about both the spatial and temporal incidence of measles [Fine and Clarkson, 1982]. Weekly notifications of the numbers of cases of measles are available from as far back as 1940 until the present. The data from 1950–1968 shows a consistent biannual pattern of major and minor epidemics before the introduction of a mass vaccination program 1968. This comprehensive data set provides the ideal testing ground for epidemiological modelling, not only of the dynamics of disease within a large population, but also of the effects of vaccination on those dynamics. As such modelling of measles is used as much as a tool to gain understanding of the dynamics observed and their mechanisms as to make predictions.

In the early eighties HIV emerged as a major new pathogen, presenting new problems to epidemiologists. In the early days very little was known about the disease and even how it was transmitted. Due to the fact that HIV is sexually transmitted, very limited is available about how frequently transmission occurs. As such current modelling practice focuses on "black box" statistical models to predict short terms trends from incidence data (see for example Brookmeyer and Liao [1990]). More general modelling is carried out using risk structured models [Anderson et al., 1986], where the population is partitioned according to their risk of becoming infected. The usual way to do this is to partition based on the number of sexual partners a person has. However, the various parameters needed are not well known, so it can be hard to make accurate predictions.

During the 2001 foot-and-mouth outbreak three different models where used both to predict the magnitude of the epidemic and to determine the effectiveness of control measures such as culling. Planning control measures such as culling is an important problem, kill too many animals and the loss

is greater than it would have been if the epidemic was left to run its course, kill too few and the spread of disease will not be prevented. It turned out that—due to the robustness of the problem— all three models predicted that same thing: a large epidemic would result without extra control measures, and that locally targeted culling would drastically reduce the incidence of the disease resulting in a much lower overall loss of livestock [Keeling, 2005].

Another important issue addressed by epidemiological modelling is the possibility of bio-terrorist attacks [Henderson, 1999] and a likely choice of pathogen would be smallpox. Modelling a scenario, such as an outbreak of smallpox within a large urban environment poses a challenge for epidemiologists. As time passes the consequences of such an attack become more severe due to the waning level of immunity with the population. One of the difficulties in modelling this scenario is the lack of suitable data about the spread of smallpox, the data that is available is old, from the times when smallpox was endemic, and does not reflect well the structure of a modern population. Various strategies have been proposed, depending on the perceived level of risk. Actions include the re-introduction of mass vaccination, just the vaccination of key health care workers [Bozzette et al., 2003], or the reliance of contact tracing and targeted vaccination [Kaplan et al., 2003]. Good quantitative predictions are hard, because of the high sensitivity on initial conditions.

Of a similar nature to the threat of bio-terrorist attack is the prospect of pandemic influenza, as has been much covered in the media in recent months (late 2006), possibly emerging from the mutation of the H5N1 strain of avian influenza. Here the focus is on protection and protection strategies. Some recent work in this field, such as that of Ferguson et al. [2006], has utilised large scale individual based models to perform full scale simulations *in silico*. Though this strategy yields detailed predictions it can be hard to know how robust they are.

Other recent examples include SARS, where quarantine was successfully used to control an emerging disease and BSE/CJD where due to the very limited data, statistical modelling is used to try and compute parameters.

There are many justifications to use mathematical model in epidemiology. Roberts and Heesterbeek [1993] cite the main ones as the following.

Insight Models provide insight into, and understanding of, the relationships

between the mechanisms operating at the individual level and the resultant phenomena at the population level.

Precision The precision required in formulating the assumptions underlying a mathematical model can shed light on working hypotheses otherwise undiscovered. Furthermore, the analysis of models can lead to the formulation of important epidemiological concepts such as R_0 (see Section 1.3 on page 9).

Parameters Modelling can clarify which parameters are critical in determining the disease dynamics. Some parameters that are difficult to measure may turn out not to be very important, or values may be found for hitherto unmeasured parameters.

Experiments The ability to perform thought experiments, for example to evaluate control measures, in cases where real experiments are unethical or uneconomic.

Roberts and Heesterbeek [1993] also note that models should be used with care for making quantitative predictions about future trends. This is because even complex models can be grossly simplified versions of reality. Making models more complex can actually make the problem worse as this leads to a proliferation of unmeasurable parameters—although recently large scale simulations underpinned with accurate, comprehensive data have been used to make quantitative predictions—see for example recent work by Ferguson et al. [2006], Keeling et al. [2003]

In recent years there has been a great surge in the amount of published work on modelling of infectious diseases. This can most probably be attributed to the increased availability and increasing power of computers. Figure 1.1 shows how dramatic this rise is from a mere handful in the late sixties to in excess of 250 papers in 2005.

1.2 SIR models

The SIR model, developed in 1927 by Kermack and McKendrick [1927] is now one of the standard epidemiological models [Anderson and May, 1991]. The model itself is quite simple; The population is partitioned into three classes:

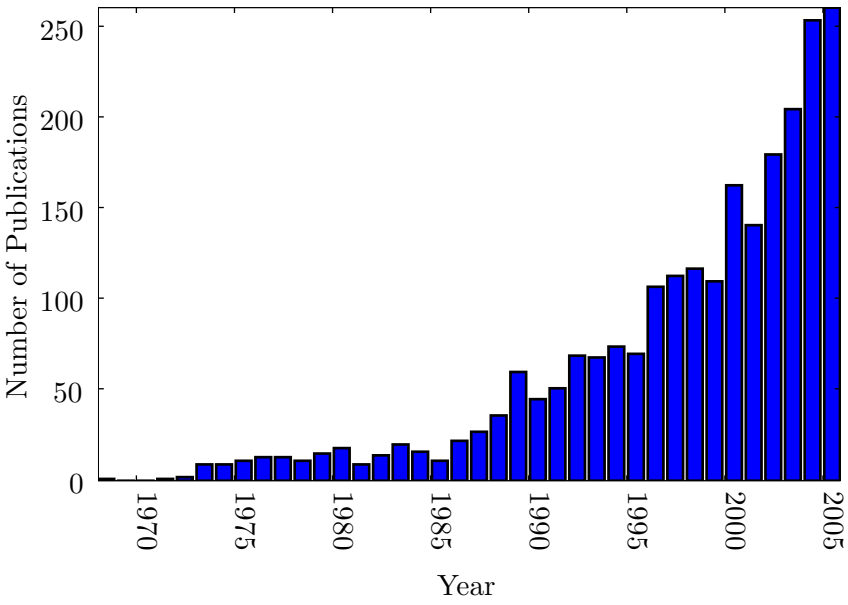

Figure 1.1: Showing how the number of papers on modelling of infectious diseases has increased since 1968 to present. Data from Scopus, the query used was: `(epizootic OR epidemic) AND infect* AND (model* OR simulat*)`.

Susceptibles have not been exposed to the disease and are able to become infected.

Infecteds have the disease and can infect members of the susceptible class. *i.e.* they are infectious.

Recovereds have recovered from the disease and are unable to become infected again. Also known as removed, because they play no further part in the dynamics.

The SIR model assumes that :

- An individual can only have the disease once.
- The birth rate is constant and all newborns are susceptible.
- Susceptible and infected individuals are well mixed so that infection moves at a rate proportional to both the level of infected and susceptibles.
- Individuals recover at a constant rate.

- The natural death rate is constant and equal across all three classes.
- The population is conserved. The only flux in and out is from births and deaths respectively.

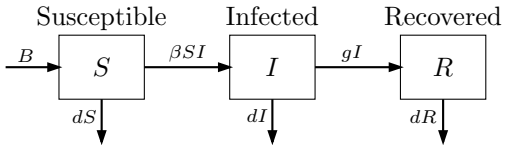

Figure 1.2: Box diagram for the standard SIR model.

The structure of the model is described graphically in Figure 1.2. The model can be expressed as three first order nonlinear ODEs:

$$\begin{aligned} \dot{S} &= -\beta SI + B - dS \\ \dot{I} &= +\beta SI - gI - dI \\ \dot{R} &= gI - dR. \end{aligned} \tag{1.1}$$

Here, the variables are:

S is the density of susceptibles within the population

I is the density of infecteds within the population.

R is the density of recovereds within the population.

And the parameters are:

β is the transmission or contact rate, which can be thought of as the rate that contacts are made multiplied by the probability of transmission across a contact.

B is the birth rate.

d is the per capita death rate which is equal to the inverse of the average life expectancy.

g is the recovery rate. This is the reciprocal of the infectious period.

The dimensionality of the state variables is discussed in Section 1.6 on page 15. In order to maintain a constant population size the sum

$$S + I + R$$

must be constant, so

$$\dot{S} + \dot{I} + \dot{R} = 0,$$

requiring that $B = d$. In other words births and deaths are balanced so that the population stays a constant size. For convenience, the densities are normalised , so that

$$S + I + R = 1.$$

The interactions between susceptibles and infecteds are modelled by the term βSI. This is historically dubbed *mass-action* as if being derived from thinking about a system of randomly moving particles (*e.g.* a gas). This assumes that as the level of both classes increases so does the level of interactions thus speeding the spread of infection. This is a realistic assumption for most animal populations. Another scheme, historically referred to as *pseudo mass-action* models the interaction by $\beta SI/N$, where N is the total size of the population. In this case it is the proportion of susceptibles and infecteds within the population, not the total population size that affects the level of interactions. This is a better model for human populations where contacts remains fairly independent of population size and density. The derivation of these two different transmission terms is discussed in detail in Section 1.6 on page 15, where a new, more descriptive, terminology is introduced.

Typical behaviour of this model is a large epidemic, followed by a series of epidemics decreasing in size. Asymptotically the system tends to an endemic equilibrium.

One special case of the standard SIR model worth considering is when $B, d = 0$: the simple SIR model, sometimes also known as the simple epidemic. Then the dynamics simplify to a single epidemic followed by disease extinction. Typical dynamics of the simple SIR model are shown in Figure 1.4 on the following page.

After introducing an ODE model it is normal determine its fixed points and perform a stability analysis on them. This is done in Section 1.4 on page 11. However, before doing that it is necessary to introduce an important concept in epidemiological modelling: the basic reproductive ratio.

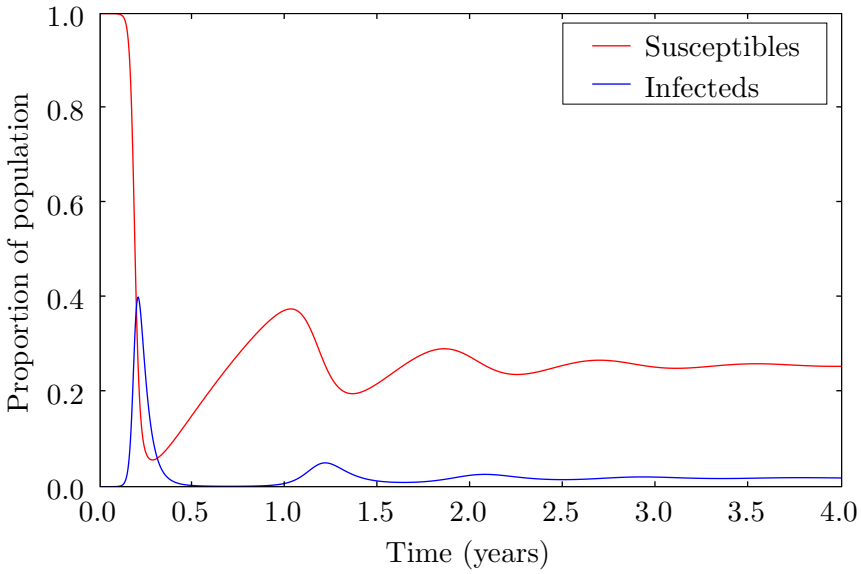

Figure 1.3: Typical dynamics of the standard SIR model. Here $\beta = 0.3$, $B = d = 1.9 \times 10^{-3}$ and $g = 0.075$.

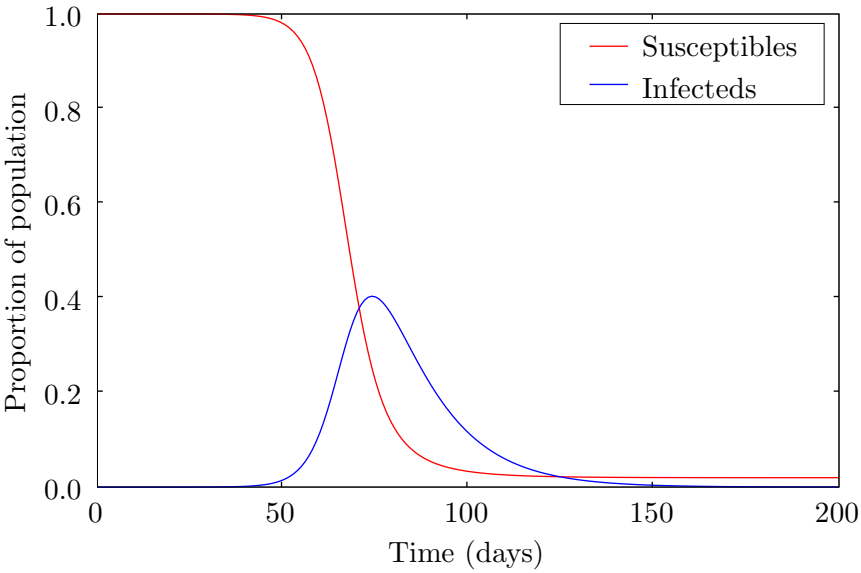

Figure 1.4: Typical dynamics of the simple SIR model. Here $\beta = 0.3$ and $g = 0.075$.

1.3 The basic reproductive ratio

The basic reproductive ratio, denoted by R_0, is one of the most important epidemiological/epizootilogical parameters. For micro-parasites, such as viruses and parasitic protozoa, the basic reproductive ratio R_0 is defined by Anderson and May [1991] as:

> The average number of secondary cases produced by an average infectious individual in a totally susceptible population.

R_0 is a so called threshold parameter. For a given infection in a given population R_0 tells us whether a disease can invade a naive population. If $R_0 > 1$ then each infectious individual will give rise to more than one new case and the disease will spread. However, when $R_0 < 1$ less than one new case occurs and the disease dies out.

R_0 is sometimes also referred to as the basic reproductive number [Diekmann et al., 1990, Hethcote, 2000] or the basic reproductive rate [Anderson and May, 1991].

From the above definition the following formula for R_0, is derived:

$$R_0 = (\text{infectious period}) \times \begin{pmatrix} \text{average rate at which} \\ \text{secondary cases are produced} \end{pmatrix}.$$

See Keeling and Rohani [2007, chap. 2] or Anderson and May [1991].

Table 1.1 on the following page shows a selection of values for R_0 for different diseases, both in animals and humans. It is clear that R_0 shows great variation from just greater than unity for Feline immunodeficiency virus to 50–100 for malaria.

For the standard SIR model, as described in Equations 1.1 on page 6, the basic reproductive ratio is given by

$$\begin{aligned} R_0 &= \begin{pmatrix} \text{rate at which secondary} \\ \text{cases are produced} \end{pmatrix} \times (\text{average infectious period}) \\ &= \beta S \times \frac{1}{g+d} \\ &= \frac{\beta}{g+d}. \end{aligned} \tag{1.2}$$

Disease	R_0 (approx)	Reference
Chickenpox	10–12	Anderson and May, 1991
Ebola virus (Congo and Uganda)	1.34 and 1.83	Chowell, Hengartner, Castillo-Chavez, Fenimore, and Hyman, 2004
Feline immunodeficiency virus	1.1–1.3	Courchamp, Pontier, Langlais, and Artois, 1995
Foot and mouth disease	3.5–4.5	Ferguson, Donnelly, and Anderson, 2001
HIV (male homosexuals in England and Wales)	4	Anderson and May, 1991
HIV (female prostitutes in Kenya)	11	Anderson and May, 1991
Influenza	3–4	Murray, 1989
Malaria	50–100	Macdonald, 1957
Measles	16.8–18.8	Anderson and May, 1982, Bjørnstad, Finkenstädt, and Grenfell, 2002
Phocine distemper	2.8	Swinton, Gilligan, Harwood, and Grenfell, 1998
Rabies in hyaenas	1.9	East, Hofer, Cox, Wulle, Wiik, and Pitra, 2001
Rubella	6-7	Anderson and May, 1991
Smallpox (Europe and US)	3.5–6	Gani and Leach, 2001, 2002
Smallpox (Nigeria 1967)	1.5–10.1	Eichner and Dietz, 2003
TB in badgers	15	Ruxton, 1996
TB in cattle	2.6	Goodchild and Clifton-Hadley, 2001
Whooping cough	16–18	Anderson and May, 1982

Table 1.1: Example R_0 values for various diseases in both humans and animals.

It follows that for the simple SIR model that,

$$R_0 = \frac{\beta}{g}.$$

1.4 Stability analysis of the standard SIR model

The long term behaviour of the standard SIR model (Equations 1.1 on page 6) is now briefly derived analytically, for a more detailed exposition see, for example Hethcote [1976]. First notice that R only appears in the equation for $\dot{R}$, so it suffices to only consider the $\dot{S}$ and $\dot{I}$ equations because given S and I, R can always be calculated using the relationship $S + I + R = 1$.

The fixed points of the system are given when $\dot{S}$ and $\dot{I}$ are simultaneously zero. Considering the I equation:

$$0 = \beta S^* I^* - g I^* - d I^*$$

which is satisfied by $I^* = 0$, or $S^* = \frac{g+d}{\beta} = 1/R_0$. Now the S equation is:

$$0 = -\beta S I - dS + d.$$

Substituting $I^* = 0$ implies $S^* = 1$ and substituting $S^* = 1/R_0$ gives:

$$\begin{aligned} 0 &= -\frac{\beta}{R_0} I^* - \frac{d}{R_0} + d \\ \frac{\beta}{R_0} I^* &= d - \frac{d}{R_0} \\ I^* &= \frac{d R_0}{\beta}\left(1 - \frac{1}{R_0}\right) \\ I^* &= \frac{d}{\beta}\left(R_0 - 1\right) \end{aligned}$$

The fixed point $(S_0^*, I_0^*) = (1, 0)$ is the *disease free equilibrium*. Which describes the state where no infection is present in the population. Similarly $(S_1^*, I_1^*) = (1/R_0, \frac{d}{\beta}(R_0 - 1))$ is the *endemic equilibrium*, where the infection persists at a fixed level. The eigenvalues of the Jacobian evaluated at these points will determine their linear stability. Now the Jacobian of the standard SIR model (only considering the S and I equations) is given by

$$J(S,I) = \begin{pmatrix} -\beta I - d & -\beta S \\ \beta I & \beta S - (g+d) \end{pmatrix} \tag{1.3}$$

At the endemic equilibrium this evaluates to

$$J(S,I) = \begin{pmatrix} -dR_0 & -(g+d)) \\ d(R_0 - 1)) & 0 \end{pmatrix}$$

which has characteristic equation:

$$\lambda^2 + \lambda d R_0 + d(\beta - (g+d)) = 0.$$

By the quadratic formula the eigenvalues are

$$\lambda_{\pm} = \frac{-dR_0 \pm \sqrt{(dR_0)^2 - 4d(\beta - (g+d))}}{2}.$$

For the fixed point to be stable the real part of both eigenvalues must be negative. If the discriminant is negative then the eigenvalues will be complex but will both have negative real part because the part out side the square root is negative. When the discriminant is positive λ_- will always be negative real, but λ_+ is only negative when

$$\begin{aligned} -4d(\beta - (g+d)) &< 0 \\ \beta - (g+d) &> 0 \\ \frac{\beta}{g+d} &> 1 \\ R_0 &> 1 \end{aligned}$$

Hence the endemic equilibrium $(S_1^*, I_1^*) = (1/R_0, \frac{d}{\beta}(R_0 - 1))$, is stable if $R_0 > 1$ and unstable if $R_0 < 1$. When $\lambda_{\pm}$ are complex oscillatory dynamics about the endemic equilibrium will result.

At the disease free equilibrium

$$J(S,I) = \begin{pmatrix} -d & -\beta \\ 0 & \beta - (g+d) \end{pmatrix} \tag{1.4}$$

which has characteristic equation:

$$-(d+\lambda)(\beta - (g+d) - \lambda) = 0$$

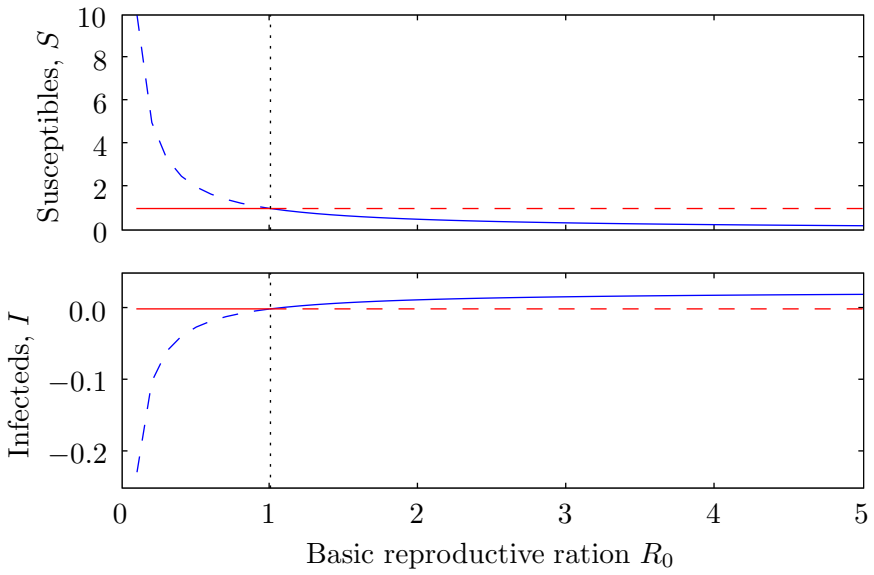

Figure 1.5: Bifurcation plot showing the stability of both the endemic (blue lines) and disease free (red lines) equilibriums for the standard SIR model (Equations 1.1 on page 6), as R_0 varies. Solid lines show the position of stable fixed points, and dashed lines unstable ones. Here $g = 0.075$ days^{-1} and $d = 1.9 \times 10^{-3}$.

and eigenvalues $\lambda_1 = -d$ and $\lambda_2 = \beta - (g + d)$. Which is stable if $R_0 < 1$ and unstable if $R_0 > 1$.

Figure 1.5 shows the bifurcation structure of these two fixed points. Notice how the endemic and disease free equilibriums coalesce as $R_0 \to 1$. It is also clear that for $R_0 < 1$ the unstable branch of the endemic equilibrium has $S_1^* > 1$ and $I_1^* < 0$ which are clearly infeasible.

It is also possible to calculate the natural period of oscillation about the endemic equilibrium in the case where $\lambda_\pm$ are complex. The period of oscillation is given by

$$\begin{aligned} T &= \frac{2\pi}{\mathrm{Im}(\lambda_\pm)} \\ &= \frac{4\pi}{\sqrt{(dR_0)^2 - 4d(\beta - (g + d))}} \end{aligned}$$

The natural value of the natural period is show in Figure 1.6 on the following page. It is clear that for lower values of both the death rate d and the

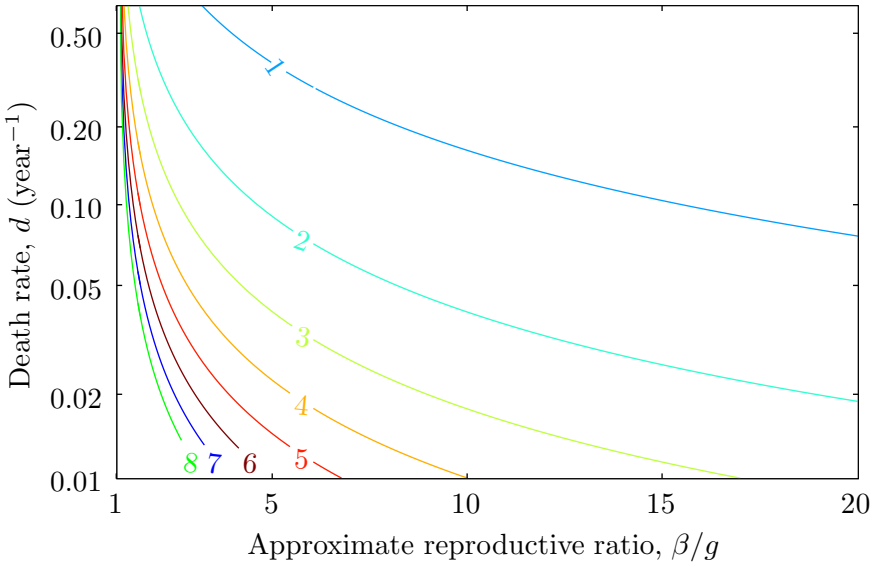

Figure 1.6: Natural period of the standard SIR model (Equations 1.1 on page 6). Here $g = 0.075$ days^{-1}.

transmission rate β the natural period is higher.

1.5 Kermack and McKendrick

Returning to the history of epidemiological modelling, it is discussed how the SIR model can be derived as a special case of a modelling framework developed by Kermack and McKendrick. In their seminal 1927 paper, 'A contribution to the theory of epidemics', Kermack and McKendrick [1927] first describe the class of epidemiological models for which they are famous.

The assumptions of Kermack and McKendrick's models are summarised by Diekmann et al. [1995] as:

1. a single infection triggers an autonomous process within the host (*i.e.* they look at 'micro-parasites' and not at 'macro-parasites');
2. the disease results in either complete immunity or death;
3. contacts are according to the law of mass action;
4. all individuals are equally susceptible;

5. the population is closed, *i.e.* at the time scale of disease transmission the inflow of new susceptibles into the population is negligible;

6. the population size is large enough to warrant a deterministic description.

This leads to the integral equation:

$$\dot{S}(t) = S(t) \int_0^\infty \bar{A}(\tau)\dot{S}(t-\tau)\mathrm{d}\tau.$$

Where

$\bar{A}(\tau)$ = expected infectivity of an individual that became infected τ units of time ago.

and $S(t)$ is the number individuals in the population that are susceptible to the disease.

The simple SIR model,

$$\begin{aligned} \dot{S} &= -\beta SI \\ \dot{I} &= +\beta SI - gI \\ \dot{R} &= gI, \end{aligned} \tag{1.5}$$

often mistakenly referred to as *the* Kermack and McKendrick model [Diekmann et al., 1995], arose from the special case where

$$\bar{A}(\tau) = \beta e^{-\gamma\tau}$$

By defining

$$\begin{aligned} I(t) &:= -\frac{1}{\beta}\int_0^\infty \bar{A}(\tau)\dot{S}(t-\tau)\mathrm{d}\tau \\ &= -\frac{1}{\beta}\int_{-\infty}^t \bar{A}(t-\tau)\dot{S}(\tau)\mathrm{d}\tau \end{aligned}$$

and differentiating the familiar equations can be obtained.

1.6 Transmission terms

When using compartmental models the state variables can represent either the number of individuals in each compartment or the density of individuals

in that compartment. In the case where the population size is constant the proportion of the population in each compartment can also be chosen to be the state variables. Each of these different cases leads to different dimensions for the transmission parameter β as well as the state variables. This problem is tackled by Begon et al. [2002]. There is much confusion about the exact assumptions behind different types of transmission: mass action, pseudo-mass action, true mass action, density-dependent transmission, frequency-dependent transmission amongst others. Here the confusing terms mass action, pseudo-mass action are dropped in favour of the terminology suggested by Begon et al. [2002]. Their derivation of transmission terms is outlined below.

First of all let s and i denote the number of susceptible and infected individuals respectively, and n denote the total number of individuals in the population. For clarity only the rate of increase of the infected class due to new infection is considered. This is denoted by $\mathrm{d}i/\mathrm{d}t$. The rate at which the number of infected individuals increases is in direct proportion to the number of susceptibles available multiplied by the per capita rate of infection commonly referred to as the force of infection. The force of infection is the product of several factors: the rate at which contacts with other individuals occur c, the probability p that a contact is actually with an infectious host, and the probability ν that the contact leads to successful transmission. Thus the prototype transmission term is given by:

$$\frac{\mathrm{d}i}{\mathrm{d}t} = scp\nu \tag{1.6}$$

The probability that a transmission event is successful ν is usually assumed to be a function of the host-pathogen combination in question. Now the probability that the contact is indeed with an infectious host is i/n. Thus the factor that usually distinguishes different types of transmission term is the rate of contact c. There are several possibilities for the form of c.

The most frequently used form is $c = \kappa n/a$, where a is the area occupied by the population and κ is a constant depending on the particular host-pathogen combination. Here the contact rate, and thus the per capita force of infection, increases with the total population density. Combining the constants κ and ν in to a single term β, usually referred to as the transmission

coefficient the following transmission term is obtained:

$$\begin{aligned}\frac{\mathrm{d}i}{\mathrm{d}t} &= s\kappa\frac{n}{a}\frac{i}{n}\nu \\ &= \beta\frac{si}{a}.\end{aligned} \tag{1.7}$$

Notice how in this case not only does the contact rate increase with the total population density, but also the per capita force of infection increases with the density of infecteds. Thus Equation 1.7 is said to describe *density dependent transmission*. This transmission term is generally used to describe the transmission of infection with in animal populations, where the contact rate increases with the total population density [Hudson et al., 2002]. This type of transmission has been traditionally referred to as *mass action*.

A second possibility is to assume a constant contact rate $c = \eta$ and thus is independent of the population density. In this case the transmission term is given by:

$$\begin{aligned}\frac{\mathrm{d}i}{\mathrm{d}t} &= s\eta\frac{i}{n}\nu \\ &= \beta'\frac{si}{n}.\end{aligned} \tag{1.8}$$

Where $\beta' = \eta\nu$ is another transmission term with different dimensions to the previous β. In this case the per capita force of infection increases with the prevalence of infection within the population i/n, which could feasibly be described as the "frequency" of infected hosts with in the population. Thus Equation 1.8 is said to describe *frequency dependent transmission*. This type of transmission may be a more suitable for modelling transmission in human populations Anderson and May [1991], and has traditionally been referred to as *pseudo-mass action*.

The two transmission terms described above can be rewritten in terms of the density of susceptibles and infecteds, denoted as S and I respectively, by substituting $I = i/a$ and $S = s/a$. Then under the assumptions that the area occupied by the population does not vary with time, the transmission term for density dependent transmission is given by

$$\frac{\mathrm{d}I}{\mathrm{d}t} = \beta SI$$

and equivalently for frequency dependent transmission

$$\frac{\mathrm{d}I}{\mathrm{d}t} = \beta' \frac{SI}{N}$$

In the following chapters the density dependent transmission is assumed throughout because highly synchronous seasonal breeding patterns, considered in Chapter 2 on page 24 and modelled by a birth pulse, are predominantly a feature of wildlife populations. The exception Subsection 3.3.5 on page 117, which looks specifically at the effects of considering frequency dependent transmission.

1.7 Seasonality

Within nature many seasonal patterns exist, for example many animals give birth in the Spring time, birds often migrate to warmer climbs during the winter and numerous other examples. These seasonal patterns play a part in driving the annual, and in some cases multi-annual, incidence patterns observed for many infectious diseases. As such, seasonality can be considered the driving force of the recurrent epidemics observed in many host pathogen systems.

Although the standard SIR and simple SIR compartmental models presented in Section 1.2 on page 4 are useful for understanding a simple epidemic, their dynamics (as shown in Figure 1.3 on page 8 and Figure 1.4 on page 8) fail to capture the recurring patters of epidemics exhibited by many host-pathogen systems.

One of the key uses of seasonality in modelling infectious diseases is the study of measles. Soper [1929] determined that, at least in the case of measles, significant seasonal variation in the transmission rate must occur. The suggested cause was congregation of children during school terms. This was confirmed around 50 years later by Fine and Clarkson's [1982] careful analysis of weekly incidence reports. Other studies have found similar patterns for other childhood diseases. Seasonality is also key in vector transmitted diseases such as Malaria [Hoshen and Morse, 2004], Dengue fever [Watts et al., 1987], tick-borne encephalitis [Randolph et al., 2000] or West Nile virus [Campbell et al., 2002], where the seasonal variations in the population of the vector cause seasonal variations in incidence. Grassly

and Fraser [2006] provides a recent overview of modelling seasonal infectious diseases in humans.

Seasonality also plays a major role in the dynamics of wildlife diseases [Altizer et al., 2006, Dowell, 2001, Hudson et al., 2002]. With diseases such as phocine distemper[Swinton et al., 1998], rabies in skunks [Gremillion-Smith and Woolf, 1988] and ebola in gorillas [Pinzon et al., 2004] showing strong seasonal variation in their incidence. Many factors drive the seasonal variation, such as aggregation or dispersal of hosts during or after the breeding season. Altizer et al. [2006] provides a good overview of seasonality in modelling infectious diseases in wildlife populations, including a discussion on the effect of seasonal birth rate within the host population.

Most models incorporating seasonality focuses on seasonal variation in the transmission rate. However, this thesis focuses on the effect of adding seasonal variation in the birth rate. Seasonality in births is dynamically less destabilising than seasonality in transmission terms [Keeling and Rohani, 2007]. An in depth review of animal populations with highly seasonal birth rates is carried out in Chapter 2.

1.8 Resonance

It is surprising the phenomenon of resonance has received little study in relation to epidemiological modelling [Choisy et al., 2006]. Early theoretical work on considering the dynamical consequences of seasonal forcing in the transmission rate started with the work of Soper [1929], Bartlett [1956] and Bailey [1975]. Their aim was establish the required level of variation in the transmission term to reproduce the large fluctuations in the level of infection.

Bailey [1975] considering the standard SIR model, without deaths but modified so that the transmission rate β is a function of time. Thus his model was given by :

$$\begin{aligned} \dot{S} &= -\beta(t)SI + B \\ \dot{I} &= +\beta(t)SI - gI \\ \dot{R} &= gI, \end{aligned} \tag{1.9}$$

with

$$\beta(t) = \beta_0(1 + \beta_1 \cos(\omega t)),$$

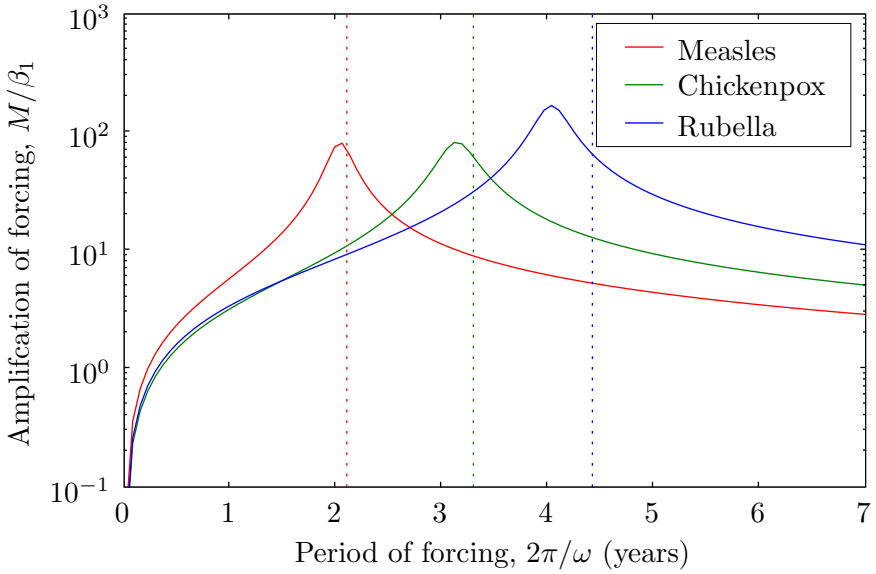

Figure 1.7: The predicted amplification of small amounts of sinusoidal forcing for three childhood diseases. Dashed vertical lines show the natural period of oscillation $2\pi/F$. Parameters: $B = 0.02$ per year throughout, measles: $R_0 = 17$; $1/g = 13$ days, chickenpox: $R_0 = 11$; $1/g = 20$ days, rubella: $R_0 = 6$; $g = 1/18$ days.

where β_0 is the average transmission rate, ω is the period of the forcing and $\beta_1 \in [0, 1]$ is the amplitude of the forcing. The basic reproductive ratio, R_0 for this system is β_0/g. Bailey [1975] analysed the effects of small perturbations from the un-forced equilibrium, in the presence of low levels of seasonality, $\beta_1 \ll 1$. He then derived the following formula for the amplitude M, of the oscillations:

$$M = \beta_1 \omega g \left((B\beta_0 - \omega)^2 + (\omega B R_0)^2 \right)^{-\frac{1}{2}}.$$

Figure 1.7 shows how the amplitude magnification factor M/β_1 varies with the period of the forcing, for several childhood diseases. There are clear peaks that show a reasonable correspondence to the natural frequency of the system. Which for this system is given by

$$F^2 = B(g + B)(R_0 - 1) - \left(\frac{BR_0}{2} \right)^2.$$

This is an example of harmonic resonance. The biological implications

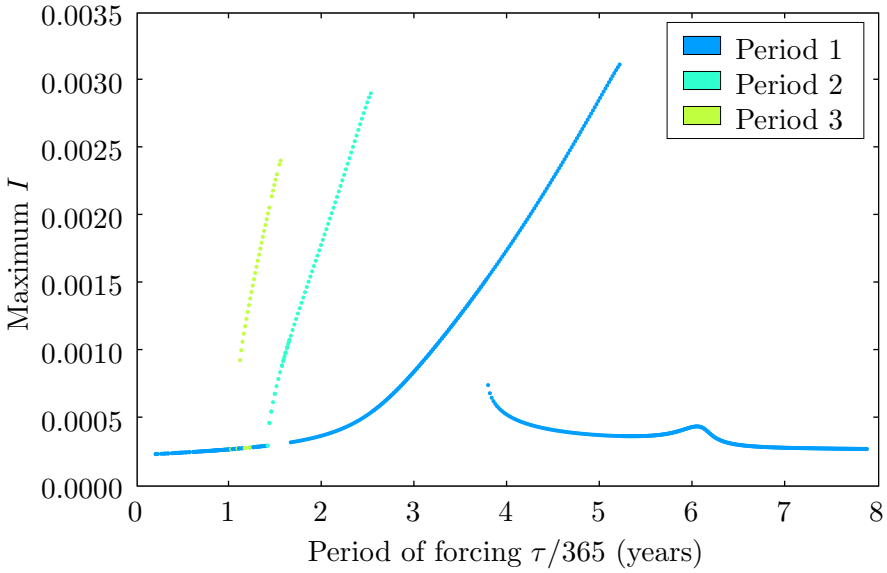

Figure 1.8: Resonance response curve of the standard SIR model with seasonally forced transmission. Parameters: $\beta_0 = 500/365 \approx 1.37$, $\beta_1 = 0.025$, $d = 0.01$ and $g = 40/365 \approx 0.11$.

are that if a system is forced at near its natural frequency, then only a small level of seasonal fluctuation in the transmission rate is necessary to cause a large fluctuation in the level of infection.

Another phenomenon exhibited by seasonally forced systems is nonlinear resonance. This can be demonstrated by looking at the standard SIR model with sinusoidal forced transmission. Hence

$$\begin{aligned} \dot{S} &= -\beta(t)SI - dS + B \\ \dot{I} &= +\beta(t)SI - gI - dI \\ \dot{R} &= gI - dR, \end{aligned} \tag{1.10}$$

with

$$\beta(t) = \beta_0 \left(1 + \beta_1 \cos\left(\frac{2\pi t}{\tau}\right)\right),$$

and $B = d$, so that births and deaths are matched and the population size remains constant. The length of the period of forcing is given by τ measured in days.

This system is studied by Greenman et al. [2004], and some of that work is reproduced here. Figure 1.8 recreates Greenman et al.'s Figure 4a and

shows the resonance response curve of the above system, though only stable branches are show here.

The behaviour is much more complicated that the simple harmonic resonance shown in Figure 1.7 on page 20. Firstly the curve has breaks at the tops of the resonant peaks which appear to lean to the right. The breaks are caused by that particular branch becoming unstable–if the unstable branches were shown the curve would be continuous apart from the disconnected period three peak. Also there is hysteresis in the system, so that at some points on the curve two stable periods exists simultaneously. This curve is typical of nonlinear resonance.

Resonant effects are not restricted to epidemiological models, for example Brassil [2006] uses these techniques to look at resonance in predator-prey models.

1.9 Overview

This chapter has reviewed the field of epidemiological modelling, from its roots in the work of Bernoulli, to its use in modern public health, planning for emerging pathogens. The derivation of one of the most common epidemiological models, the SIR model is considered in some detail, introducing some more universal elements of disease models, such as the basic reproductive ratio and transmission terms. A brief overview how seasonality in nature can be included into models, and used to explain patters of seasonal variation in incidence levels and other phenomena. Finally, the role of resonance is considered, showing how interactions between times scales can result in large epidemics.

Chapter 2 on page 24, begins with a review of seasonality in birth rates in animal populations, illustrating that in many cases births are highly synchronised. To model diseases within populations exhibiting this phenomenon, the standard pulsed SIR model is introduced. It is noted that there is little work in the literature where a pulse has been used to model births. After a review of the available numerical techniques, suitable ones are chosen and refined to analyse the behaviour of the model. In particular, techniques are reviewed and developed to calculate the period of attractors, and a predictor-corrector based continuation method to determine the extent of these attractors in parameter space.

These methods are then utilised to catalogue various properties of the attractors. An analysis of the role of resonance plays in the dynamics is made, showing that nonlinear resonance plays a significant part in explaining the complex dynamics. Finally a bifurcation analysis is undertaken, and the locations of unstable period one limit cycles are tracked.

The next chapter, Chapter 3 on page 89, builds on the results of Chapter 2 on the next page, showing how robust they are to a variety of perturbations. Firstly Floquet multipliers are used to asses the stability of attractors to small perturbations in state space. Secondly, the birth pulse function used is varied to determine how sensitive the results are to the exact choice of this function. Finally, the structure of the model itself is altered to get a sense of how pulsed births affect other epidemiological models.

The final chapter, Chapter 4 on page 142, presents progress made analytically to describe the dynamics of the pulsed SIR models. Approximations are formulated to describe the dynamics in particular regions of parameter space where it can be challenging to evaluate the behaviour numerically.

Chapter 2

Pulsed births

Many simple population and disease models use a constant birth rate [Hethcote, 2000] and for certain populations this is a realistic assumption. For example, humans, in general, only show slight variation throughout the year [Brewis et al., 1996, Lam et al., 1994, Rojansky et al., 1992] [1]. However, many animal populations show significant seasonal variation to the point where a model using the mean as a constant birth rate is unrealistic. This chapter starts to investigate the effect of going to an extreme by modelling the births within a population as an instantaneous pulse. Ims [1990] suggests that strong reproductive synchrony such as this is a reproductive strategy that can lead to greater success.

Pulsed births have been studied in population models [Barlow and Barron, 2005, Tang and Chen, 2003] but very little work has been done on disease models with pulsed births. Tang and Chen [2003] take a similar approach to the one taken here. They formulate a population model for a generic wild animal population with a birth pulse once per time period. Gao and Chen [2005] implement a single species discrete population model with stage structure and birth pulses to consider the effect of seasonal harvesting on fish populations. Both Tang and Chen [2003], and Gao and Chen [2005], then go on to show that the model exhibits small scale annual cycles, larger scale multi-annual cycles and, through period doubling, chaos. Similar work is done by Dong and Chen [2005].

Barlow [1993] utilised birth and dispersal pulses in a model for the spread

[1] This is, however, not universally true for humans, some communities show great seasonal variation. See for example Chatterjee and Acharya [2000].

of bovine TB in the New Zealand possum population. Roberts and Kao [1998] deals again with TB in possums using an SI model with birth pulses and analyse its stability. Later Barlow and Barron [2005] take a different approach. They aim to model stoat populations in New Zealand forests for the evaluation of control measures. A comparison is made of a series of three models of increasing complexity, with the second and third having pulsed births. These two models exhibited more complex dynamics. Reluga [2004] models "population dynamics with disturbance", using the effects of wildfire on shrub populations as the main example. Wildfire is modelled as a variable annual death pulse. Reluga observes multi-annual dynamics—where the population grows for several seasons before a collapse—and period doubling cascade leading to chaos. Later in this chapter similar behaviour is seen from the standard pulsed SIR model (Equations 2.1 on page 29). Finally density dependent birth pulses are considered by Gao et al. [2005], again showing complex dynamics, period doubling and chaos.

Many animal populations show strongly pulsed births. The following paragraphs illustrate a range of poignant examples. Making it clear that pulsed births are a widespread phenomenon.

A particularly good example of a population with strongly pulsed births is Saiga antelopes (*Saiga tatarica*) [Milner-Gulland, 2001]. Saiga live in the desert, semi-desert and steppe of Central Asia. Pregnant females gather together in late spring to form large temporary aggregations. Mass calving then occurs with most of the females in the aggregation giving birth within 3–8 days (see Figure 2.1 on the following page). By choosing to give birth in an aggregation females reduce the risk of predation on their calves. The price they pay for this is the increased likelihood of disease [Milner-Gulland, 2001].

Berger and Cain [1999] observed that within the bison populations of Yellowstone that 50% of all births occur within a one month period and 95% occur within 61 days.

The Mongolian gazelle (*Procapra gutturosa*) is another species documented as a strongly seasonal breeder. Despite the rutting season lasting from the middle of November until the first week in February females give birth between mid June and mid July with about 90% of births occurring within the same 4-7 day period [Milner-Gulland and Lhagvasuren, 1998].

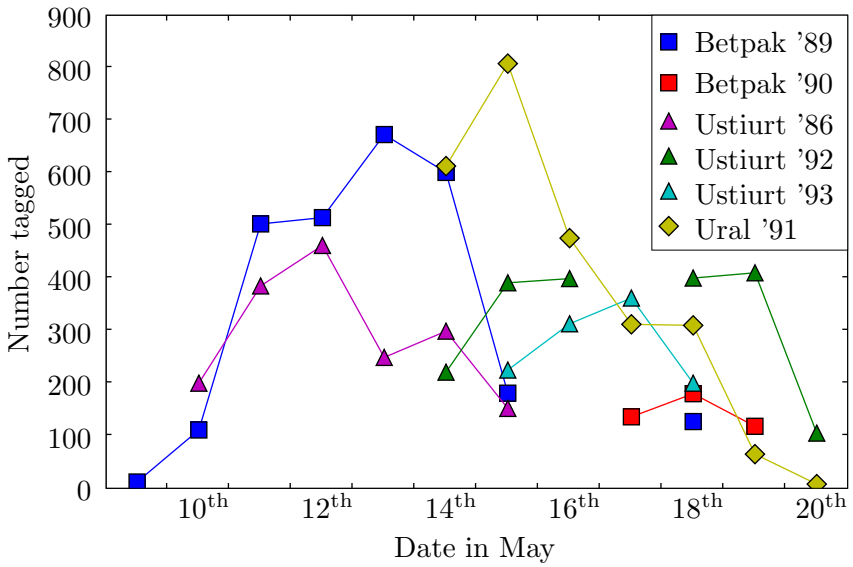

Figure 2.1: Field data showing the number of newborn Saiga Antelope captured and tagged each day in different locations and years [Milner-Gulland, 2001] during the breeding month of May. As with all field data it is subject to a certain amount of interpretation. The issues are explained in the source.

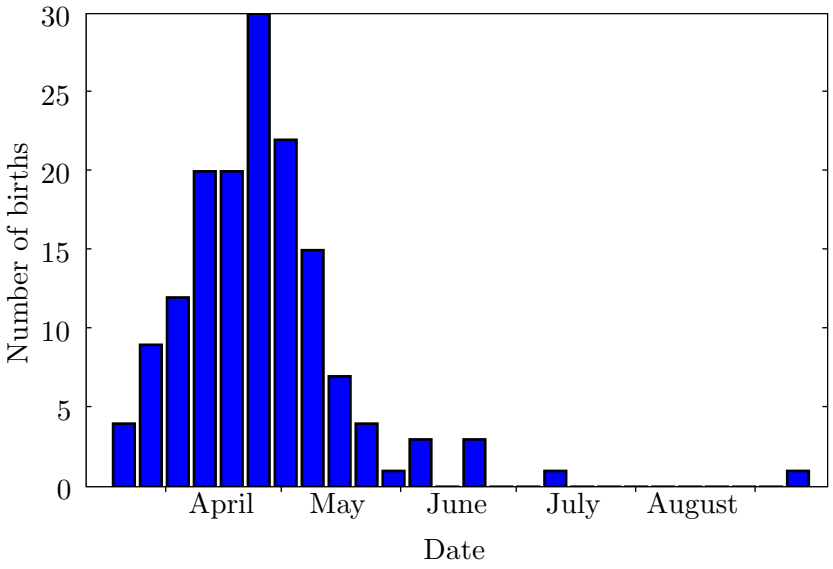

Figure 2.2: Field data showing the temporal spread of births of the common brushtail possum in Australia. The number of births per week in the study area summed over three years. Data from Clinchy [1999], Clinchy et al. [2004].

Lesser Snow geese (*Anser caerulescens caerulescens*) migrate each summer to the Canadian tundra to hatch their young. Due in part to the pressures of breeding in the short arctic summer, the whole process from the hatching of the eggs in the first nest to the hatching of the eggs in the last one usually occurs within a two week period [Cooke et al., 1995]. A more detailed study of the factors influencing this synchrony can be found in Findlay and Cooke [1982a,b].

Common brushtail possums (*Trichosurus vulpecula*) in Australia also have a distinct seasonal pattern to their births. Field data from Clinchy et al. [2004] and Clinchy [1999], reproduced in Figure 2.2, shows how the majority of the births are in a two month period from mid March until mid May.

Even cattle on UK farms show strong seasonal variation in their birth rate. The general pattern consists of two annual peaks, one in spring of about $13,000$ births per day, followed by a second smaller peak in the autumn and a trough at around the year's end of $6,000$ births per day. Figure 2.3 on the following page shows time-series data from mid 1996 until mid 2005 and the regularity of this annual pattern is immediately obvious. See Mitchell et al.

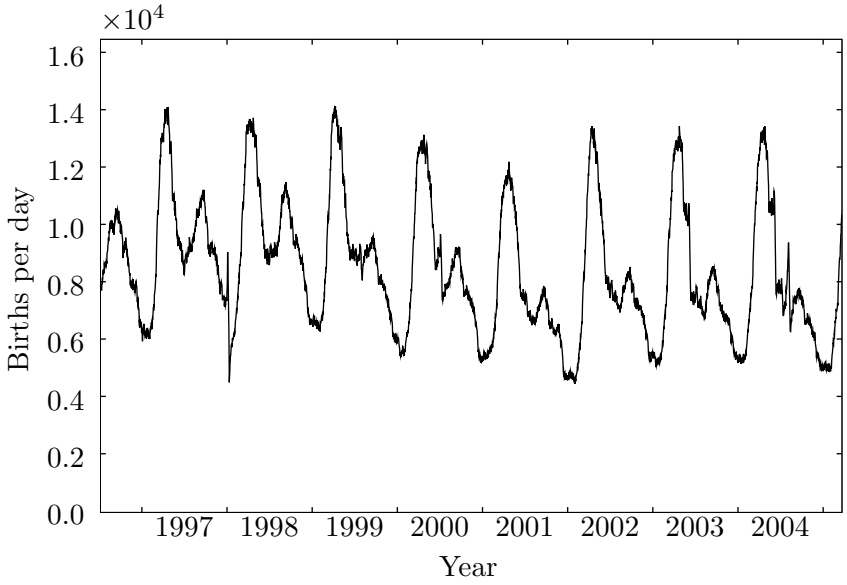

Figure 2.3: Time-series of daily UK cattle births from mid 1996 until mid 2005. The data is smoothed by a 7 day rolling average. Data provided by DEFRA from the British cattle movement service's cattle tracing system via DEFRA's RADAR [a] information management system.

[a] `http://www.defra.gov.uk/animalh/diseases/vetsurveillance/radar/project.htm`

[2005], Robinson and Christley [2006] for a more detailed discussion.

Other examples of reproductive synchrony include grey seals where more than half of the births in a colony can occur within a 7 day period [Boness et al., 1995]. Also black headed gulls have been observed to breed more successfully when in reproductive synchrony [Patterson, 1965].

If modelling a known disease in a specific population then the birth pulse could be fitted from data about when births occur. This could be a polynomial function fitted from daily birth totals or the births could be added to the susceptible class on a daily basis. However, the aim here is not to study a particular disease but to analyse the general effects of pulsed births on disease dynamics. Thus the simplest possible method was chosen to model the pulse—every year at a single time-point the births are simply added to the susceptible class. From a modelling perspective this shares one of the main advantages of having a constant birth rate: it only utilises a

single parameter, in this case, the number of births each year. The effect of other birth functions is analysed in Chapter 3 on page 89.

2.1 The standard SIR model with pulsed births

Replacing the constant birth rate with a birth pulse in the standard SIR model (Equations 1.1 on page 6) the equations become:

$$\begin{aligned} \dot{S} &= -\beta SI - dS + B'(t) \\ \dot{I} &= +\beta SI - gI - dI \\ \dot{R} &= gI - dR. \end{aligned} \tag{2.1}$$

Here $B'(t)$ gives the instantaneous birth rate, and the cumulative birth rate since $t = 0$ is given by

$$B(t) = \left\lfloor \frac{t}{\tau} \right\rfloor x. \tag{2.2}$$

Here $\lfloor \cdot \rfloor$ is the floor function, *i.e.* the largest integer less than the argument, τ is defined to be 365, the number of days in a year, and $x = 1 - e^{-d\tau}$ so that annual births and deaths over a year are balanced. Essentially the model is like the standard SIR model (Equations 1.1 on page 6), except at the transition from one year to the next where there is a jump of size x in the susceptible class. This model could equally well be written as the standard SIR model without births and the following state-reset equation:

$$S(t^+) = S(t^-) + x \qquad \text{where } t = n\tau,\ n \in \mathbb{N}.$$

The model uses density dependent transmission as this is more appropriate for animal populations.

Typical dynamics are displayed in Figure 2.4 on the following page. This pulsed SIR model behaves much like the simple SIR model during the year. After an epidemic in the simple in SIR model the disease dies out [Keeling and Rohani, 2007, chap. 2], but in the pulsed model the addition of more susceptibles prevents this from happening. If the pulse raises the level of susceptibles sufficiently then another epidemic is triggered that year.

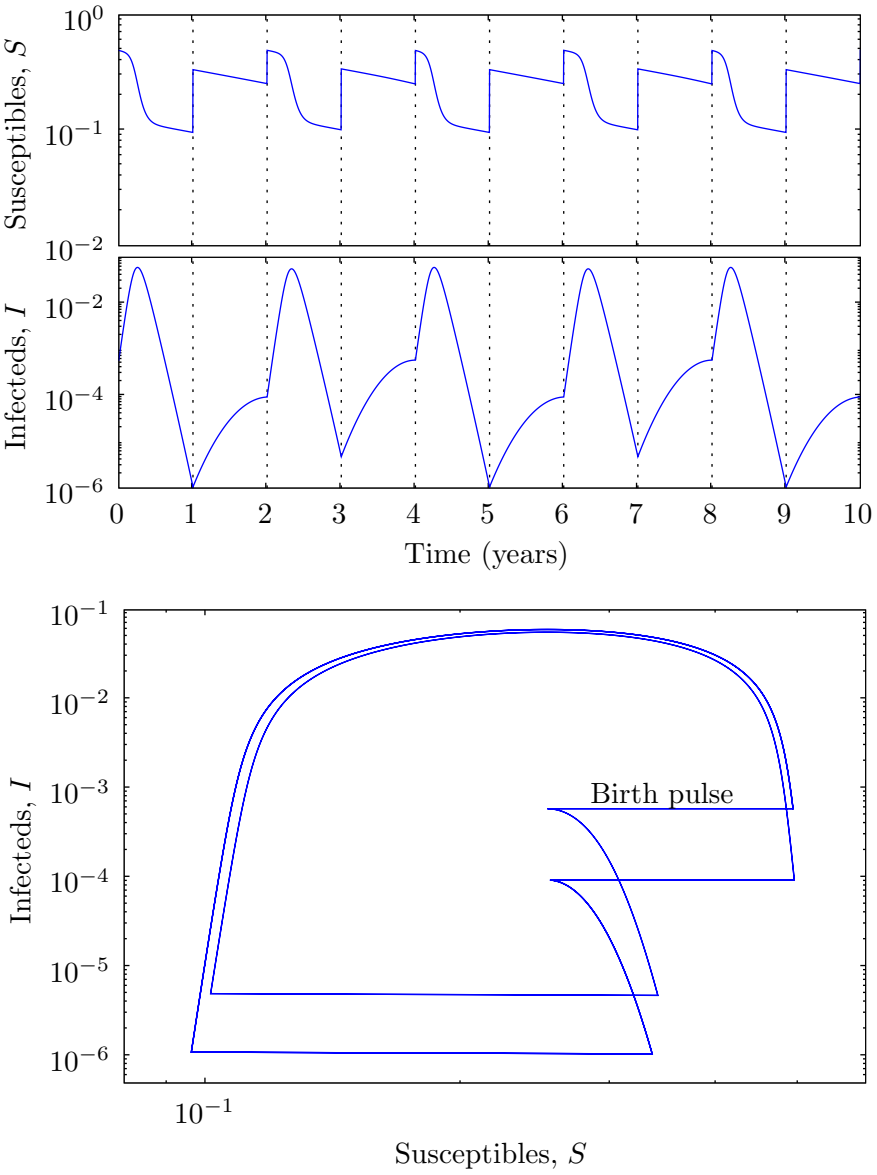

Figure 2.4: Typical dynamics for the pulsed SIR model described in Equations 2.1 on the preceding page. The birth pulse is clearly seen in the time-series plot as an instantaneous change in S on each of the annual vertical dashed gird lines. Similarly in the phase portrait the birth pulses are the four horizontal lines. Looking at the time-series data it initially looks biannual, with a large epidemic in the first half of every other year. However, upon closer inspection it actually has a period of four years which is clearly evident in the phase portrait. This phenomenon is investigated in Section 2.4 on page 53. Parameters: $g = 0.075$, $\beta/g = 4$, $x = 0.24$, $d \approx 0.274$.

Lemma 2.1 *The basic reproductive ratio R_0 for the system described in Equations 2.1 on page 29 is*

$$\frac{\beta x}{(g+d)d\tau}.$$

Furthermore $R_0 = 1$ defines a transition point, so that if I is initially small then $\dot{I} > 0$ initially iff $R_0 > 1$.

Proof:

First note that by setting $I = 0$ the susceptible dynamics during the year, between birth pulses, can be described by

$$\dot{S}\Big|_{I=0}(t) = -dS,$$

so

$$\begin{aligned} S|_{I=0}(t) &= S_0 e^{-dt} \\ &= e^{-dt} \qquad \text{as } S_0 = 1. \end{aligned}$$

The choice of $S_0 = 1$ is not entirely arbitrary as it represents the disease free equilibrium. Consider the following difference equation for S at the end of each year in the absence of infection:

$$\begin{aligned} S_{(n+1)\tau} &= S_{n\tau} e^{-d\tau} + x \qquad \text{for } n \in \mathbb{N} \\ &= S_{n\tau} e^{-d\tau} + 1 - e^{-d\tau}. \end{aligned}$$

Solving this equation for a steady state S^* yields

$$\begin{aligned} S^* &= S^* e^{-d\tau} + 1 - e^{-d\tau} \\ S^* &= 1. \end{aligned}$$

Showing that the choice of relationship between x and d is justified. Thus it suffices to take the average over a single year because the birth pulse resets S back to the value at the start of the year.

From Section 1.3 on page 9, R_0 is calculated as:

$$\begin{aligned} R_0 &= (\text{infectious period}) \times \begin{pmatrix} \text{average rate over one year at which} \\ \text{secondary cases are produced} \end{pmatrix} \\ &= \frac{1}{g+d} \times \frac{\beta}{\tau} \int_0^\tau S|_{I=0}\, \mathrm{d}t \\ &= \frac{\beta}{(g+d)\tau} \left(\int_0^\tau e^{-dt} \mathrm{d}t \right) \\ &= \frac{\beta}{(g+d)\tau} \left(\frac{1}{d} - \frac{1}{d} e^{-d\tau} \right) \\ &= \frac{\beta}{(g+d)d\tau} \left(1 - e^{-d\tau} \right). \end{aligned}$$

If it is assumed that $I \ll 1$ then S behaves approximately like $S = e^{-dt}$ Assuming this for $0 < t < \tau$ it is possible to directly integrate the $\dot{I}$ equation so that

$$I(\tau) \approx I(0) \exp \left(\int_0^\tau \beta S - (g+d) \mathrm{d}t \right). \tag{2.3}$$

Then I is increasing, over a one year period iff

$$\begin{aligned} \int_0^\tau \beta S \mathrm{d}t &> (g+d)\tau \\ \beta \left[-\frac{-e^{-dt}}{d} \right]_0^\tau &> (g+d)\tau \\ \beta \left(1 - e^{-d\tau} \right) &> d(g+d)\tau \\ \frac{\beta x}{(g+d)d\tau} = R_0 &> 1. \end{aligned}$$

□

In the limit as $d \to 0$ the pulsed SIR model (Equations 2.1 on page 29) becomes the simple SIR model (Equations 1.5 on page 15). It is now shown that in the limit as $d \to 0$ the value of R_0 for the simple SIR model is recovered. To demonstrate this it suffices to show that

$$\lim_{d \to 0} \frac{1 - e^{-d\tau}}{d\tau} = 1.$$

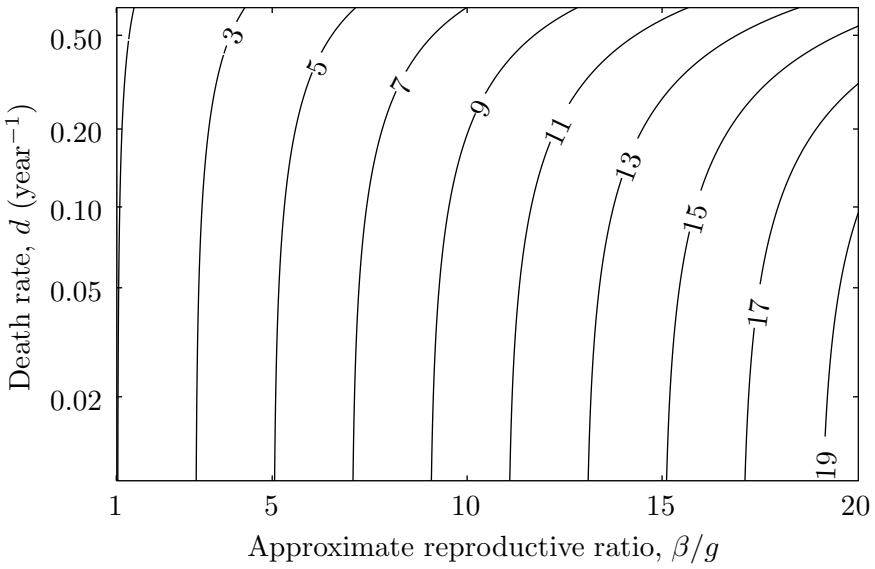

Figure 2.5: How R_0 for the pulsed SIR model (Lemma 2.1 on page 29) compares to $R_0 = \beta/g$ for the simple SIR model over parameter space. In this case $g = 0.075$. The two values are the same for $d = 0$, but diverge as d increases.

Noting that $\lim_{d\to 0} 1 - e^{-d\tau} = 0$ and $\lim_{d\to 0} d\tau = 0$, by l'Hôpital's rule

$$\begin{aligned}\lim_{d\to 0} \frac{1-e^{-d\tau}}{d\tau} &= \lim_{d\to 0} \frac{\frac{\mathrm{d}}{\mathrm{d}d}\left(1-e^{-d\tau}\right)}{\frac{\mathrm{d}}{\mathrm{d}d}\left(d\tau\right)} \\ &= \lim_{d\to 0} \frac{\tau e^{-d\tau}}{\tau} \\ &= 1.\end{aligned}$$

Whence the R_0 equation for the simple SIR model is recovered.

Figure 2.5 illustrates the relationship between R_0 for the two models. For small d $R_0 \approx \beta/g$, and as d increases they diverge. This relationship is exploited in the following work. For simplicity many graphs are plotted as β/g against d (for example Figure 2.5) as this approximates R_0. While in reality plotting a graph on these axes involves changing β along the x-axis, it is scaled as β/g in the hope that this is more meaningful to the reader.

2.2 Periodic orbits

Motivated by the attracting periodic orbits illustrated in Figure 2.4 on page 30, it is clear that one of the key features of the pulsed SIR model (Equations 2.1 on page 29) is the annual and multi-annual periodicity inherent from the forcing. As such it was decided to try and classify the existence and periodicity of attractors throughout a biologically relevant parameter space.

Due to the nature of this system it is some what cumbersome to treat analytically, although some progress is made in Chapter 4 on page 142. Thus the use of numerical methods is necessitated in order to gain a quantitative understanding of the dynamics. This section describes the numerical techniques developed to quantify and then analyse the periodic nature of this system. The mainstay of this is the period finding algorithm (discussed in Box 2.1 on page 40) which calculates how many years it takes for the system to return to the same state.

Many tools exist to analyse dynamical systems numerically. A review of the several of the available tools was conducted to determine their suitability for the study of the pulsed SIR model presented in the previous section.

`AUTO` [Doedel, 2007] is probably the oldest of the available tools, dating back to the late '70s, and it is still in active development, with the recent release of `AUTO-07p`. In fact `AUTO` is used as a back end by several of the other packages reviewed here. However, it seems that `AUTO` is unable to deal with the birth pulse natively. This is illustrated by one of the example files supplied with `AUTO`, where a sinusoidally forced system is encoded by augmenting the system with two extra variables governed by ODEs such that the two extra variables converge to a limit cycle that is the unit cycle, so that one can be used to provide the sinusoidal forcing required. It is immediately obvious that this approach would not be able to adequately describe a system forced by a pulse.

`DSTool` [Guckenheimer, 2004] provides an interactive graphical environment for exploring dynamical systems. It has roots dating back to around 1995, but has seen little development in recent years, and even the authors recommend other software that make use of more modern algorithms. However, `DSTool` is not able to directly represent the birth pulse.

`CONTENT` [Kuznetsov, 2001] is another interactive tool described as an 'integrated environment for analysis of dynamical systems'. It too seems

to have had little development in the last decade. Unfortunately it seems that it is only able realise continuous systems of ODEs, and as such it is not possible to express the pulsed SIR model within its framework.

A much newer piece of software, still under active development, is `MATCONT` [Govaerts and Kuznetsov, 2007] builds on the ODE solvers built into `MATLAB`^{TM} [MathWorks, 2007], and it is the limitations of these that cause this software to be unsuitable. This is because the `MATLAB`^{TM} ODE solvers are only able to represent a continuous system of ODEs.

Another more modern tool is `PyDSTool` [Clewley, 2007], in fact it was not available when this research was started. `PyDSTool` 'provides a powerful suite of computational tools for the development, simulation, and analysis of dynamical systems'. Although not feature complete yet, it seems to provide some support for what it calls *hybrid systems*, which consist of smooth flows punctured by discrete events. This is a framework into which the standard pulsed SIR model would fit.

Given that, at the start of this research, no preexisting dynamical system tools could be found that where able directly deal with the pulsed SIR model (presented in Section 2.1 on page 29), is was necessary to create a *de-novo* implementation. This was done in `C++` [Stroustrup, 2000], which provides the necessary performance, but at a high enough level to ease the implementation. The `C++` objects are then exposed to the `Python` scripting language [van Rossum, 2007] via the `SWIG` interface generator [Beazley, 2007]. This allowed interactive investigation and plotting using the `pylab` interface to `matplotlib` [Hunter, 2007]. `pylab`, in conjunction with the `IPython` shell [Perez, 2007] provides an interactive numerical computing environment similar to `MATLAB`^{TM}.

One of the advantages of undertaking a *de-novo* implementation is that it gives a greater opportunity to gain insight into the behaviour of the system in question. In the light of this, the next section reviews some of the available algorithms for determining the existence of periodic orbits to determine a suitable method to employ in this case.

2.2.1 Numerical integration

Discretisation is an essential part of numerical simulations of ODE models. It is not possible to simulate directly the dynamics of a system of ODEs on

a digital computer. Thus the system must be discretised using a numerical integration scheme. This is a non-trivial problem and much work has been done in this field, see for example Hairer et al. [2002]. The central issue is how closely the dynamics of the discrete approximation provided by the numerical integrations scheme relates to the dynamics of the continuous system. There are two ways inaccuracies can occur: discretisation errors and floating point errors.

Discretisation errors occur when the numerical integration scheme ceases to become a good approximation to the continuous system. This can happen for a variety of reasons, but one of the most common is too large a time step. If the time step is too large then the approximation may fail to capture dynamics that occur between time steps. However, having a very small time step is computationally costly and can cause rounding or floating point errors. Truncation errors also fall into this class. They derive from the approximations implicit in the make up of numerical integration schemes.

Floating point errors arise from the finite precision floating point arithmetic used in modern computers. Only a subset of the real numbers can be stored, for example IEEE double precision equates to roughly fifteen significant figures. To compound this further errors are introduced when arithmetic is carried out in these floating point numbers.

Many schemes for numerical integration of ODEs exist, varying in their complexity, robustness, computational expense and accuracy. There is usually a trade off between these factors. A detailed discussion of the available methods is given in Hairer et al. [2002]. As a general rule, however, a forth order Runge-Kutta method is considered a good method to start with, because although it is not the most computationally efficient, and does not give the highest orders of accuracy, it is relatively simple and very robust. For simplicity it was chosen to implement this method with a fixed time step.

In order to gauge the effects of the discretisation errors described above an error analysis was performed. Figure 2.6 on the following page shows how, for a selection of attractors, the relative error decreases as the number of time steps per day increases. The error is measured relative to a trajectory calculated using a very large number of time steps per day. Linear regression reveals that the slope of the lines is approximately 3.9, which is a good fit for the fourth order Runge-Kutta method in use.

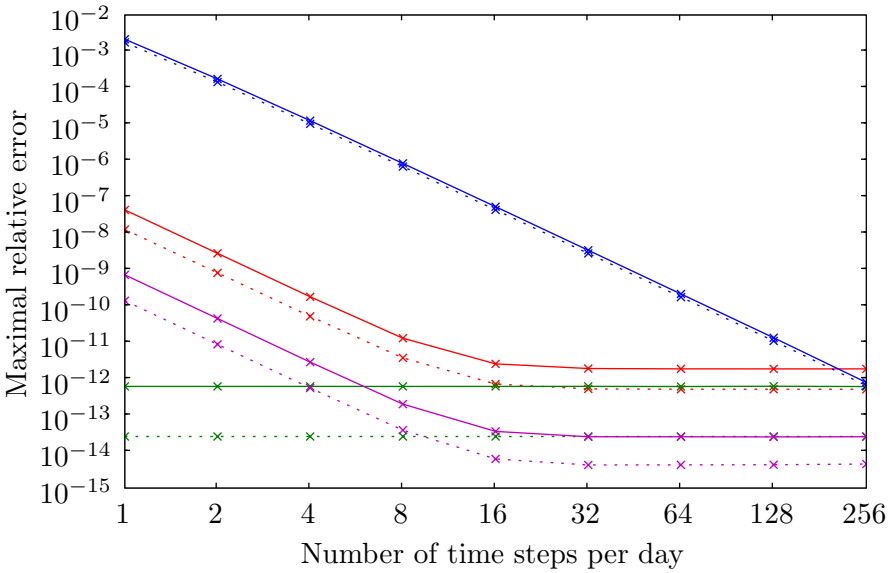

Figure 2.6: Comparison of maximal relative error around a selection of attractors for different time step sizes for the pulsed SIR model (Equations 2.1 on page 29). The error is calculated relative to the path of the attractor calculated using 512 steps per day. Solid lines and dashed lines show the relative error in S and I respectively. Parameters given as $(\beta/g, x)$, $g = 0.075$ throughout. Blue: $(20, 0.5)$ period 1, green: $(2, 0.01)$ period 1, magenta: $(7.5, 0.05)$ period 3, red: $(4, 0.24)$ period 4.

Four steps per day was chosen as a compromise between accuracy and the computational effort required to perform the simulation. The larger error for the blue line in Figure 2.6 is not an issue as it occurs in an area of parameter space where only period one dynamics are seen, thus there is very little scope for errors to occur. Moreover, the relative error is still small compared to the dynamic range within an orbit.

Thus the forth order Runge-Kutta method with a fixed time step of 0.25 days gives a robust method for numerically calculating trajectories of the pulsed SIR model.

2.2.2 Period finding algorithms

There are a variety of possible algorithms that could be used to find periodic solutions of dynamical systems. Two of the most popular are described

below.

The simplest and most obvious method, to find attracting limit cycles, is to use forward numerical integration. Starting at a point in the basin of attraction of a stable limit cycle, then the trajectory converges to the limit cycle as $t \to \infty$. The main advantage of this method is that it is simple, and if it is the initial point is in the basin of attraction of an attracting limit cycle, then its success is only dependent on the accuracy of the numerical integration routine. However, this method does have its drawbacks. Firstly it can only find stable periodic orbits (although it is possible to some unstable periodic orbits through reverse time integration), and secondly it can be computationally expensive, especially if it takes a long time to converge to the attractor. Also, a stopping criterion has to be defined, to determine when the trajectory is close enough to the periodic orbit, and what its period is.

Another method, that is capable of finding both stable and unstable limit cycles involves reformulating the problem as either as a root finding, or minimisation problem over the state space [Parker and Chua, 1989]. This is achieved by considering the annual map of the system, which is the case of the pulsed SIR model is given by

$$\Phi_\tau(S_0, I_0) = \begin{pmatrix} S_0 + x \\ I_0 \end{pmatrix} + \int_0^\tau \begin{pmatrix} \dot{S(t)} \\ \dot{I(t)} \end{pmatrix} \mathrm{d}t.$$

Then the annual points of a period p limit cycle (that it points on the trajectory when $t = n\tau$, $n \in \mathbb{N}$) will be fixed by the p^{th} composition of Φ with itself, that is they satisfy

$$\Phi_\tau^p(S_0, I_0) - \begin{pmatrix} S_0 \\ I_0 \end{pmatrix} = 0. \tag{2.4}$$

Of course there is no closed form for Φ and it must be determined by numerical integration. Then the above expression can be solved, by for example a 2D Newton's method. Alternatively, this can be expressed as a minimisation problem where

$$f(S_0, I_0) = \left\| \Phi_\tau^p(S_0, I_0) - \begin{pmatrix} S_0 \\ I_0 \end{pmatrix} \right\|$$

is minimised over the state space. This can then be minimised using a conjugate gradient, or simplex method [Nocedal and Wright, 1999]. These

methods have the advantage of being less computationally intensive than the simple use of forward numerical integration, although each evaluation of Φ^p does require integrating the system p years forward in time. Another advantage is the possibility to check for the existence of an attractor of a particular period, though this can be a disadvantage as they each have to be checked individually. The main disadvantage of this technique is that it there is no guarantee that the minimisation will find a zero of f, it could for example get stuck at a non zero local minimum. In other words it is less robust and more sensitive to the choice of starting point (S_0, I_0). Techniques similar to this are used by Schwartz and Smith [1983] in the study of an SEIR model with seasonally forced transmission.

One other advantage of restating the problem is this form is that it allows the use of preexisting tools that are able to find periodic solutions of discrete maps. Of the tools reviewed above at least `AUTO` and `PyDSTool` would be suitable for this. However, this approach was not pursued.

Both of these methods have their advantages and disadvantages. The main advantage of the direct integration method is that it is guaranteed to find a attractor (even chaotic ones), but that is can be computationally intensive under certain circumstances, also there is no need to explicitly check for each period. While the minimisation method is the reverse: it may not always find an attractor, but can be fast. However, in order for this method to find every possible attractor it must test every period in each basin (although of course the number and locations different basins will not be known). As such it may be optimal to use a hybrid method, where direct integration is used to get close, followed by minimisation to achieve the desired level of accuracy.

2.2.3 Chosen algorithm

This subsection describes in detail the implementation and development of the direct forward integration algorithm described in the previous section. This method was chosen initially for simplicity, and as described in Subsection 2.2.4 on page 43, it achieves good results, when combined with certain refinements to the algorithm. The fact that this algorithm is unable to find unstable limit cycles is not of major concern, because they biologically less important. The details of the precise algorithm used are discussed in Box 2.1.

First of all, a parameter space was chosen to represent biologically realistic ranges for each of the three parameters. $\beta/g(\approx R_0)$ was chosen to run from 0.98—just less than unity to test that the numerics show the infection dying out—to 20. x was chosen to run from 0.01 to 0.5. This corresponds to a birth/death rate varying from 2.7535×10^{-5} to 1.8990×10^{-3} per day or an average life expectancy of about 100 years to 18 months. Realistic values of g were considered to be between 0.075 and 0.5, so that the infectious period ranges from about two weeks to two days. A grid was then placed on this space and the dynamics considered at discrete points in this space. For β/g the range was covered by 318 points, including the end points, with a regular spacing of 0.06. The x range was covered by 301 logarithmically spaced points including the end points. This grid in β/g-x space will from here on in be referred to as parameter space. For g however, only 4 values 0.075, 0.100, 0.250 and 0.500 were chosen. This was done for g rather than one of the other two parameters because in practise it is much easier to measure g. Out of the three parameters g is, to a greatest extent, a function of the disease rather than the population—or even a combination of the two. Thus when trying to fit the model to a real disease this approach makes comparing epidemics, of the same disease, across different populations possible.

2.1 Calculating the period

Accurately determining the period of an attractor numerically has proved to be a challenging problem. Firstly, the possibility that a point may not have converged to a limit cycle and indeed may never do so must be considered! In some areas of parameter space the convergence can be very slow (of the order of several thousand years) so determining when to stop and assume a periodic attractor doesn't exist can be problematic. How the algorithm works is now described. All the numerics only consider the state variables S and I, together denoted here by `P`. The value of R is not calculated because it is simply a function of I. A fixed time step fourth order Runge-Kutta scheme was used for integration [Hairer et al., 2002], as discussed in Subsection 2.2.1 on page 35.

The core of the period finding is the function `try_periods()`:

```
function period=try_periods(P) :
```

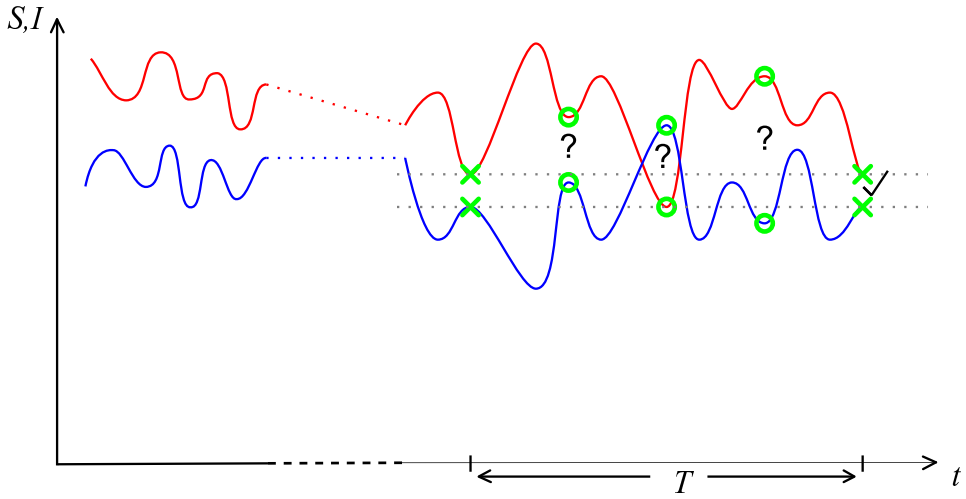

Figure 2.7: The period calculation algorithm explained graphically, showing how `try_periods()` works. The system starts at `P_start`—denoted by the left most pair of crosses. Iterating forward in time—moving to the right—`try_periods()` checks if the state—denoted by circles—is close to `P_start`. After four years the system returns to the original state `P_start`—right most pair of crosses.

```
P_start=P
for period = 0 to MAX_PERIOD :
  iterate_forward(ONE_YEAR,P)
  if is_close(P,P_start) : return period
return -1
```

This function simply checks if the the system returns to the same state (up to a tolerance, see Box 2.2 on page 43) indicating that the system maybe on, or converging to a limit cycle. If the system doesn't return the the same state within `MAX_PERIOD` years it terminates and returns a period of -1 signifying failure. This function is illustrated in Figure 2.7.

The above process works well when starting on or close to an attractor, but will fail if the system has not yet converged. The next function `check_again()` deals with this by iterating the system forward for `TRY_AGAIN_YEARS`, usually 100, before calling `try_periods()` again:

```
function period=check_again(P) :
  for k = 1 to MAX_TRIES :
```

```
    period = try_periods(P)
    if period == -1 :
      iterate_forward(TRY_AGAIN_YEARS,P)
    else if period == 1 :
      if I < 1e-200 : return 0
    else :
      if period is even : check_half_period(P,period)
      return period
  return -1
```

There is a limit of `MAX_TRIES` (usually 50) calls to `try_periods()` to avoid an infinite loop. If this limit is reached -1 is returned.

If the system fails to get back to the same state again within `MAX_PERIOD` years one of three things could be happening:

- `P` is not in the basin of attraction of a periodic attractor and thus will never converge.
- `P` has not yet converged to an attractor.
- It is on a periodic orbit with period greater than `MAX_PERIOD`.
- It is on a chaotic attractor.

In all four cases `try_periods()` will return -1. When this happens `check_again()` will iterate the system forward for `TRY_AGAIN_YEARS` and call `try_periods()` again, assuming `MAX_TRIES` has not been reached. When `MAX_TRIES` is reached the presence of a chaotic attractor is usually presumed. A possible improvement would be to confirm this by checking the Lyapunov exponent to confirm if the dynamics are in fact chaotic.

The `check_again()` function also deals with a couple of special cases. If `try_periods()` returns 1, the state is the same after only one year, then it is quite possible that the state has not changed at all. Some basic analysis shows that the only time that this can happen is through extinction, thus a check of whether I is approaching machine precision is carried out in the period 1 case. In the case that the period returned by `try_periods()` is even, the half period check is applied. This is discussed in detail in Box 2.4 on page 50.

Before finally returning the period the top level function `calc_period()`, if it has locked on to an attractor, moves `P` to the annual point on the attractor with maximal I:

```
function period=calc_period(P){
  period=check_again(P)
  if period > 0 :  minimise_I(P)
  return period
}
```

2.2 Closeness

A key method in these numerics is to decide if two points in phase space are in some sense close. To determine this the following function was chosen. Given two points $P_1 = (S_1, I_1)$ and $P_2 = (S_2, I_2)$ they are said to be close if

$$d(P_1, P_2) = \left|1 - \frac{S_1}{S_2}\right| + \left|1 - \frac{I_1}{I_2}\right| < \epsilon$$

This function was chosen instead of the Euclidean metric because it gives a more comparable measure of closeness for both large and extremely small numbers. In essence it ensures that the relative error is small, not just the absolute error when $S, I \leq 1$. This is important because I can range from order 1 to order 10^{-15} or smaller. In most calculations, including period calculations, $\epsilon = 10^{-8}$.

It is worth noting that d is not a metric on $\mathbb{R}^2$. While d satisfies the non-negativity and identity axioms it is obviously not symmetric. This could be rectified by defining

$$D(P_1, P_2) = d(P_1, P_2) + d(P_2, P_1).$$

This was not done for performance reasons.

2.2.4 Results

Preliminary investigations showed that the system exhibited periodic attractors at the vast majority of points in the chosen parameter space. Initial

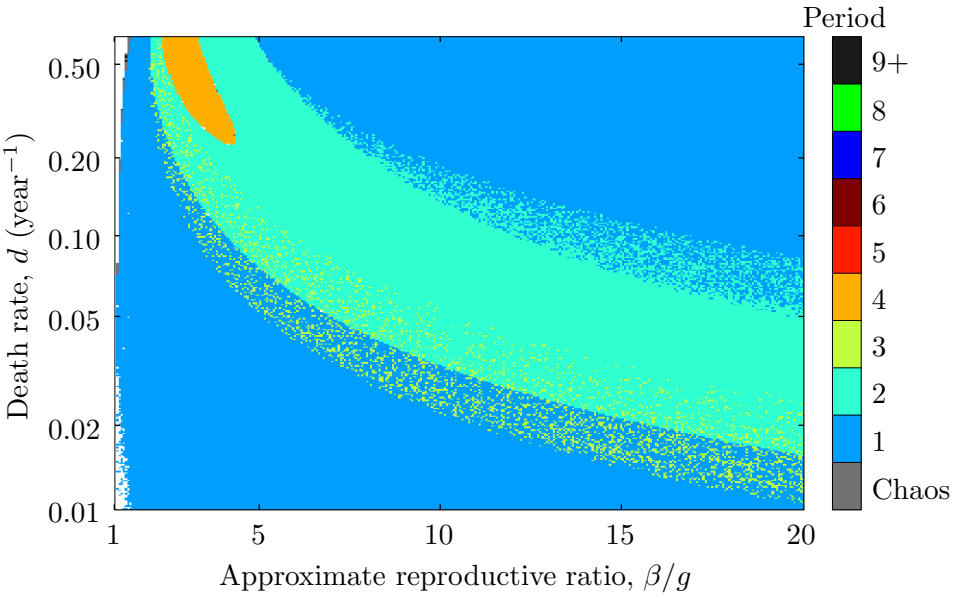

Figure 2.8: Period of resultant attractors for with $S_0 = 0.02$, $I_0 = 0.0005$ for $g = 0.075$.

attempts to classify the period of attractors throughout parameter space can be seen in Figure 2.8. The majority of parameter space exhibits annual dynamics. The major feature though is the 'banana' shaped region of period two dynamics. This kind of behaviour has been observed in other systems.

There is also a smaller 'tongue' of period four dynamics. The 'speckling' around some of the transition areas is interesting. Points close in parameter space converge to different attractors. This suggests that there may in fact be two attractors of different periods in that region.

By superimposing R_0 contours on the data of Figure 2.8, Figure 2.9 on the next page shows that the $R_0 = 1$ isoline is clearly a transition from annual dynamics to extinction showing how well the numerics and analysis agree.

The algorithm used to classify these attractors is described in Figure 2.7 on page 41, and in Box 2.1 on page 40. The same data was also calculated for $g = 0.100$, 0.250 and 0.500, though the figures are not shown as this data is only preliminary. This will become apparent in the following section where coexisting attractors are explored.

Several things were learnt in producing the data for Figure 2.8:

- Convergence in some areas of parameter space (specifically small x

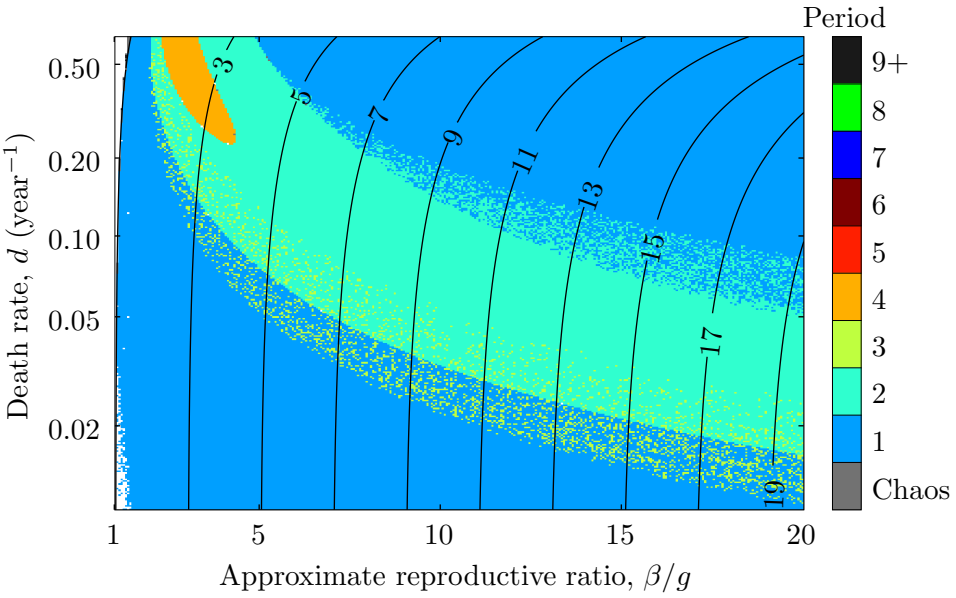

Figure 2.9: Data from Figure 2.8 on the preceding page superimposed with the R_0 contours of Figure 2.5 on page 33. The $R_0 = 1$ contour closely follows the left hand edge of the period one region. The period one region should extend right into the bottom left corner, but in this region of parameter space convergence is extremely slow and the period finding algorithm has not given them sufficient time to converge.

and/or β/g) is very slow, of the order of several thousand years.

- It seems that attracting periodic orbits exist throughout parameter space as expected, with the exception of the region $R_0 < 1$ in which extinction occurs.

- There is evidence of multiple coexisting attractors in some areas of parameter space.

The last point is covered in depth in the next section.

Some improvements could be made to this algorithm, for example to check if an attractor is in fact chaotic the Lyapunov exponents could be calculated. Also the use of alternative algorithms, such as the minimisation techniques discussed in Subsection 2.2.2 on page 37, could be investigated, these would be able to find unstable limit cycles too, but at they are less robust. Perhaps as discussed in a Subsection 2.2.2 a hybrid approach could

be most successful, combining the robustness of direct integration, with the speed of a minimisation method.

2.3 Coexisting attractors

This section attempts to uncover the extent of the coexisting attractors who's existence was suggested in the previous section. Finding these attractors requires the use an other range of numerical algorithms: continuation methods.

2.3.1 Continuation algorithms

In general continuation methods involve computing approximate solutions to a system of parameterised, usually nonlinear, equations:

$$F(y, \lambda) = 0, \quad F : \mathbb{R}^n \times \mathbb{R}^m \to \mathbb{R}^n \tag{2.5}$$

where F is assumed to be smooth so that by the inverse function theorem a solution exists, parameterised by λ. Take for example the autonomous system of ODEs

$$\dot{y} = F(y, \lambda),$$

where λ is scalar. In this case the solutions of Equation 2.5 are the fixed points of the system of ODEs. A plot of λ against y (or one component of y) forms the familiar bifurcation diagram.

There are two main algorithms for approximating solutions of Equation 2.5 simplicial continuation, and predictor-corrector continuation. Both assume an initial point (y_0, λ_0), with $F(y_0, \lambda_0) = 0$ is known.

Simplicial continuation, also known as piecewise linear continuation, algorithms [Allgower and Georg, 2000] work on a similar premise to the bisection method. Consider the example above where the solution is a curve in $\mathbb{R}^2$ and an initial point (y_0, λ_0) is known, also F is defined so that it is positive on one side of the solution curve and negative on the other. Then any line segment AB, such that $F(A) > 0$ and $F(B) < 0$ must intersect the solution curve. Now let a line segment AB containing y_0 form the base of a triangle, ABC, then the solution curve must also pass though either AC or BC, the location of this intersection can be determined by linear interpolation or bisection, if a higher accuracy is required. This yields a second known

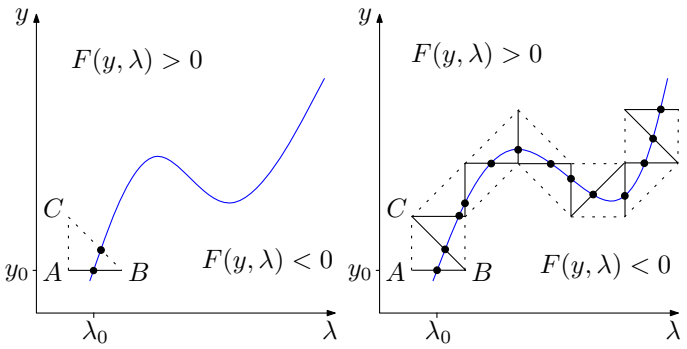

Figure 2.10: A graphical representation of simplicial continuation. The left hand side shows how the first step is made given that (y_0, λ_0) is known to lie on the solution curve. Given that the solutions curve enters the triangle ABC though edge AB, it must leave though either AC or BC, depending on the sign of F at C, that is which side of the curve C lies on. The right hand axes show how the algorithm progresses, solid lines show simplexes that intersect the solutions curve, dotted lines represent simplexes that don't.

point on the solutions curve, as illustrated on the left of Figure 2.10. The process is now repeated with either AC or BC as the base of the triangle. In this way the solution curve can be followed, as is shown on the right of Figure 2.10. Different triangulation patters can be used, Figure 2.10 illustrated a square lattice with cells subdivided along the diagonals to form triangles, however, an isometric grid has also been used [Wheeler, 2006, Section 3.8.3].

The second class of continuation methods use a two stage predictor-corrector process to determine an approximation to the next point on the solution curve [Doedel, 1997]. They work by making an initial guess for a next point on the solution curve, using the known point(s), or other information, for example the gradient. This is the predictor part of the process, and is denoted by the arrows in Figure 2.11 on the next page yielding a first estimate $(\bar{y_1}, \bar{\lambda_1})$ for the next point. There are several methods for making the predictor step, and Figure 2.11 on the following page shows the simplest. The parameter λ is incremented by a fixed amount and the previous value for y is used, that is $\bar{y_1} = y_0$, this could be considered a zeroth order extrapolation. If, for example there is knowledge of the derivative of F, then an Euler step could be used, or multiple previous points could be used to extrapolate the

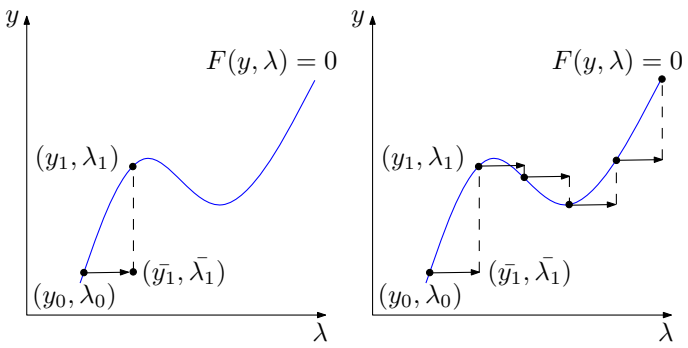

Figure 2.11: Predictor-corrector continuation, following a solution curve, $F(y, \lambda) = 0$, shown in blue. Given a known point on the curve (y_0, λ_0), left hand axes, then an initial guess $(\bar{y_1}, \bar{\lambda_1})$ is made–the predictor step–illustrated by an arrow. Then this guess is refined in the corrector step, using some kind of iterative method, dashed line yielding an approximation to a second point on the solution curve (y_1, λ_1). The right hand axes show how the algorithm proceeds with multiple steps.

position.

The corrector step, illustrated by dashed lines in Figure 2.11, attempts to improve on the estimate given, usually by using a iterative approach to get closer to the solution curve. What iterative algorithm is used will vary depending on the problem but if the problem is finding stable fixed points of a map, or system of ODEs then is could involve forward integration or repeated application of the map. Alternatively minimisation or Newton methods may be used, depending of the formulation of F.

Predictor-corrector algorithms can be taken one step further by allowing the increment in the parameter λ to vary with each step. One such adaptive predictor-corrector algorithm featuring a tangential predictor, and Newton corrections was utilised by Kuznetsov and Piccardi [1994] to perform a bifurcation analysis of SIR and SEIR models with a sinusoidally varying contact rate. The same system is studied by Schaffer and Bronnikova [2007] and continuations of periodic orbits are this time performed using a secant predictor and again Newton-Raphson for the corrector stage.

The extension of these techniques into two or more parameter dimensions, m, can lead to complex algorithms to deal with the potentially more complex topology of the solution manifolds. These are reviewed in Henderson [2002], and not discussed here. However, if the problem is on a fixed two dimensional

grid in parameter space then the simple approach of using the one dimensional predictor-corrector algorithm to approximate the value at an adjacent grid point in parameter space can be used. In fact, this is the method that was chosen, in conjunction with zeroth order extrapolation for the predictor stage, and direct forward integration for the corrector stage. The details of the implementation of this algorithm are described in the next subsection.

2.3.2 Chosen algorithm

To explore the extent of coexisting attractors a program was written, implementing some of the continuation techniques discussed above. The process of finding these new attractors was dubbed *pushing out* and the details the precise methods used are described in Box 2.3 and Figure 2.7 on page 41. In brief they comprise a predictor-corrector algorithm with a zeroth order extrapolation predictor and direct forward integration corrector.

In order to search for new attractors several assumptions are made. Firstly, it is assumed that regions of the same period are connected, or at least connected to a currently known area of the same period. That is to say there are assumed to be no isolated points, and should any exist they will not be found. Secondly, there are no areas where multiple distinct attractors of the same period exist. If this were to happen, no attempt would be made to distinguish between them.

2.3 Pushing out

Pushing out is the algorithm used to find attractors in new regions of parameter space. It works on attractors of each period independently. Taking the regions in parameter space where attractors of the given period are known to exist, it finds all the points adjoining these regions and stores them in a list paired with an adjoining point inside the region where the attractor is know to exist. For each pair it tests if the same attractor still exists at the adjoining point using a simple predictor corrector algorithm. If it exists the point is added to the region, if not it is marked as an edge point. When it has finished all the points in the list it goes back and makes a new list of adjoining points and tests them. This process continues until all regions are surrounded by edge points.

To test if an attractor exists at an adjoining point one could just use the values of S and I from the point inside the region as initial conditions at the adjoining point and see if it converges to the same period. There is a risk here that if the grid is not fine enough then you could be outside the basin of attraction of the attractor one seeks at the adjoining point. Thus, rather than move between adjoining grid points in a single step many small steps are taken to ensure that the system stays within the same basin of attraction. Typically twenty steps are taken and the model is iterated forward for two years at each intermediate point.

This algorithm is explained graphically in Figure 2.12 on the next page.

2.4 Half period

It was found that in some places the period calculation algorithm would sometimes return double the real period. This seems to be because of the way trajectories converge to a limit cycle. Figure 2.13 on page 52 shows a typical pattern of convergence. Notice that the annual points oscillate about the limit point in such a way that they are closer to themselves after two years than they are after one. Once the biannual separation falls below the tolerance used by the period calculation algorithm the algorithm will think it is on a period 2 attractor.

To circumvent this issue, whenever the period finding algorithm returns an even period $2p$, a check is made to see if the distance between points p years apart is also fairly small. If so it iterates the system forward to see if it can get the p separation to within its tolerance. The following pseudo code shows how this is done:

```
function check_half_period(P,period) :
  P_start=P
  iterate_forward(period/2,P)
  if is_close(P,tolerance=0.05) :
    iterate_forward(START_YEARS*5,P)
    period=try_periods(P)
```

The function stores the stating point, `P_start`, and iterates `P` forward half a cycle, that is p years. If it is still reasonably close to the starting

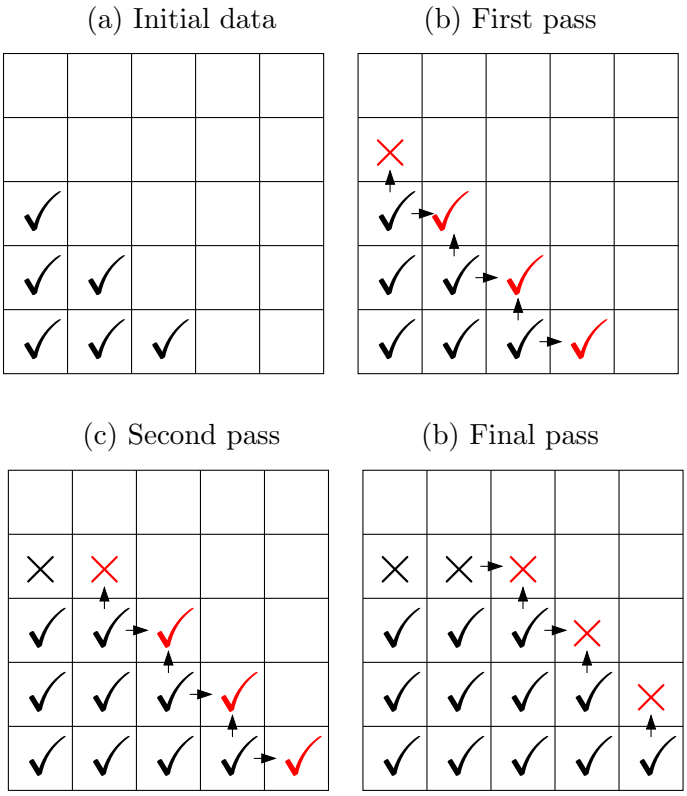

Figure 2.12: How pushing out works, explained graphically on a 5 by 5 test grid. (a) Shows the initial data for just the period being pushed out. The initial data as obtained by using the same initial conditions at each point on the grid. The symbol ✓marks grid points where an attractor of this period exists. Empty boxes are as yet untested as to whether or not an attractor of this period exists or not. (b) Shows the first pass. Arrows point from the points where existence is known to adjoining untested points. At most of the adjoining points the attractor still exists, marked with ✓, but at one point an attractor of the period in question no longer exists, denoted by a ×. (c) Shows the second pass which repeats the same process at with the first pass. (d) Shows the final pass, no more new points can be added because the region where the attractor of the period in question exists is bounded by either the edge of the grid or the points where an attractor of the same period doesn't exist.

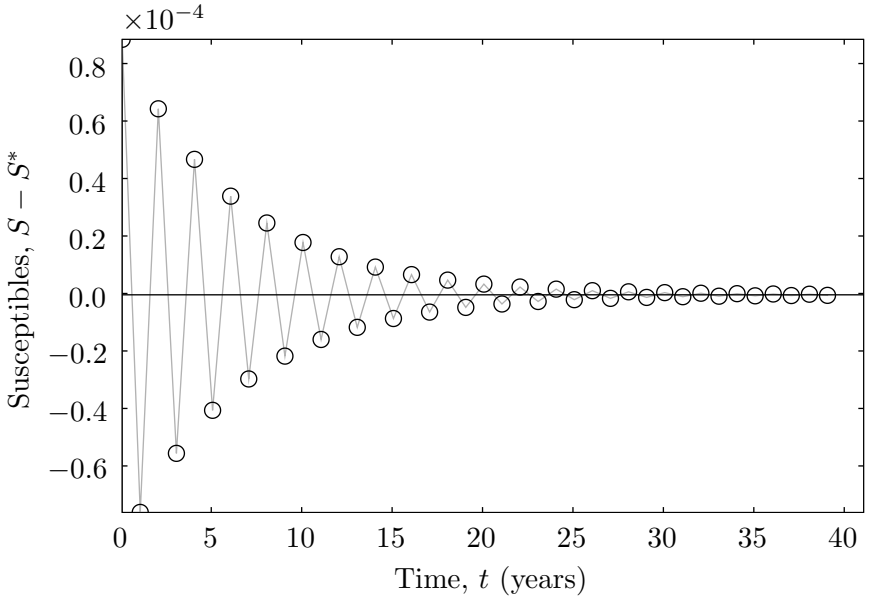

Figure 2.13: How trajectories converge to an attractor. The grey line represents a point on the attractor. The circles are annual points taken from a trajectory. Notice how a point is closer to the next-but-one point than it is to the next. The fixed point $S^* \approx 0.240$

point this suggests that the the system not be on a period $2p$ attractor, but converging to a period p one. To check this, the code iterates `P` forward for $5\times$`START_YEARS`. The the idea is that if a period p attractor exists the system has converged close enough for `try_periods()` to lock on to it rather that the period $2p$ one.

2.3.3 Results

The data sets for all four g values are displayed in Figure 2.14 to Figure 2.17 on pages 54–55. Comparing the data before and after pushing out for $g = 0.075$ (Figure 2.8 on page 44 and Figure 2.14 on page 54) two changes become apparent. Firstly, the speckled area on the upper boundary between periods one and two has become an overlap. Secondly the period three speckles have merges to form a contiguous region overlapping both the lower period one, and period two regions. There is now a substantial proportion of parameter space—roughly 29% in terms of number of grid points—where two attractors coexist.

Now comparing the data for different values of g it is clear that the complexity increases with g. Although it is important to not e that because a constant range of β/g (approximately the reproductive ratio) is considered, increasing g also has the effect of increasing the transmission rate β. Higher periods appear and there are more overlaps. With $g = 0.075$ there is a single 'tongue' of period four. At $g = 0.100$ there are tongues of period four eight and nine that have emerged from the top left. As g increases further to 0.100 the tongues move down and right. At the highest value $g = 0.500$ most of the tongues heads have passed out of the parameter space to the bottom and right leaving only their tails. In their wake is a large chaotic region.

Looking more closely (at for instance $g = 0.100$) there is clear evidence of period doubling, period two becomes period four then eight, sixteen. Similarly for period three though this is harder to pick out.

Another observation from Figure 2.15 on the next page ($g = 0.100$) is the existence of two distinct overlapping tongues of period six attractors. Figure 2.19 on page 56 shows an enlargement of just the two period six tongues. To distinguish them, they are coloured by the value of I at the fixed point at which I is minimal. Figure 2.18 on page 56 shows phase plots of two of the period six attractors at a point in the overlap. The two attractor have clear structural differences. The blue attractor looks like a period three attractor that has undergone period doubling. Where was the period three could be a period two attractor that has undergone a period tripling bifurcation.

2.4 Attractor properties

To further understand the properties of the attractors, several other properties were computed over the whole parameter space. The hope is that by calculating some properties of the attractor it will be come clear which are more likely to manifest them selves in reality. Firstly, the minimal value of I attained on each attractor across parameter space is calculated. This can give an indication of how likely the infections is to die out due to stochastic effects, that any real population is likely to experience. Secondly, the modal frequency component of the time-series representing one cycle each attractor. This is compared to the period of the attractor.

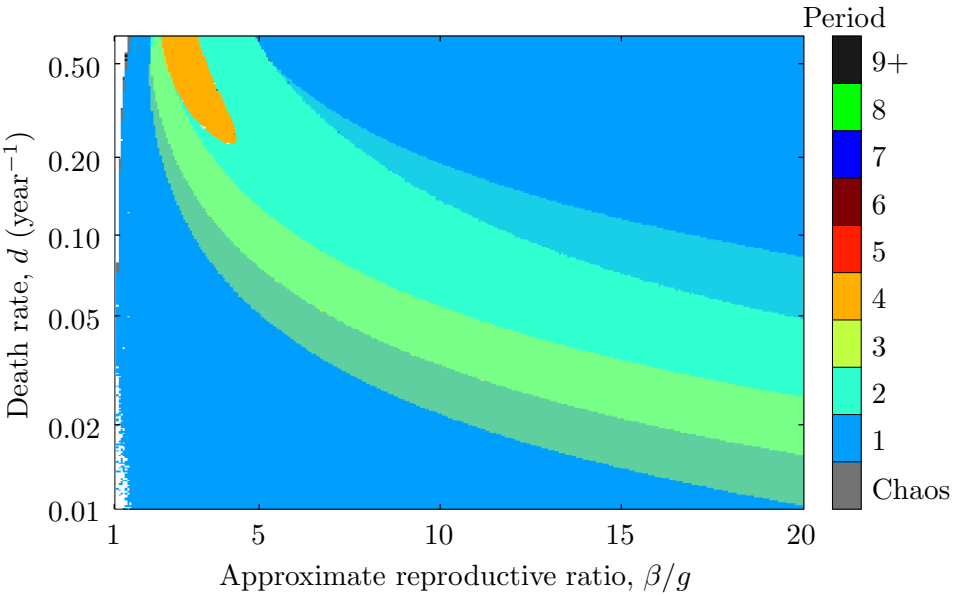

Figure 2.14: Attractors found after pushing out for $g = 0.075$.

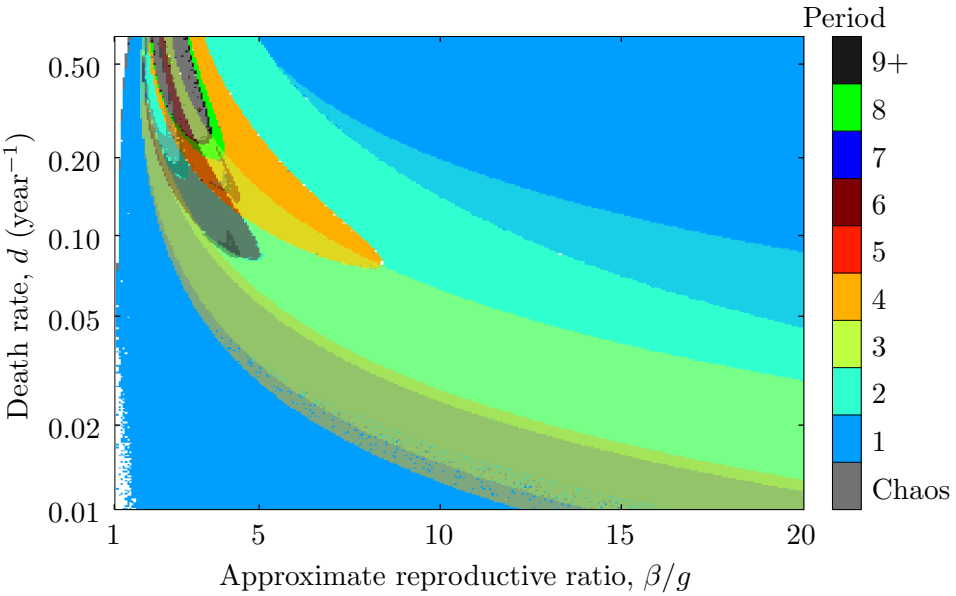

Figure 2.15: Attractors found after pushing out for $g = 0.100$.

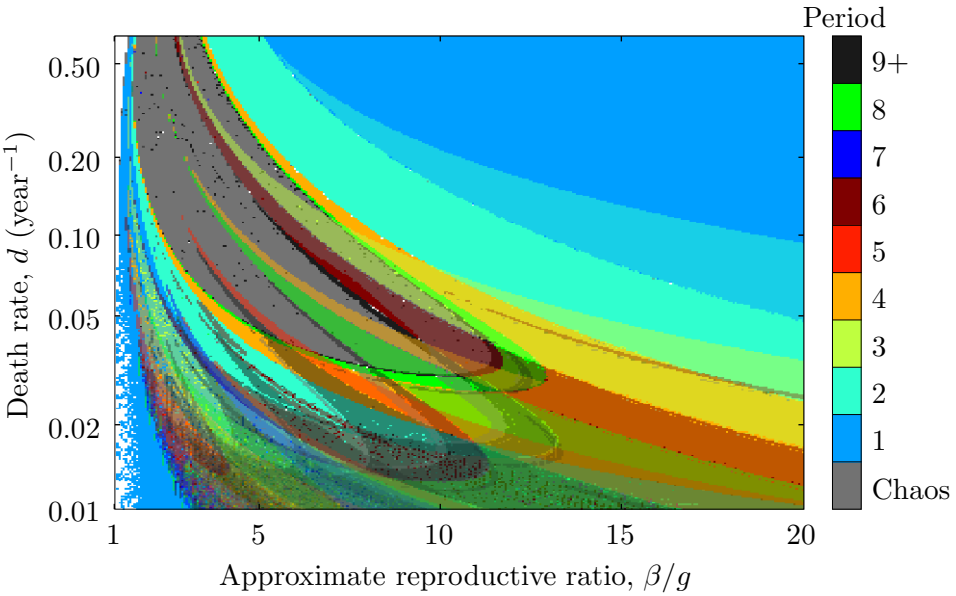

Figure 2.16: Attractors found after pushing out for $g = 0.250$.

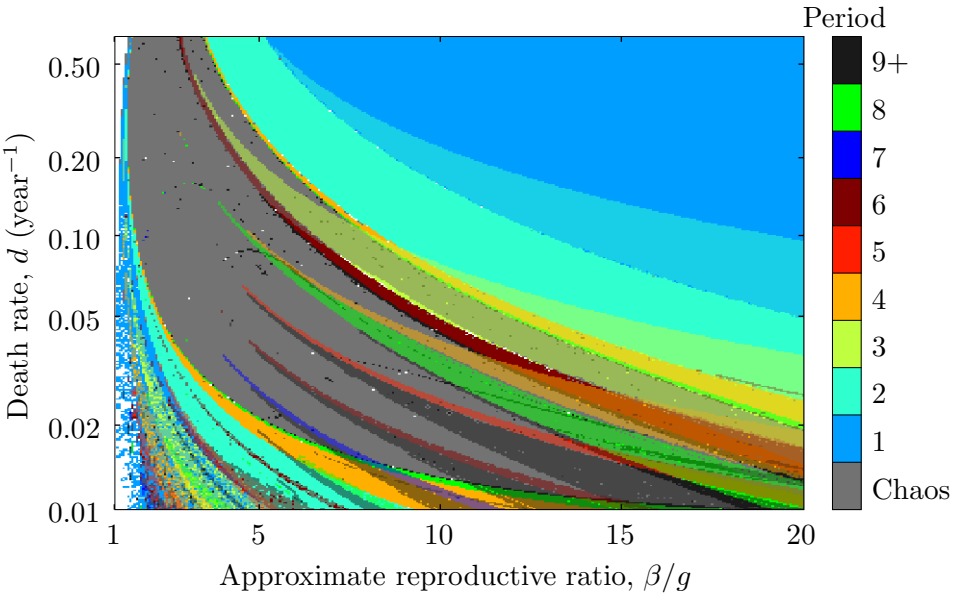

Figure 2.17: Attractors found after pushing out for $g = 0.500$.

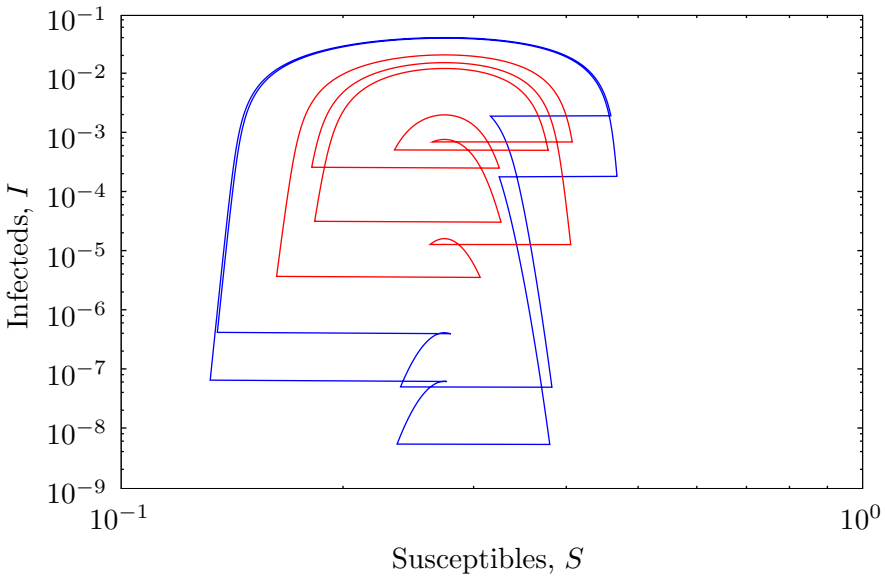

Figure 2.18: Coexisting period 6 attractors for the pulsed SIR Model. The blue line clearly shows a period three attractor that has under gone a period doubling bifurcation. Parameters: $R_0 = 3.68$, $x = 0.143$, $g = 0.100$.

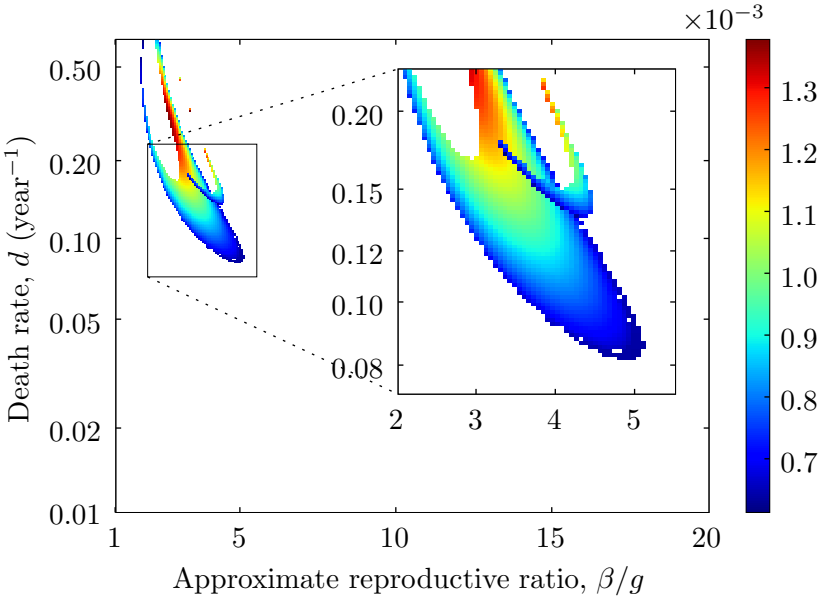

Figure 2.19: The value of I, at the fixed point at which it is minimal, for the two coexisting regions of period 6 attractors. The data was obtained by first deleting all the points in one of the regions and then pushing out. The process is them repeated for the other region.

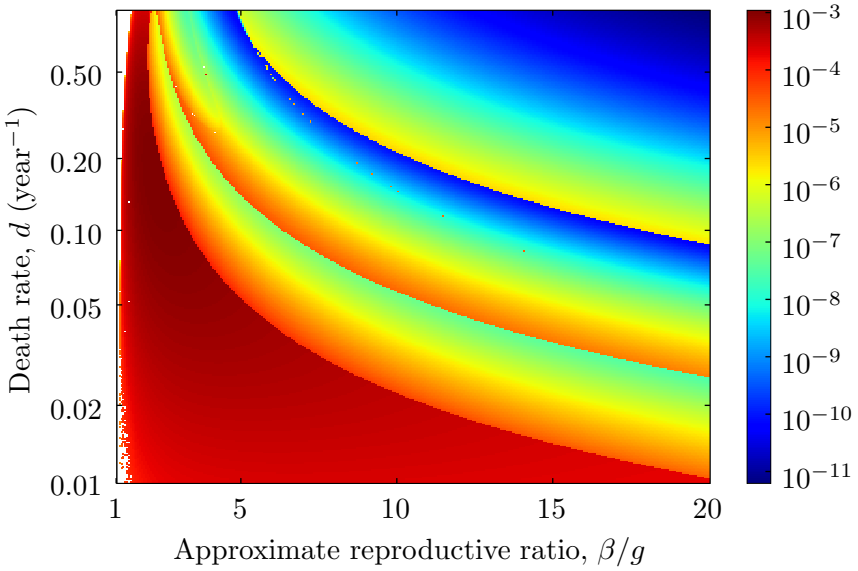

Figure 2.20: The minimum value of I attained around the attractor, or attractors, at each point in parameter space. In this case $g = 0.075$.

2.4.1 Minimum I

First of all the minimum value of I attained around each attractor was determined. This is important because it helps in understanding if a disease will die out. Real populations are discrete, so if $I < 1/N$—where N is the size of the population—the disease will certainly die out. In fact it may only be necessary for I to be close to $1/N$ as there will inevitably be stochastic variations in a real system that may lead to extinction. The result of calculating the minimum of I over the whole of the the chosen parameter range for $g = 0.075$ is shown in Figure 2.20. It is clear that the density of infection does reach very low levels in some regions of parameter space. Two regions show particularly small values of I, the top of the period two region and the top left corner, where both d and β/g are large. This is not surprising. With a high transmission rate an epidemic will quickly take off and the supply of susceptibles will quickly be exhausted, so the epidemic will peak early allowing time for most of the infecteds to recover before the next birth pulse arrives. The high death rate will also aid in diminishing the level of infecteds in this period.

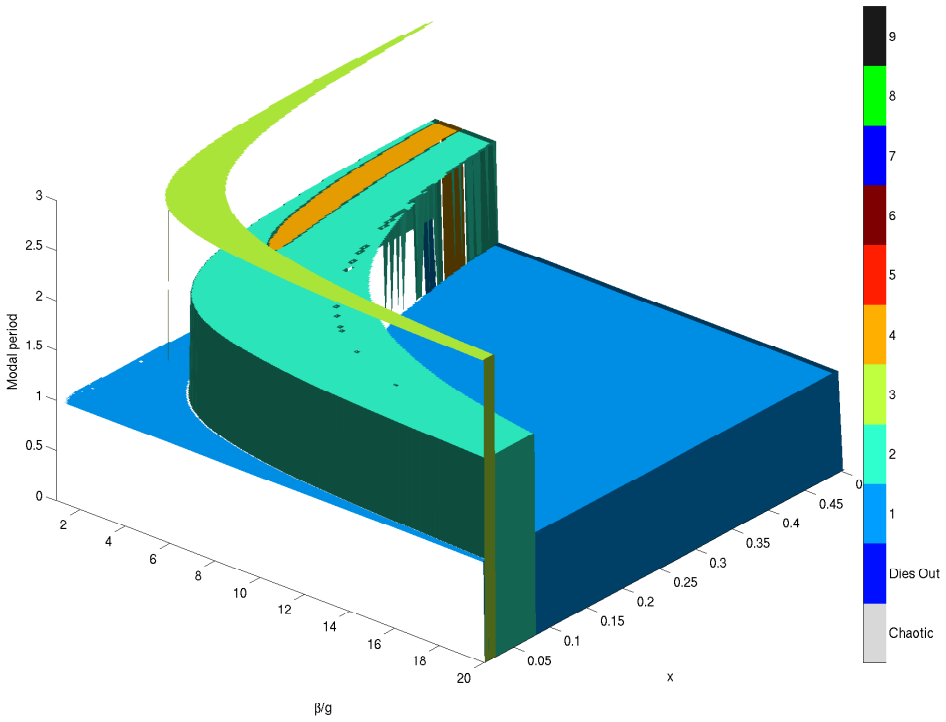

Figure 2.21: The modal frequency component on each attractor. In this case $g = 0.075$.

2.4.2 Modal frequency

When looking at the time-series in Figure 2.4 on page 30 the dynamics appear to be period two, but on closer inspection it becomes apparent that they are infect period four and the phase plane plot confirms this. So in a real system if exhibiting this kind of behaviour, what is important it that it is having a major epidemic every two years, it is not so important that the size of these major epidemics alternates slightly.

Here, to try and detect this phenomenon, the *modal frequency* component of the time-series representing one orbit around the attractors is calculated at each point in parameter space. The calculation is performed using a fast Fourier transform, and taking the largest component.

The result of calculating the modal frequency over the whole parameter space for $g = 0.075$ is shown in Figure 2.21. This shows that the only area where the modal frequency is not equal to the period is the period four region. This means that when ever period four dynamics occur they will, behave like

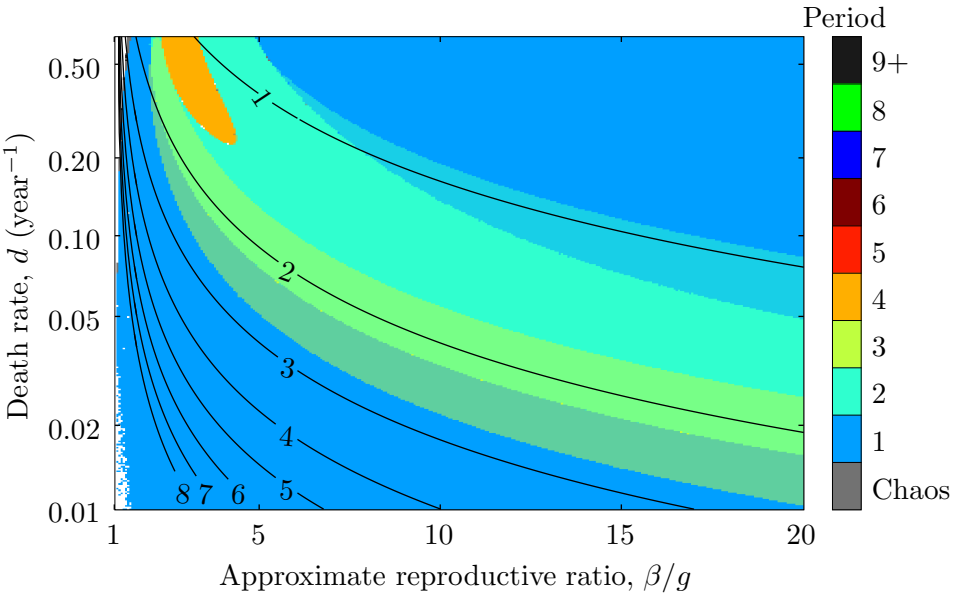

Figure 2.22: Comparison of the natural period of the un-forced standard SIR model (Equations 1.1 on page 6), and the period standard pulsed SIR model (Equations 2.1 on page 29). In this case $g = 0.075$.

period two dynamics, with a major epidemic every two years.

2.4.3 Interaction of time-scales

Another way to help elucidate the dynamics of the system is to consider the time-scales present in the system. The pulsed SIR model presented in this chapter has two inherent time-scales, the natural period of the un-forced system and the annual time-scale induced by the forcing. It is the interaction between these two time-scales that causes the complex annual and multi-annual cycles.

Figure 2.22 shows the actual period of the system, overlaid with the natural period of the system across parameter space. There is no clear correspondence between the actual and natural periods. Even in the region where the natural period is annual, and therefore equal to the period of the forcing, the two periods do not agree. Of course, it is worth bearing in mind that the natural period calculation relies on a local linearisation of the system, and this is only valid locally around the fixed point of the un-forced system. Thus this simple analysis alone cannot explain the complex multi-annual

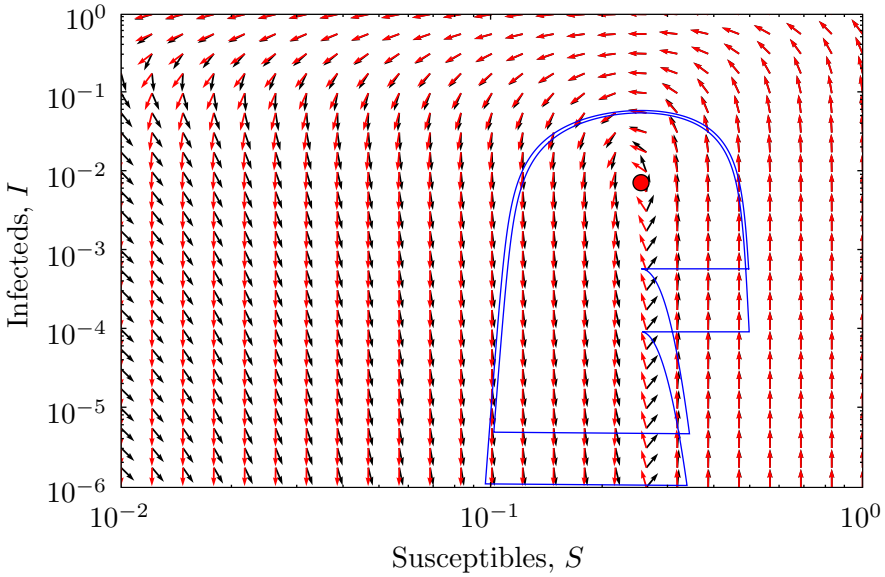

Figure 2.23: Black arrows show the vector field for the un-forced standard SIR model (Equations 1.1 on page 6) Red arrows are for the same equations, but without the birth term, which are the ODEs used in the pulsed SIR model (Equations 2.1 on page 29). The blue line shows a period four attractor of the pulsed SIR mode, and the red circle shows the endemic fixed point of the standard SIR model (with births). Parameters: $\beta/g = 4$, $x = 0.24$ and $g = 0.075$.

dynamics. Further understanding of the causes of the multi-annual dynamics is gained in Section 2.5 on page 62, where they are shown to be an example of nonlinear resonance.

Figure 2.23 shows the vector fields associated with the un-forced model (*i.e.* an SIR model with a constant death rate, but no births), and standard SIR model (*i.e.* with constant birth and death rates) overlaid with a period 4 attractor. It is proposed that the time scale of the forcing interacts with the time-scale of the underlying ODEs. For example a period one attractor exists where the continuous dynamics over a year (that is up until just before the birth pulse) map a point such that its image is in exactly the right place for the pulse to take it back to the initial point. Higher period dynamics occur when multiple years continuous dynamics and multiple pulses cause the initial point to be regained.

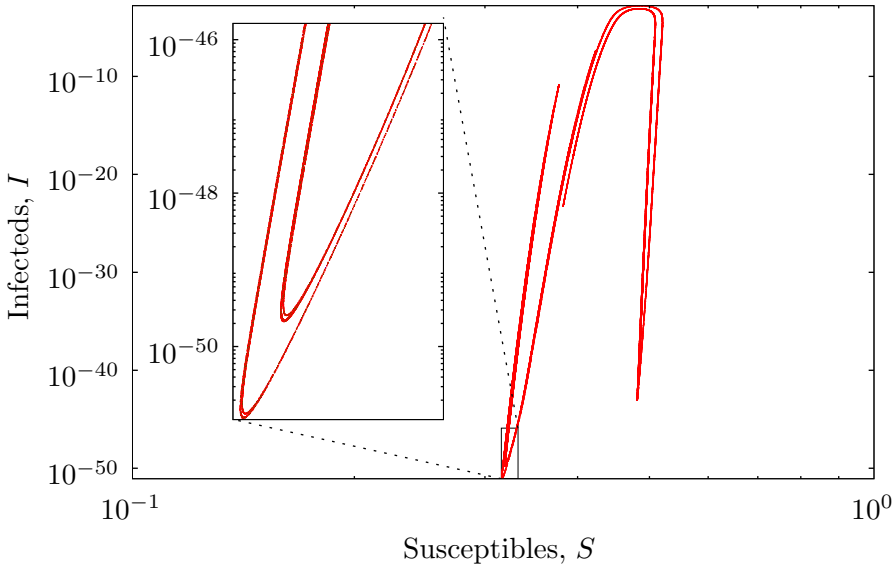

Figure 2.24: Annual points on a strange attractor for the pulsed SIR model. Parameters: $\beta/g = 4$, $x = 0.24$ and $g = 0.500$.

2.4.4 Chaotic attractors

For values of $g \geq 0.100$, the pulsed SIR model presented in this chapter has been shown to exhibit dynamics, where the period finding algorithm (Box 2.1 on page 40) was unable to determine the period of the dynamics. This subsection shows that at least some of those dynamics are indeed chaotic.

Figure 2.24 shows the distribution of annual points of a chaotic attractor, in other words the strange attractor of the annual map associated with the pulsed SIR model. Together the points form an 's' shaped curve. The insert shows one area of the curve enlarged, and it can be observed that the curve consists of two lines. In fact, enlarging again (not shown), those two curves can be seen themselves to be made of up two curves. The attractor seem to have structure on many levels. The Floquet multiplier (see Section 3.1 on page 90) for this attractor was calculated to be about 1.387 which is clearly greater than unity and hence the attractor shows strong sensitivity to initial conditions and chaos in the truest sense.

This attractor is similar to that of the Hénon map [Hitzl and Zele, 1985]. It also bear resemblance to chaotic attractor exhibited by SEIR models with sinusoidally forced transmission rates used to model childhood diseases such

as measles [Kuznetsov and Piccardi, 1994, Schaffer and Bronnikova, 2007].

2.5 Resonant effects

To investigate if the multi-annual dynamics exhibited by the standard pulsed SIR model are caused by nonlinear resonance the following analysis was undertaken, based, in part, on the techniques described by Greenman et al. [2004]. These techniques are reviewed in Section 1.8 on page 19 in the context of a sinusoidally forced transmission rate. Ireland et al. [2004] used these techniques to look at a similar model, where the births where forces sinusoidally.

The idea is to calculate the resonance response curve for a system with low levels of forcing birth term (that is using a simple step function that is low in the first half of the cycle and high in the second), which is expected to show harmonic resonance, and examine how the resonance response curve changes as the strength of the forcing increases and its temporal extent decreases. That is, the forcing function is zero for most of the cycle, and high for a short period at the end—so that it is essentially a pulse.

This transition is undertaken in two stages. Firstly, for the step function, the difference between the value in the first and second half of the cycle, which is initially small, is increased, until the point where it is zero in the first half of the year. The second part of the transition consists of narrowing the temporal extent of this function, form being zero in just the first half of a cycle, to being zero for all but a tiny fraction at the end of the cycle.

Greenman et al. [2004] take the approach of directly rescaling time by substituting $t' = pt$. However this approach causes the parameters to be rescaled too. Here instead, the period, τ, of the forcing function is varied and its magnitude adjusted to compensate. This leaves the parameters untouched avoiding confusion when comparing across different periods of forcing.

For the first part of the transition the birth forcing function is given as a step function

$$B_\delta(t) = \begin{cases} Q_\delta(1-\delta) & \text{for } t \leq \tau/2 \mod 365 \\ Q_\delta(1+\delta) & \text{for } t > \tau/2 \mod 365. \end{cases} \tag{2.6}$$

Where Q_δ is calculated so that births and deaths are balanced over the period of forcing τ, so that $N(t)$ is cyclic, with period τ. Furthermore, the

dynamics are constrained so that $N(t) = 1$ for $t = n\tau$, $n \in \mathbb{N}$. The parameter δ is varied from 0 to 1 to give the desired transition.

Lemma 2.2 *For the standard SIR model, Equations 2.1 on page 29, forced with the birth function $B_\delta(t)$ given by Equation 2.6 on the previous page, then for N to be cyclic and satisfy the condition that $N(t) = 1$ for $t = n\tau$ where $n \in \mathbb{N}$, Q_δ must be given by*

$$Q_\delta = \frac{(1+\xi)d}{(1+\xi)+\delta(1-\xi)} \qquad \text{with } \xi = e^{-d\tau/2} \ . \tag{2.7}$$

Proof: By using for birth forcing function given in Equation 2.6 on the preceding page and summing Equations 2.1 on page 29 an equation for the rate of change of the populations density is obtained:

$$\dot{N} = -dN + B_\delta(t)$$

The proof proceeds by integrating this equation, given the boundary values of N are known, and solving the resulting expression for Q_δ. There are two cases to consider, $0 < t < \tau/2$ and $\tau/2 < t < \tau$. The value of $N(\tau/2)$ is denoted by $\hat{N}$, which is then equated across both cases.

In the case $0 < t < \tau/2$

$$\dot{N} = -dN + Q(1-\delta).$$

This can be solved by separation of variables, given the constraints $N(0) = 1$ and $N(\tau/2) = \hat{N}$. Thus

$$\int_1^{\hat{N}} \frac{\mathrm{d}N}{-dN + Q_\delta(1-\delta)} = \int_0^{\frac{\tau}{2}} 1\mathrm{d}t$$

integrating yields

$$\left[-\frac{1}{d}\log\left(-dN+Q_\delta(1-\delta)\right)\right]_1^{\hat{N}} = \left[t\right]_0^{\frac{\tau}{2}}$$
$$-\frac{1}{d}\log\left(\frac{-d\hat{N}+Q_\delta(1-\delta)}{-d+Q_\delta(1-\delta)}\right) = \frac{\tau}{2}$$
$$\frac{-d\hat{N}+Q_\delta(1-\delta)}{-d+Q_\delta(1-\delta)} = e^{-\frac{d\tau}{2}}.$$

For brevity $e^{-\frac{d\tau}{2}}$ is denoted by ξ. So that

$$-d\hat{N}+Q_\delta(1-\delta) = -\xi d+\xi Q_\delta(1-\delta)$$
$$-d\hat{N} = -Q_\delta(1-\delta)-\xi d+\xi Q_\delta(1-\delta). \tag{2.8}$$

Now in the other case $\tau/2 < t < \tau$, the same procedure is followed. In this case

$$\dot{N} = -dN+Q_\delta(1+\delta).$$

Again this can be solved by separation of variables, but this time with the constraints $N(\tau/2)=\hat{N}$ and $N(\tau)=1$. Thus

$$\int_{\hat{N}}^{1}\frac{\mathrm{d}N}{-dN+Q_\delta(1+\delta)} = \int_{\frac{\tau}{2}}^{\tau}1\mathrm{d}t$$

again integrating yields

$$\left[-\frac{1}{d}\log\left(-dN+Q_\delta(1+\delta)\right)\right]_{\hat{N}}^{1} = \left[t\right]_{\frac{\tau}{2}}^{\tau}$$
$$-\frac{1}{d}\log\left(\frac{-d\hat{N}+Q_\delta(1+\delta)}{-d+Q_\delta(1+\delta)}\right) = \frac{\tau}{2}$$
$$\frac{-d+Q_\delta(1+\delta)}{-d\hat{N}+Q_\delta(1+\delta)} = e^{-\frac{d\tau}{2}}.$$

Then with ξ as before

$$-d + Q_\delta(1+\delta) = -\xi d\hat{N} + \xi Q_\delta(1+\delta).$$

Now using Equation 2.8 on the preceding page to substitute for $-d\hat{N}$ in the above, eliminating $\hat{N}$, thus making it possible to solve for Q_δ. Whence

$$\begin{aligned}
-d + Q_\delta(1+\delta) &= -\xi Q_\delta(1-\delta) - \xi^2 d + \xi^2 Q_\delta(1-\delta) + \xi Q_\delta(1+\delta) \\
d(\xi^2-1) &= Q_\delta\left[2\delta\xi + \xi^2(1-\delta) - (1-\delta)\right] \\
&= Q_\delta\left[-\delta(\xi^2 - 2\xi + 1) + \xi^2 - 1\right] \\
d(\xi-1)(\xi+1) &= Q_\delta\left[-\delta(\xi-1)^2 + (\xi-1)(\xi+1)\right],
\end{aligned}$$

finally yielding

$$Q_\delta = \frac{d(\xi+1)}{(\xi+1) + \delta(1-\xi)}$$

as required. □

For the second stage of the transition, the forcing is given by:

$$B_w(t) = \begin{cases} 0 & \text{for } t < \tau - w \mod 365 \\ Q_w & \text{for } t \geq \tau - w \mod 365. \end{cases} \tag{2.9}$$

Again w is calculated so that the total populations density N is cyclic, with period τ and $N(t) = 1$ at the start of every cycle. The parameter w is varied from $\tau/2$ to ϵ, where ϵ is small. Thus for small w the effect is similar to a pulse.

Lemma 2.3 *For the standard SIR model, Equations 2.1 on page 29, forced with the birth function $B_w(t)$ given by Equation 2.9, then in order for N to be cyclic, with period τ, and satisfy the condition $N(t) = 1$ for $t = n\tau$ where $n \in \mathbb{N}$, Q_w must be given by*

$$Q_w = \frac{(1 - e^{-d\tau})d}{1 - e^{-dw}}. \tag{2.10}$$

Proof: As in the previous lemma the proof proceeds by integrating the

equation go the rate of change of the total population density

$$\dot{N} = -dN + B_w(t),$$

over a cycle. This is split into two cases, $0 < t < \tau - w$, and $\tau - w < t < \tau$, and the resulting expressions are equated to solve for Q_w. Here $\hat{N}$ denotes the mid value $N(\tau - w)$.

In the first case where $0 < t < \tau - w$

$$\dot{N} = -dN.$$

As was done previously this can be solved by separation of variables,

$$\int_1^{\hat{N}} \frac{\mathrm{d}N}{N} = \int_0^{\tau-w} -d\mathrm{d}t \tag{2.11}$$

$$\Big[\log(N)\Big]_1^{\hat{N}} = \Big[-dt\Big]_0^{\tau-w} \tag{2.12}$$

$$\hat{N} = e^{d(\tau-w)}. \tag{2.13}$$

The second case has $\tau - w < t < \tau$, and here the equation for growth of the population is given by

$$\dot{N} = -dN + Q_w.$$

This is solved by separation of variables:

$$\left[-\frac{1}{d}\log(-dN + Q_w)\right]_{\hat{N}}^{1} = \Big[\,t\,\Big]_{\tau-w}^{\tau}$$

$$\log\left(\frac{-d\hat{N} + Q_w}{-d + Q_w}\right) = dw$$

$$-d\hat{N} + Q_w = (Q_w - d)e^{dw}.$$

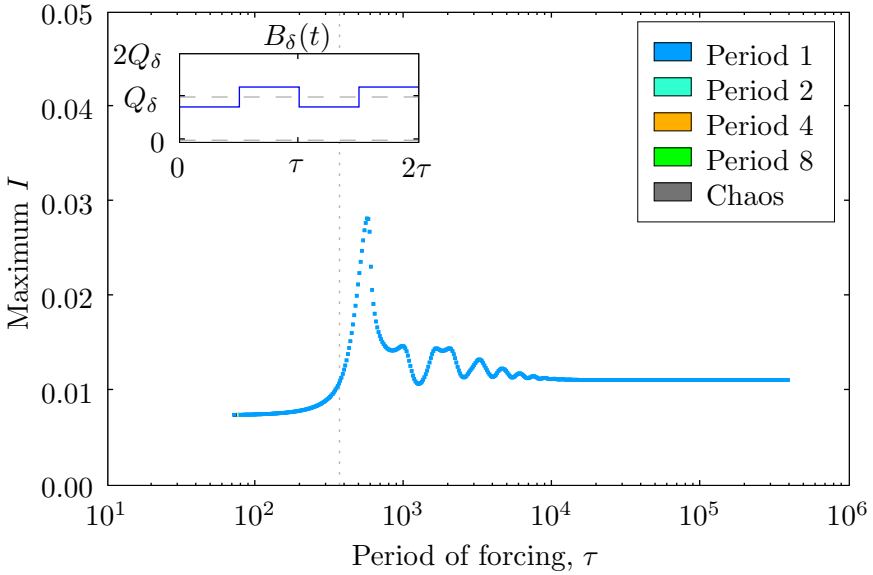

Figure 2.25: Resonance response curve of the standard SIR model, forced with the birth function $B_\delta(t)$ for $\delta = 0.23$. Parameters: $\beta/g = 4$, $d = 7.5 \times 10^{-4}$ (equivalent to $x = 0.24$ when $\tau = 365$), $g = 0.075$ and τ runs from 71 days to $\sim$1056 years. Note the scale on the vertical axis differs from the following figures.

Now substituting for $\hat{N}$ using Equation 2.13 on the previous page yields

$$\begin{aligned} -de^{-d(\tau-w)} + Q_w &= (Q_w - d)e^{dw} \\ Q_w &= \frac{d\left(e^{-d(\tau-w)} - e^{dw}\right)}{1 - e^{dw}} \\ Q_w &= \frac{d\left(1 - e^{-d\tau}\right)}{1 - e^{-dw}}. \end{aligned}$$

□

Notice that for $\delta = 1$ and $w = \tau/2$ $B_\delta(t) = B_w(t)$ for $0 \leq t < \tau$, so that the two functions coincide at the crossover point.

Snapshots of the transition are shown in Figure 2.25 to Figure 2.29 on pages 67–69 for $\delta = 0.23$, $\delta = 0.54$, $\delta = 1$ (or equivalently $w = \tau/2$), $w = 0.19$ and finally pulsed forcing. Note that only stable fixed attractors are shown, and that there may exist attractors that are not shown. This is because the

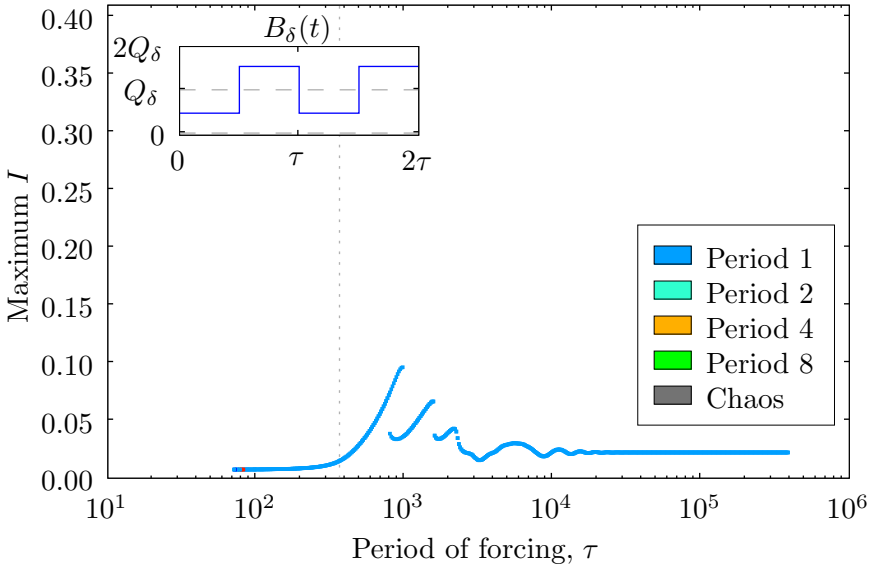

Figure 2.26: Resonance response curve of the standard SIR model, forced with the birth function $B_\delta(t)$ for $\delta = 0.78$. Other parameters as Figure 2.25

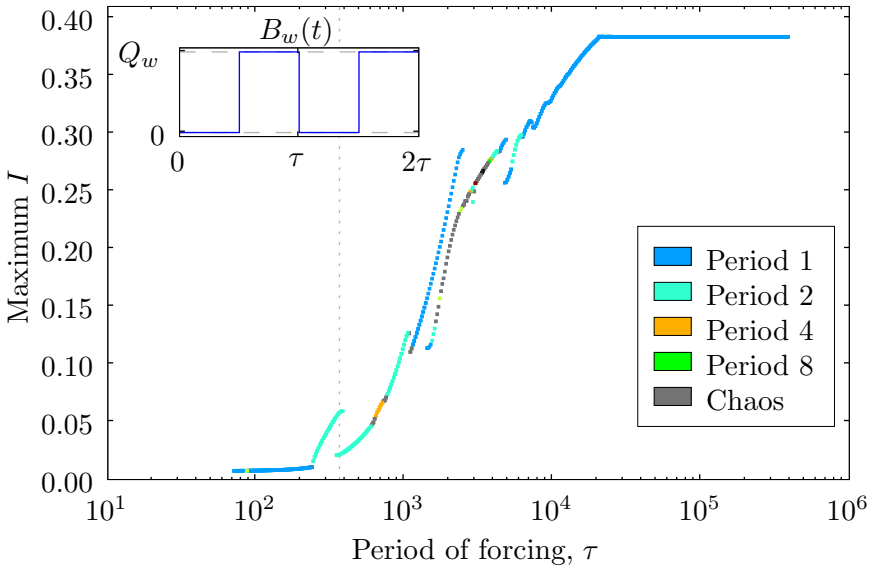

Figure 2.27: Resonance response curve of the standard SIR model, forced with the birth function $B_\delta(t)$ for $\delta = 1.0$, or equivalently using the birth function $B_w(t)$ with $w = \tau/2$. Other parameters as Figure 2.25.

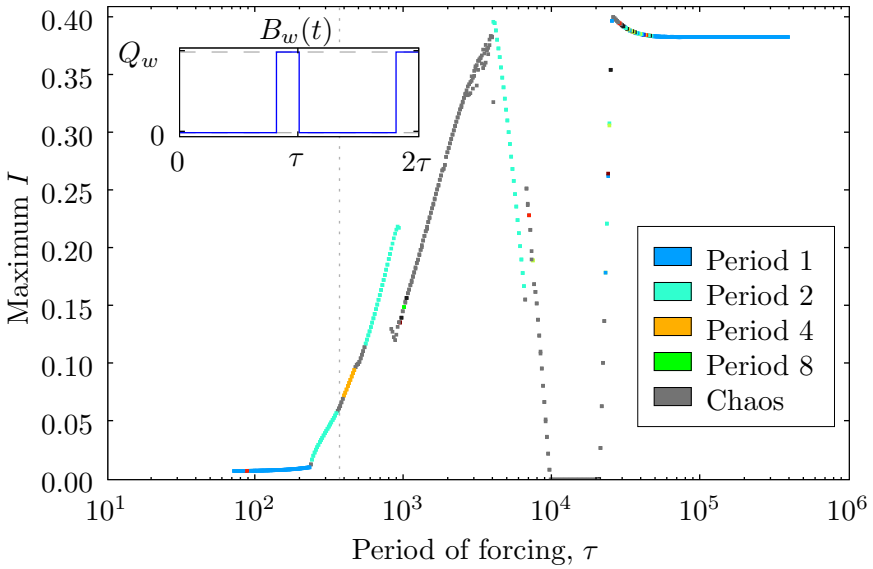

Figure 2.28: Resonance response curve of the standard SIR model, forced with the birth function $B_w(t)$ for $w = 0.19$. Other parameters as Figure 2.25.

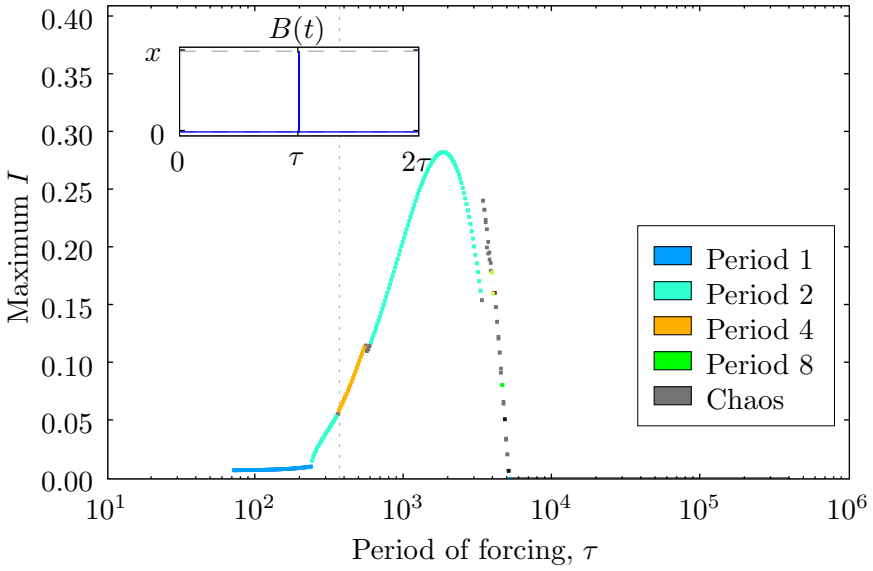

Figure 2.29: Resonance response curve for the standard pulsed SIR model pulsed forcing. Other parameters as Figure 2.25.

data was produced using two stages. The first where τ increases, and the previous fixed point is used as an initial condition, and the second where the process is repeated for τ decreasing. This means that when bifurcations occur, *i.e.* waves break and overlap, than more than one branch can be detected.

Resonance is usually associated with low levels of forcing leading to a large amplitude oscillations at certain forcing frequencies, and this is the behaviour shown in Figure 2.25 on page 67. The response is a smooth curve with the main resonant peak at $\tau \approx 550$ days, and above that there are several peaks representing subharmonics of the main peak.

As the level of forcing is increased, the resonance becomes nonlinear as illustrated in Figure 2.26 on page 68 showing the classic breaking wave formation. There are several breaks, and further subharmonics can bee seen building at the right hand side.

At the mid point of the transition, Figure 2.27 on page 68, where the crossover between B_δ and B_w occurs, the number of breaks has increased. There is more complexity and some waves now consist entirely of subharmonic oscillations. There are also large regions of chaotic dynamics.

As temporal extent of the pulse narrows, as shown in Figure 2.28 on the previous page, the number of breaks reduces. However, the region of chaotic dynamics is much larger.

Finally, when the pulse is reached at the end of the transition, shown in Figure 2.29 on the preceding page, the response curve is significantly simplified. For very short periods of forcing the dynamics are period one, but as the length of the period of forcing increases the dynamics become period two, then four and back to period two at the top of the resonant peak where $\tau \approx 2000$ days. Beyond the peak some chaotic dynamics exist. To put these results into context, the standard pulsed SIR model is normally considered with annual forcing,$\tau = 365$, this places it just on the left edge of the period four region in Figure 2.29 on the previous page.

Of course this series of results only considers one set of parameters, $\beta/g = 4$, $d = 7.5 \times 10^{-4}$ (equivalent to $x = 0.24$ when $\tau = 365$) and $g = 0.075$. In order to determine if this behaviour is typical is necessary to look at representative sample of points in parameter space. Figure 2.30 on the following page shows the resonance response curves of the standard pulsed SIR model at six extra points in parameter space, points A–F, as well as

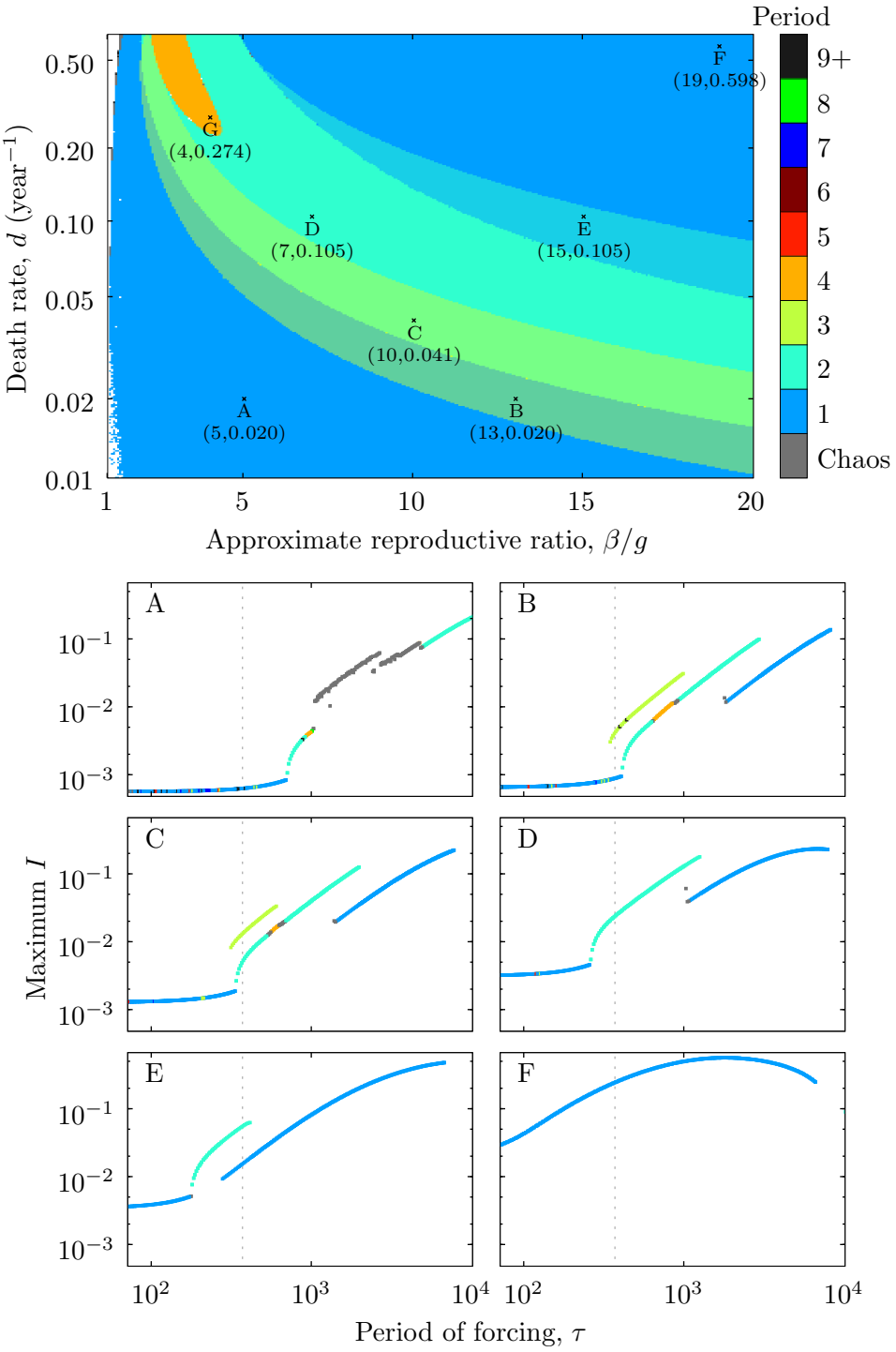

Figure 2.30: Resonance response curves of the standard pulsed SIR model for several parameter values, and long with what period attractors exits for those parameters. Here $g = 0.075$ and point G shows the location of previous figures.

what period attractors exist at each point in point. For completeness, point G shows the parameter values used in Figure 2.29 on page 69. The points cover all periods, or combinations of periods, exhibited across parameter space. Points A–E clearly show the classic breaking wave profile, and at point B,C and E, where multiple attractors coexist, the grey dashed line, representing $\tau = 365$, clearly intersects multiple waves.

This system clearly shows nonlinear resonance, for all but the smallest levels of forcing (Figure 2.25 on page 67, $\delta = 0.23$). Although, the forcing is applied to a different biological process, the results compare well to those of Greenman et al. [2004] and also those of Ireland et al. [2004]–where these techniques are applied to SIR models with sinusoidally forced birth rates. Note though that in this thesis the amplitude of the forcing is much higher. Choisy et al. [2006] also uses these techniques to look at the dynamics of an SEIR model with a seasonally forced transmission rate and pulsed vaccination. This helps to explain the existence of multiple coexisting attractors, which coincide with a breaking waves that overlap each other.

2.6 Bifurcation structure

In order understand what causes the transitions between periods as parameter space is traversed this section studies the bifurcation structure of the pulsed SIR model. The existence of unstable period one limit cycles is observed and the level of their instability shown to relate to the higher period dynamics in the same areas of parameter space.

More detailed studies of the bifurcation structure of epidemiological models have been carried out before. For example Kuznetsov and Piccardi [1994] perform a similar bifurcation analysis on the SEIR and SIR models, but with sinusoidally forced transmission rate. Their analysis was performed over a two dimensional parameter space spanned by the mean transmission rate and the degree of seasonality in the transmission rate. A similar study on this model was also conducted by Schaffer and Bronnikova [2007] and again by Greenman et al. [2004]. However, a review of the literature found no work to have been done on the pulsed SIR model as presented here.

2.6.1 Bifurcation plots

In order to analyse the structure of the bifurcations in a meaningful way rather than look at the whole two dimensional parameter space the analysis is restricted to a one dimensional path though parameter space, where one of the parameters is fixed and the other varies. In the two cases considered the death rate d—and therefore the size of the birth pulse—is fixed and the transmission rate β is varied. As in previous sections, the axes are scaled so that β/g—which is approximately the basic reproductive ratio for the pulsed SIR model is shown as it is gives more meaningful numbers. The bifurcation plots below show the value of S at each attractors fixed points. The Floquet multipliers of the attractor are also shown. The calculations of the Floquet multipliers is explained in Section 3.1 on page 90.

Figure 2.31 on the following page shows a bifurcation plot for $g = 0.075$, which equates to an infectious period of about two weeks. The path though parameter space, illustrated in Figure 2.32 on page 75, is chosen to cross all the regions of different periods exhibited for $g = 0.075$. Starting on the left there is only period one present, this then under goes a period doubling bifurcation to become period two. Another period doubling bifurcation follows to give the period four dynamics. Moving further right the second period doubling is reversed. and the dynamics return to period two. Around $\beta/g = 5.5$ the region where period one and two overlap is reached, which is unfortunately quite narrow here. It is clear that as the overlap is approached the Floquet multipliers of the period two attractor become real and then one quickly goes to zero while the other tends to one so that the attractor becomes unstable. Approaching the overlap from the right hand distinct period one attractor goes unstable because the larger of its two real Floquet multipliers exceeds unity. The period three attractors that exist for $\beta/g \in [2, 2.5]$ seem to be distinct from the main group of attractors. They cease to exist, on both the left and the right when the Floquet multipliers become real and tend to one and zero.

Similarly Figure 2.33 on page 76 shows a bifurcation plot for $g = 0.100$, the path of which is illustrated in Figure 2.34 on page 77. The structure is much more complex in this case, and is not described in as much detail as for $g = 0.075$. The series of period doubling bifurcations that caused the period 1-2-4-1 sequence seen for $g = 0.075$ has be come much more complex. A period doubling cascade is seen and chaos results. For clarity

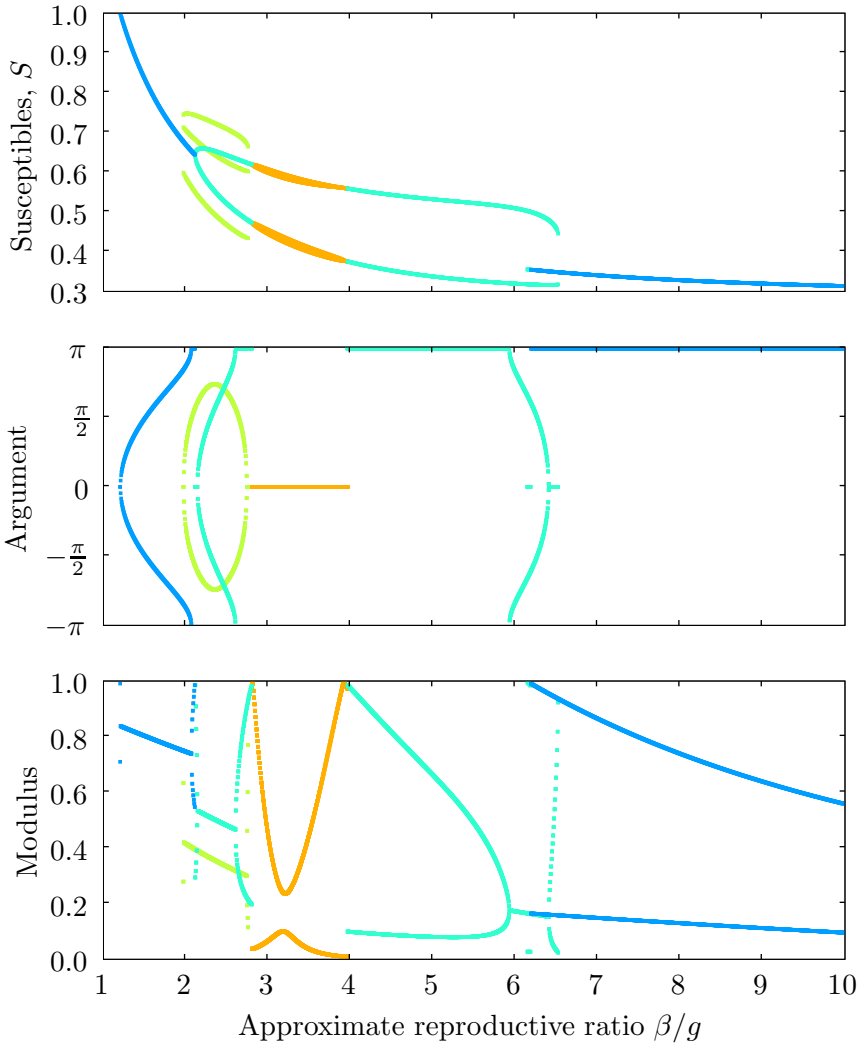

Figure 2.31: Bifurcation plot of the pulsed SIR model with $g = 0.075$, $x = 0.385$, $d = 0.486$, $\beta/g \in [0.98, 9.98]$, this path is illustrated in Figure 2.32 on the next page. The top plot shows S at the annual fixed points of the attractors. The lower two plots show the attractors Floquet multipliers.

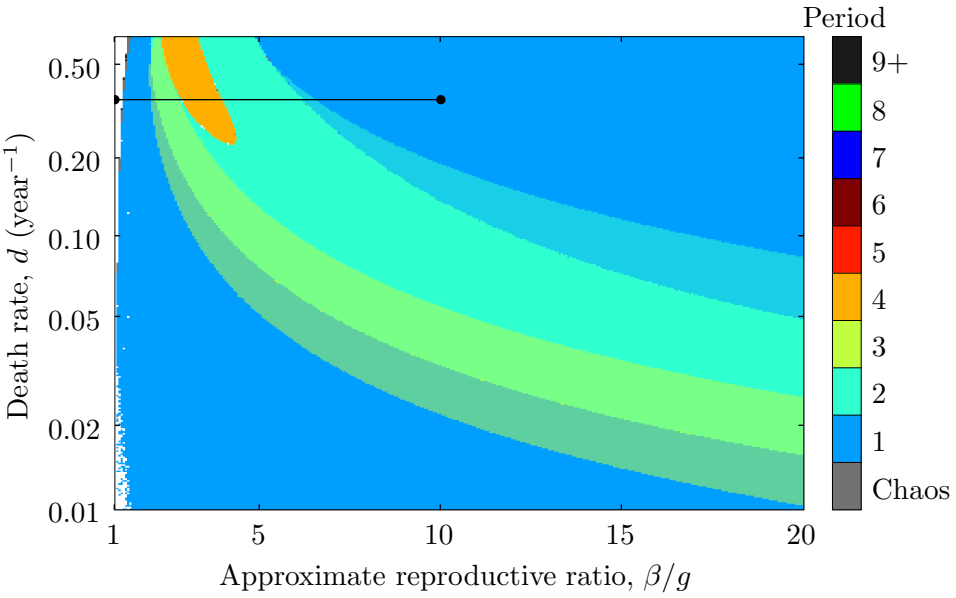

Figure 2.32: Path taken though parameter space by Figure 2.31 on the previous page—shown as a horizontal black line.

the chaotic points are omitted, as they would obscure the period three dynamics. Similarly the isolated period three attractor is now split with a period doubling cascade in between.

In the case $g = 0.075$ it has been verified that the same kinds of bifurcations as those shown in Figure 2.31 on the preceding page occur all the way along the given boundaries.

The biological interpretation of this structure comes from considering a population-pathogen combination with parameters that lie close to a bifurcation. Then, if some change occurs to the population, say for example the area occupied by the population is reduced for some reason, then this would increase the contact rate, and increase β. Equally a change could occur to the host or the pathogen, it might mutate, for example, or a change in climatic conditions may make it more easily transmitted. Either way it is conceivable that this change could vary one of the parameters, so that the population-pathogen combination resided in a region of parameter space with a different periodicity. The bifurcation analysis shows what effect this may have. If the move is across a period doubling bifurcation, where the period goes from two to four, then little noticeable change may result because the

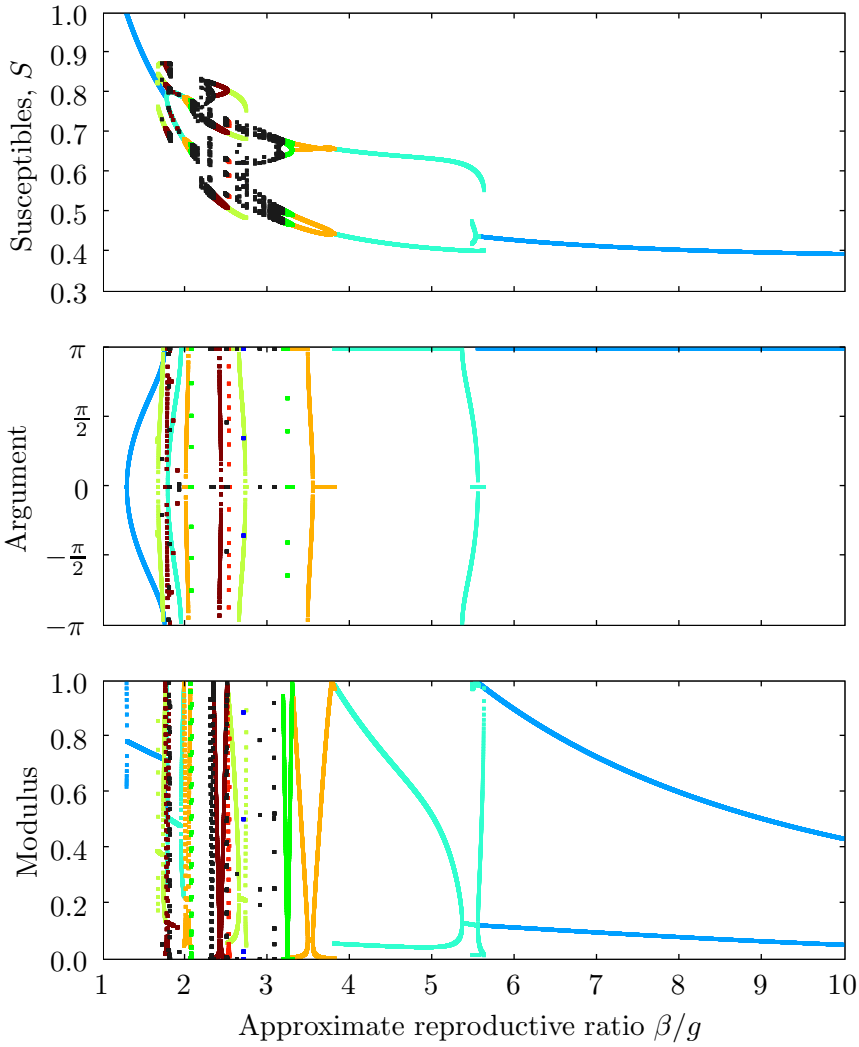

Figure 2.33: Bifurcation plot of the pulsed SIR model with $g = 0.100$, $x = 0.297$, $d = 0.352$, $\beta/g \in [0.98, 9.98]$, this path is illustrated in Figure 2.34 on the next page. The top plot shows S at the annual fixed points of the attractors. The lower two plots show the attractors Floquet multipliers.

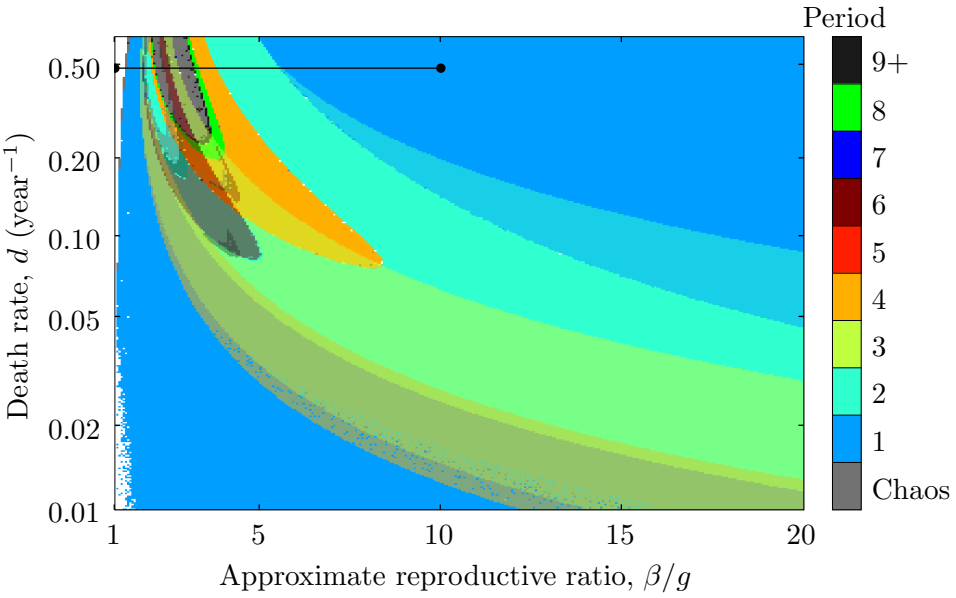

Figure 2.34: Path taken though parameter space by Figure 2.33 on the previous page—shown as a horizontal black line.

period four attractor has fixed points that lie close to those of the period two attractor. Hence the resulting pattern of epidemics will remain very similar (this is discussed in more detail in Section 2.4 on page 53). However, if the change in parameters causes the parameters to shift in such away that the attractor the system was sitting on became unstable the observed disease dynamics could change greatly.

2.6.2 Basins of attraction

When multiple attractors coexist at a point in parameter space it is not obvious which, if any, attractor would be most likely manifest itself when the model is applied to a real biological system. Studying the basin of attraction at the relevant point in parameter space is one way to try to answer this question. They can also help to understand how the model may respond to large perturbations. The modified brute force algorithm used to determine the basins of attraction is described in Box 2.5 on page 79.

Figure 2.35 on the next page shows the basin of attraction for the standard pulsed SIR model with $R_0 = 5$, $x = 0.1$ and $g = 0.075$. Note that this is the basin of attraction for $t = n\tau$, $n \in \mathbb{N}$. That is, it shows what

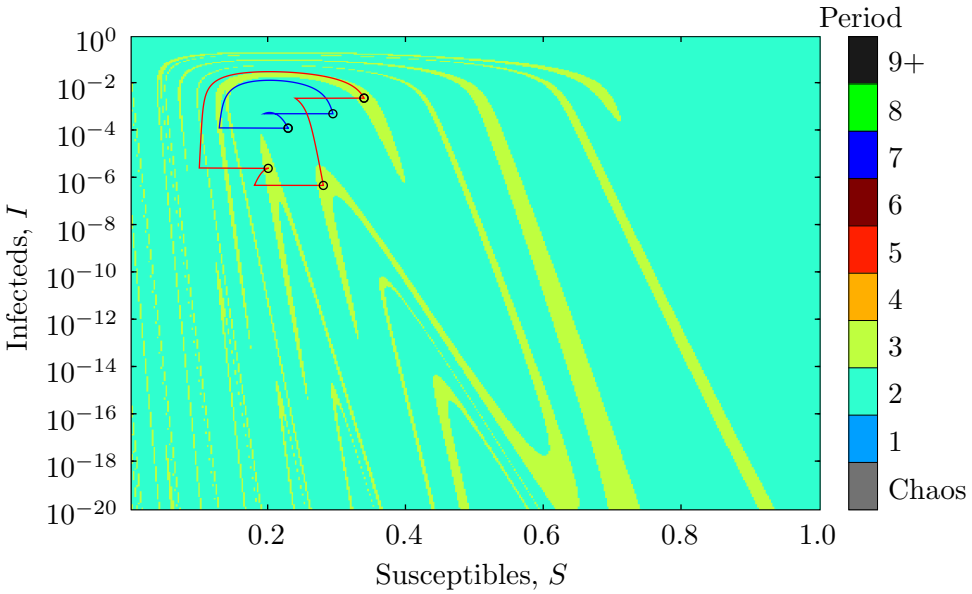

Figure 2.35: The basin of attraction of the pulsed SIR model for $t = n\tau$, $n \in \mathbb{N}$. overlaid with the attractors to which points converge. The red line shows the period three attractor, and the blue line the period two. The annual fixed points of the attractors are marked with black circles. Parameters $R_0 = 5$, $x = 0.1$, $g = 0.075$.

period attractor a point started at $t = n\tau$, $n \in \mathbb{N}$ will converge to. This is because of the seasonal forcing. Alternatively it could be thought of as the basin of attraction of the annual map.

At this point in parameter space two attractors coexist: period two and period three. It is clear from the figure that most points are in the basin of the period two attractor. The basin of the period three attractor is much smaller. Thus it is quite likely that if a trajectory on the period three attractor were to receive large perturbation then it may get pushed into the basin of the period two attractor.

This also explains why the un-pushed out data shown in Figure 2.8 on page 44 shows very little of the period three region.

It is clear that the structure is very complicated, the basins for period two and three are intertwined in a complex way. Concentrating on a smaller area, say the bottom left corner of Figure 2.35, and looking using a higher resolution, shows that same kind of pattern, but on a smaller scale. These two factors, suggest that the basin may in fact have fractal boundaries [Ott,

2002]. Using fractal terminology [Mandelbrot, 1977], the basin has detail on every scale, and is self similar. This opens up the possibility of using algorithms developed for use with fractals to reduce the computational effort required to determine basins of attraction such as illustrated in Figure 2.35.

2.5 Calculating basins of attraction

A simple algorithm to calculate the basins of a attraction is a brute force approach, that is, given a grid over state space, use each point as an initial condition for the system and calculate the period of the attractor to which the trajectory converges, using the algorithm described in Box 2.1 on page 40. This is a very computationally intensive algorithm. A significant improvement to this algorithm can be made, without significant increase in complexity, by assuming that the annual points of all possible attractors is known for the parameter values in question. Given this knowledge, rather than continuing to integrate each point in the state space grid until it converges to an attractor, it is only necessary to integrate forward until the point is close to one of the know attractors. More specifically, with each year forward the trajectory is integrated it is compared to each of the annual points of the known attractors, using the method described in Box 2.2 on page 43. If a trajectory is found to be close to a particular attractor then its starting point is classified as being in the basin of that attractor. In fact it is not necessary to have the list of attractors in advance, it can be compiled as points converge to attractors not on the list.

This technique saves a great deal of computational effort, especially in regions where trajectories are slow to converge to periodic orbits.

2.6.3 Unstable limit cycles

An examination of the bifurcation diagram for $g = 0.075$ (Figure 2.31 on page 74) and in particular the two disjoint regions of period one fixed points suggests that these may lie on the same curve and that in the gap there may exist unstable annual fixed points. This subsection calculates the location of these unstable fixed points and analyses their stability.

Calculations show that unstable period one limit cycles exits in the whole of the region between the upper and lower regions of period attractors

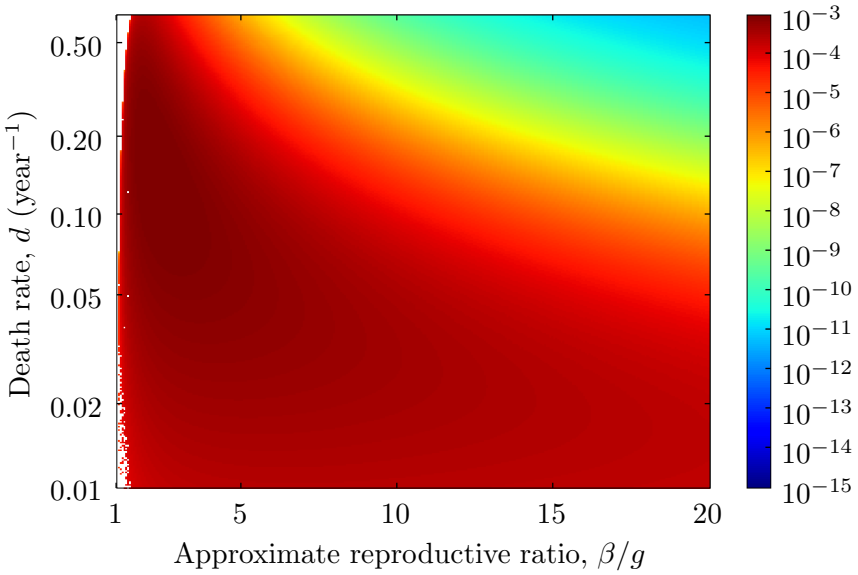

Figure 2.36: I values of stable and unstable fixed points of the Poincaré map for $g = 0.075$.

(*cf.* Figure 2.14 on page 54). The algorithm used locate these unstable fixed points, which is explained in detail in Box 2.6 on page 84, uses a brute force approach: calculating the position after one year of a grid of fixed initial conditions and seeing which point was closest to its starting point. If this point is indeed close to its starting point, then it approximates the stationary point.

The I values, at the annual fixed point, of the unstable period one limit cycles are illustrated in Figure 2.36. There is a clear continuous variation in I across from the stable to unstable and back to the stable again, to the point that it is practically impossible to distinguish the two regions. Figure 2.37 on the following page shows the same data for $g = 0.100$, again there is a smooth transition in I.

Since the locations of the unstable fixed points calculated above are only an approximation, it is wise to consider how good an approximation they are to the real fixed points. However, the real fixed point cannot be calculated directly to compare it with. Instead the distance between a point and its image after one year is calculated using the distance function described in Box 2.2 on page 43. It is worth remembering that even the locations of the stable fixed points are only approximations because they are

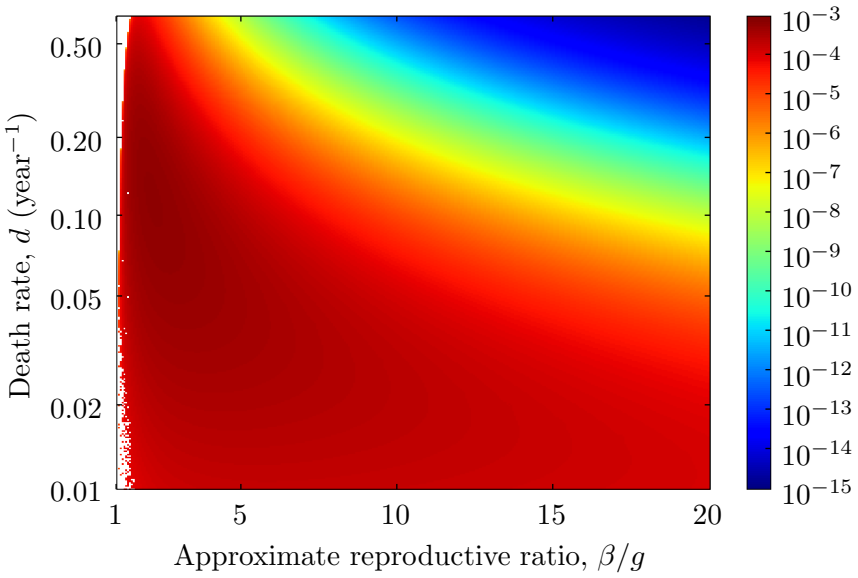

Figure 2.37: I values of stable and unstable fixed points of the Poincaré map for $g = 0.100$

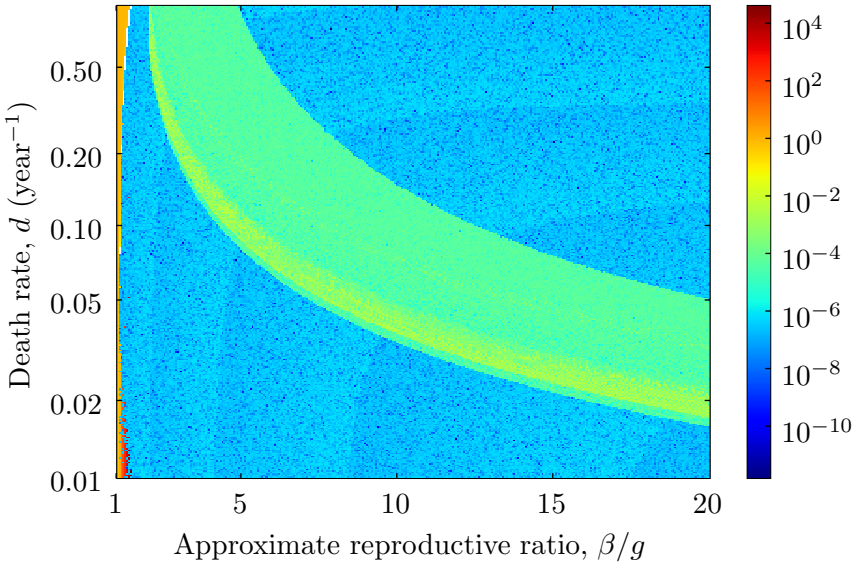

Figure 2.38: Distance between approximated stable and unstable fixed points and and their images under the Poincaré map for $g = 0.075$. Distance is measured as described in Box 2.2 on page 43.

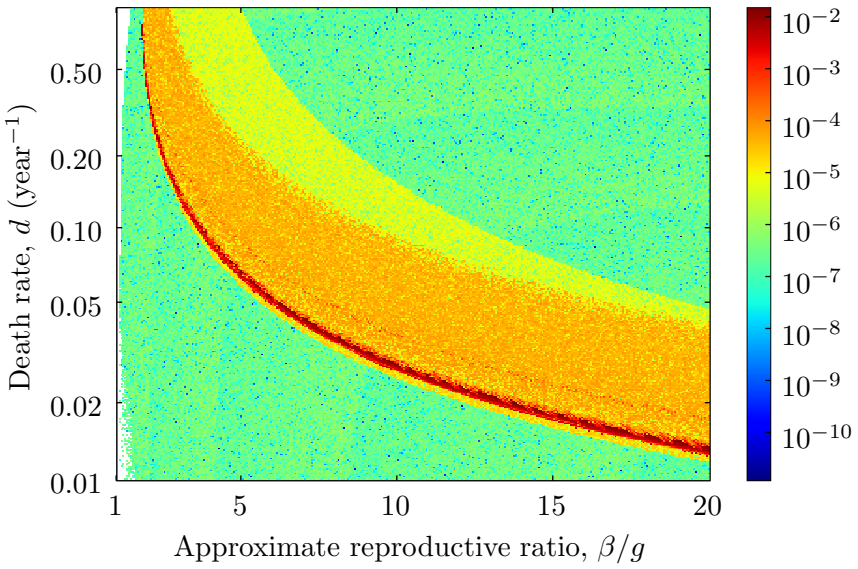

Figure 2.39: Distance between approximated stable and unstable fixed points and their image under the Poincaré map for $g = 0.100$. Distance is measured as described in Box 2.2 on page 43.

calculated numerically using Runge-Kutta, which is essentially a discrete approximations to the system (see Subsection 2.2.1 on page 35), thus the same calculation is made for the stable fixed points too. Figure 2.38 on the previous page and Figure 2.39 show the results for $g = 0.075$ and $g = 0.100$ respectively. This time there is a clear distinction between the stable and unstable regions. In the case $g = 0.075$ the distance is about 10^{-2}–10^{-3} in the unstable region and 10^{-6}–10^{-8} and in the stable region. For $g = 0.100$, the distance is larger, 10^{-2}–10^{-5} in the unstable region and 10^{-6}–10^{-7} for the stable region. Both cases share the feature that towards the lower edge the error increases, especially in the case $g = 0.100$. It was this region that required multiple passes when calculating the unstable fixed points.

The brute force method was chosen, as it is despite its inefficiency more robust. It also avoids the possibility of a minimisation algorithm converging on a local minimum. However, with hindsight, this would not have been a problem and trials of a minimisation algorithm (as discussed in Subsection 2.2.2 on page 37) gave accurate results with minimal computational effort. This may also alleviate the need for a second pass. This would very much reduce the computational effort required to calculate the unstable limit

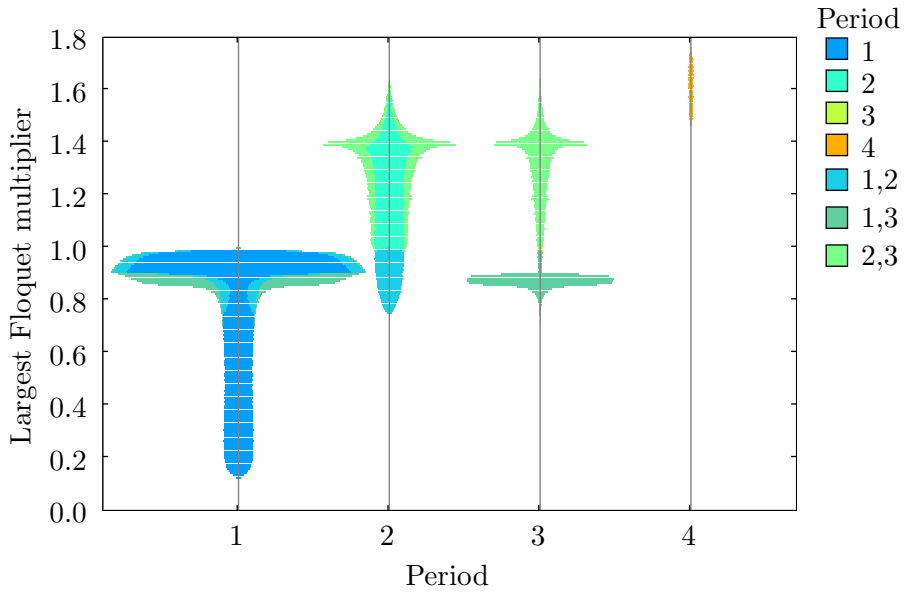

Figure 2.40: How the Floquet multipliers of the period one limit cycles, both stable and unstable, are spread over the regions of parameter space exhibiting different period attractors, for $g = 0.075$. The histogram for each period shows the distribution of the Floquet multipliers of the period one limit cycles (both stable and unstable) that exist in the regions of parameter space where stable attractors of that period exist. Moreover, each histogram is stacked—ordered by increasing period—to show what other periods overlap that period.

cycles, as well as potentially offering greater accuracy. Also it would be more feasible to look for unstable limit cycle of higher periods.

In order to calculate the level of instability of each unstable limit cycle their Floquet multipliers where calculated along with those for the stable period one attractors (see Section 3.1 on page 90 for an explanation of Floquet multipliers, and the algorithm used to calculate them). It is interesting to note that there is a correlation between the Floquet multipliers of the period one limit cycles and the period of stable attractors that existing across parameter space. The general trend is that the higher period dynamics exist where the Floquet multipliers, of the unstable period one limit cycles, are largest. This means that the level of instability of the unstable period one limit cycle in some way predicts the complexity of the stable dynamics

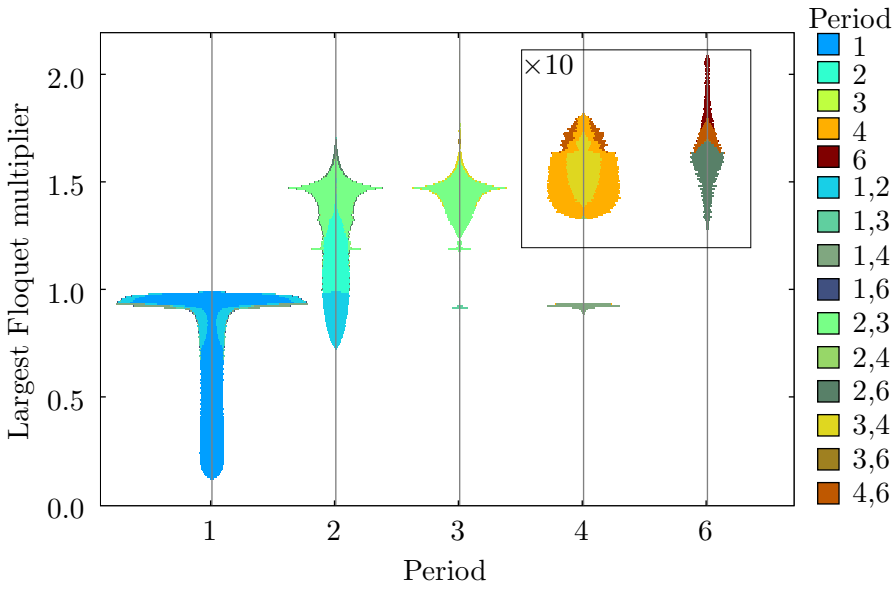

Figure 2.41: How the Floquet multipliers of the period one limit cycles, both stable and unstable, are spread over the regions of parameter space exhibiting different period attractors, for $g = 0.100$. The area in the black box has had the frequency scaled by a factor of ten for clarity. See the caption of Figure 2.40 on the previous page for a fuller explanation.

exhibited in that region. More work may be required to fully understand the implications of this trend, however it is conjectured that the period one dynamics, both stable and unstable, provide a baseline for the behaviour at each point in parameter space.

2.6 Finding unstable fixed points

It is obvious that unstable fixed points cannot be found in the same way as their stable counterparts, that is using forward integration. Instead they can be approximated as follows. Consider a grid over state space, each point is iterated forward for p years, where p is the period of unstable limit cycle being sought, the points that are 'closest' to their original position can be considered good approximations to the stationary points.

It is possible to increase the efficiency of the algorithm by using similar techniques to that of Box 2.3 on page 49. Knowledge of the position of

stationary points for nearby parameters allows the use of a finer grid, covering a smaller range of initial conditions, centred around the nearby point. This of course assumes that the position of the fixed points, locally at least, depends continuously on the parameters. To ensure that the fixed point does not lie just outside the grid a series of shifts are performed, if necessary, to centre the minimum within the gird. To increase the precision the centre of the grid is then refined. The process of shifts and refinements in continued until the desired precision is achieved. However, a stopping criterion is added in the form of a maximal number of shifts and refinements, so an infinite loop is not created. In the case this limit is reached the algorithm is considered to have failed to find an unstable fixed point at that location in parameter space.

The extent and resolution of the grid had to be tuned, as well as the maximum number of shifts and refinements to make the most efficient use of CPU time and to provide the most reliable results.

It was necessary to perform a second pass, pushing out from the new unstable region back towards the old stable region in order to fill in points where the first pass failed to find unstable fixed points. The reason for this is not well understood, but it is conjectured that it is due to a larger instability in that region of parameter space.

Perhaps these issues could be avoided by the use of a minimisation algorithm, as discussed in Subsection 2.2.2 on page 37, this would be much more computationally efficient, and would offer potentially higher accuracy, though at the cost of being less robust. This come from the fact that a minimisation algorithm can converge to a local minimum, if not given an initial condition close to the solution.

2.7 Conclusions

After a review of the literature it was found that little work had been carried out to address the inaccuracy of the modelling seasonally varying birth rates. It was noted that many animal populations have highly seasonal birth rates. Some, such as Saiga antelope, showing such tight reproductive synchrony that all mothers in a breeding group give birth in a matter of several days. A simple way to model this kind of behaviour was chosen: an annual birth pulse.

The pulsed SIR model was introduced in Section 2.1 on page 29. Although a relatively simple model, the combination of strong seasonal forcing and a nonlinear transmission term necessitated the use of numerical methods. The numerical methods where shown to be robust (Subsection 2.2.1 on page 35)

A biologically reasonable parameter space was chosen and the model was shown to exhibit periodic attractors in the region where $R_0 > 1$. Numerical methods where developed to determine the periodicity of these attractors. It was noted that in some areas of parameter space multiple attractors coexist and the method of "pushing out" was developed, based on a predictor-corrector algorithm, to ascertain their extent (Box 2.3 on page 49).

For a long infectious period ($g = 0.075$), the pulsed birth model exhibited dynamics of period one, two, three and four (Figure 2.14 on page 54). For shorter infectious periods the dynamics become more complex with higher period dynamics and chaos being observed. It is noted that, as the infectious period is decreased (increasing g), the transmission rate β is also increased, so that the approximate reproductive ratio β/g is kept constant, so as to make the results for different values of g more comparable. One chaotic attractor was studied in more detail in Subsection 2.4.4 on page 61.

Various properties of the attractors where calculated in Section 2.4 on page 53. The modal frequency was calculated, explaining why some period four attractors look very much like those of period two. Also the minimal level of infecteds on each attractor was calculated throughout parameter space showing that some areas show a high risk of disease extinction due to very low levels of infection.

The penultimate section investigates coexisting attractors in the context of resonance. Starting by looking at a modified model with lower levels of forcing and showing how the resonance response curve varies as the magnitude of the forcing is increased show a transition from a single peak, to the classic breaking wave profile of nonlinear resonance. By then looking at a representative sample of points across parameter space it is shown that nonlinear resonance occurs throughout parameter space. Moreover the overlaps in the breaking waves correspond to coexisting attractors. This provides a much greater level of understanding into the causes of the multi-annual dynamics, and coexisting attractors observed for this system.

The final section addressed the bifurcation structure present, showing that chaos ensues after a cascade of period doubling bifurcations. This

section also looked at the basins of attraction as a tool to predict the most likely of two coexisting attractors to manifest its self in an application of the model. The last subsection exposed the existence of unstable period one limit cycles in the regions of parameter space where $R_0 > 1$ and stable period one attractors do not exist. Increases in the Floquet multipliers of these period one attractors, both stable and unstable, were found to broadly correlate to increases in the periodicity of coexisting stable attractors in that region.

Further work in the analysis of this model could include a tracking of more unstable attractors as well a more details bifurcation analysis. One of the most important issues that needs to be addressed is the ability to distinguish coexisting attractors of the same period. Also the period finding algorithm described in Box 2.1 on page 40 does have its shortcomings, for example the slow convergence in some regions of parameter space and the fact that this technique only finds stable periodic orbits. These issues could be addressed by using some of the other algorithms discussed in Subsection 2.2.2 on page 37, for example using a minimisation algorithm to locate periodic orbits would allow the unstable attractors to be found by the same process as stable ones. While this approach offers the potential for a great reduction in the computational effort required, it is perhaps not as robust as the direct integration method described in Box 2.1 on page 40.

There are also perhaps improvements to be gained by the use of a more advanced numerical integration routine than the forth order Runge-Kutta employed. In a similar vein more sophistication could be added to the predictor-corrector algorithm used in pushing out. That is, investigating the possibly using a minimisation method for the corrector step, and a higher order extrapolation for the predictor.

In conclusion the addition of strong seasonal forcing, to a model with known simple behaviour, leads to very complex behaviour, especially for short infectious periods (large g). It is worth noting that biologically this is a very simplistic model, yet despite that it still shows the complex, even chaotic dynamics. Some of the other results have great biological significance, for example, the results of the minimum I calculation show there is a real chance of stochastic effects causing extinctions in real scenarios. Similarly the modal period results show that the observed frequency of epidemics could

be different from the actual period of the dynamics. However, the prediction of multi-annual cycles matches that observed in the real populations. There is much potential for the use of pulsed birth SIR models in modelling wildlife diseases.

Chapter 3

Robustness

The previous chapter focused on the behaviour of one particular model over a range of parameters. It is natural to ask how these qualitative results extend beyond the particular model considered, and to investigate, in a broad sense, their robustness. In order make these results useful, it is important to show that these results are robust. All models are, by their very nature, approximations to real systems thus if this model is to be applied to real world systems, it is important to show that similar models also display similar dynamics.

This chapter begins by assessing the stability of the pulsed SIR model with respect to small perturbations in S-I-space. This is achieved by calculating the Floquet multipliers of the attractors in order to determine the linear stability with respect to small perturbations.

The next section in this chapter determines how sensitive the results are to the function used to model the births. The results from using several different birth functions are examined and compared to the birth pulse introduced in Chapter 2.

The standard SIR model is often adapted in many ways to model different scenarios. The third section of this chapter investigates how robust the results of the previous chapter are to these changes in the structure and underlying assumptions of the model.

3.1 Small perturbations

To look at how stable the attractors found in Section 2.3 on page 46 are with respect to small perturbations their Floquet multipliers where calculated. The method is similar to that used in Shulgin et al. [1998]. In order to take the forcing into account it is necessary to consider the eigenvalues of the annual map linearised about its fixed point—these are the Floquet multipiers of the attractor. The annual map is given by

$$\Phi_\tau(S_0, I_0) = \begin{pmatrix} S_0 + x \\ I_0 \end{pmatrix} + \int_0^\tau \begin{pmatrix} \dot{S(t)} \\ \dot{I(t)} \end{pmatrix} \mathrm{d}t$$

where $S(0) = S_0$ and $I(0) = I_0$. As there is no closed form for this map, the calculation must be performed numerically. This is achieved by augmenting the system (Equations 2.1 on page 29) with two extra equations

$$\frac{\mathrm{d}}{\mathrm{d}t}\begin{pmatrix} e \\ f \end{pmatrix} = J\begin{pmatrix} e \\ f \end{pmatrix}$$

where J is the Jacobian of the S and I equations:

$$J = \begin{pmatrix} -\beta I - d & -\beta S \\ \beta I & \beta S - d - g \end{pmatrix}.$$

e and f approximate how small perturbations, in S and I respectively, evolve around an attractor. This augmented system is now used to evaluate the fundamental matrix of the system.

Now assume that S and I are on an attractor, at an annual fixed point, and set $e = 1$ and $f = 0$. Then run this four variable system forward once round the attractor. The resulting values form the first column of the fundamental matrix. The second column is formed in the same way but taking $e = 0$ and $f = 1$ initially. This matrix is (up to numerical error) the Jacobian of the annual map $\Phi_\tau(S_0, I_0)$.

The eigenvalue of this matrix with the largest real part then gives a measure of how stable this attractor is with respect to small perturbations. The result of calculating this value across all known attractors in parameter space, for $g = 0.075$, is displayed in Figure 3.1 on the following page. It is clear that there is a significant proportion of the parameter space where the attractors are only "weakly" stable (values close to one). This explains why

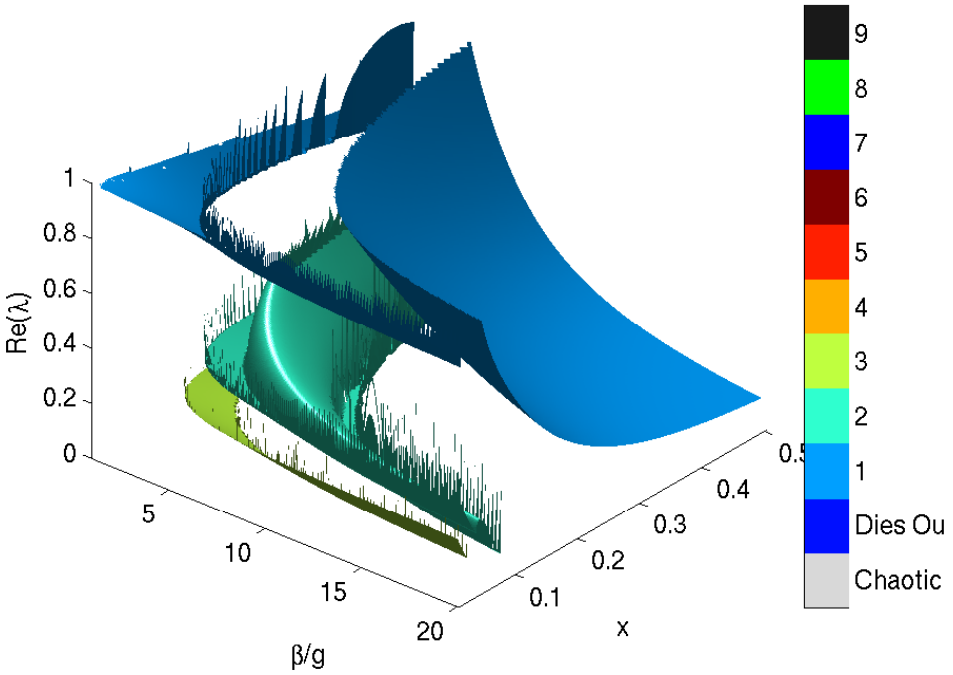

Figure 3.1: How the real part of the largest eigenvalue of the annual map varies across parameter space. In this case $g = 0.075$.

finding the attractor numerically has such a high computational cost, as it can take many years to converge towards the attractor. Biologically this means that small changes in S and I may completely change the behaviour of an epidemic, and it will show greater transient dynamics when perturbed from the attractor. Consequently, if the system is displaced from the attractor, it will take much longer to get back and if there are many small displacements the trajectory may not stay close to the attractor at all. Conversely, in the areas where the attractors are more strongly attracting the dynamics will be more predictable as any small perturbations will be quickly be damped and the dynamics will settle back towards the attractor.

Figure 3.2 on the next page shows typical dynamics for a trajectory perturbed from a period 1 attractor. As it converges back towards the attractor, the annual points cycle round the fixed point in a cycle of period 7, so that after 7 years it is very close to where it started. This can confuse the period finding algorithm, and explains why some of the speckling found

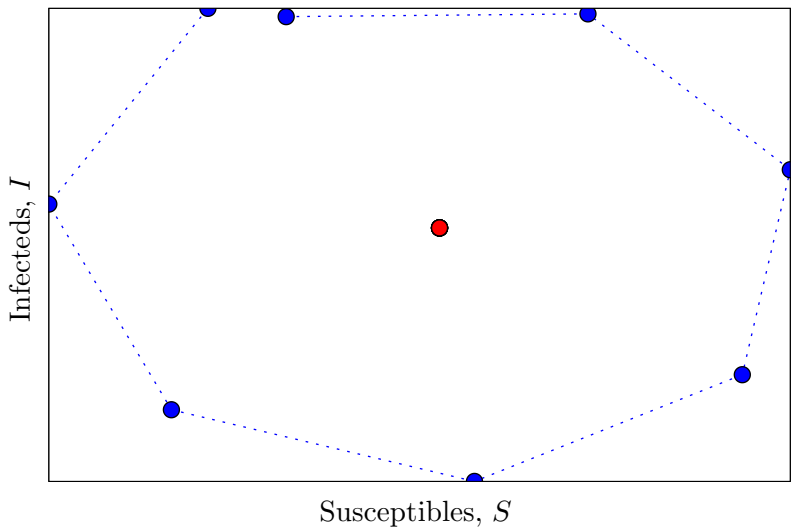

Figure 3.2: An example of the kind of slow convergence that the pulsed SIR model exhibits for small d and small R_0. The central point (red circle) is the annual fixed point of a period one attractor. The blue circles show the annual points of a trajectory that was perturbed away from the attractor. They converge towards the fixed point in a period 7 like manner.

in the small d, low R_0 region (see for example Figure 2.14 on page 54).

3.2 Change in pulse function

Although a birth pulse is, for certain populations, more true to life than a constant birth rate, it is still an unrealistic assumption that all the births within a given animal population arrive on the same day. Even very tightly grouped births occur on a time scale of about a week (*e.g.* Saiga Antelope, Milner-Gulland [2001]). Some births may be spread over several months [Berger and Cain, 1999, Clinchy, 1999, Clinchy et al., 2004]. This section explores the robustness of the results of Section 2.3 on page 46 with respect to the manner in which births are added to the population. The aim is to discover to what extent those results depend on the nature of the birth pulse. Several different ways of adding seasonal births are investigated:

- sinusoidally varying birth rate,

- a top hat function,
- a smoothed top hat function.

The results are compared to the original birth pulse.

The following system was considered:

$$\begin{aligned} \dot{S} &= -\beta SI - dS + B(t) \\ \dot{I} &= +\beta SI - dI - gI \\ \dot{R} &= -dR + gI. \end{aligned} \tag{3.1}$$

for several different birth pulse functions B.

3.2.1 Sinusoidal forcing

A common choice for a forcing function in mathematics is the sine function [Dietz, 1976, Smith, 1983], so it seems apt to consider this as a forcing function. Ireland, Norman, and Greenman [2004], Ireland, Mestel, and Norman [2007] apply this type of forcing to the SIR model with self regulation, though they do not study the same parameter space as here. They observed periodic dynamics, with periods of up to twelve years as well as chaotic dynamics.

The birth function is now given by:

$$B(t) = \frac{x}{\tau}\left(1 + a\sin\left(\frac{2\pi t}{\tau}\right)\right).$$

Where $a \leq 1$ so B is non-negative. This function is formulated so that the number of births put in throughout the year is x, so as to be comparable with the standard pulsed SIR model. Though really for comparability the magnitude of the forcing should be derived under the constraint that $N(t)$ is cyclic and that $N(n\tau) = 1$ for $n \in \mathbb{N}$. However, for simplicity the above form is used.

Figure 3.3 on the following page shows an example of a period two attractor for this model, compared with the period two attractor at the same point in parameter space for the pulsed SIR model. With the sinusoidal forcing the attractor is much more rounded as one would expect. The minimum value of I is also a lot larger than for the pulsed SIR model. Similarly the range of S is smaller. The peak of the major epidemic is also later in the year with the sinusoidal forcing.

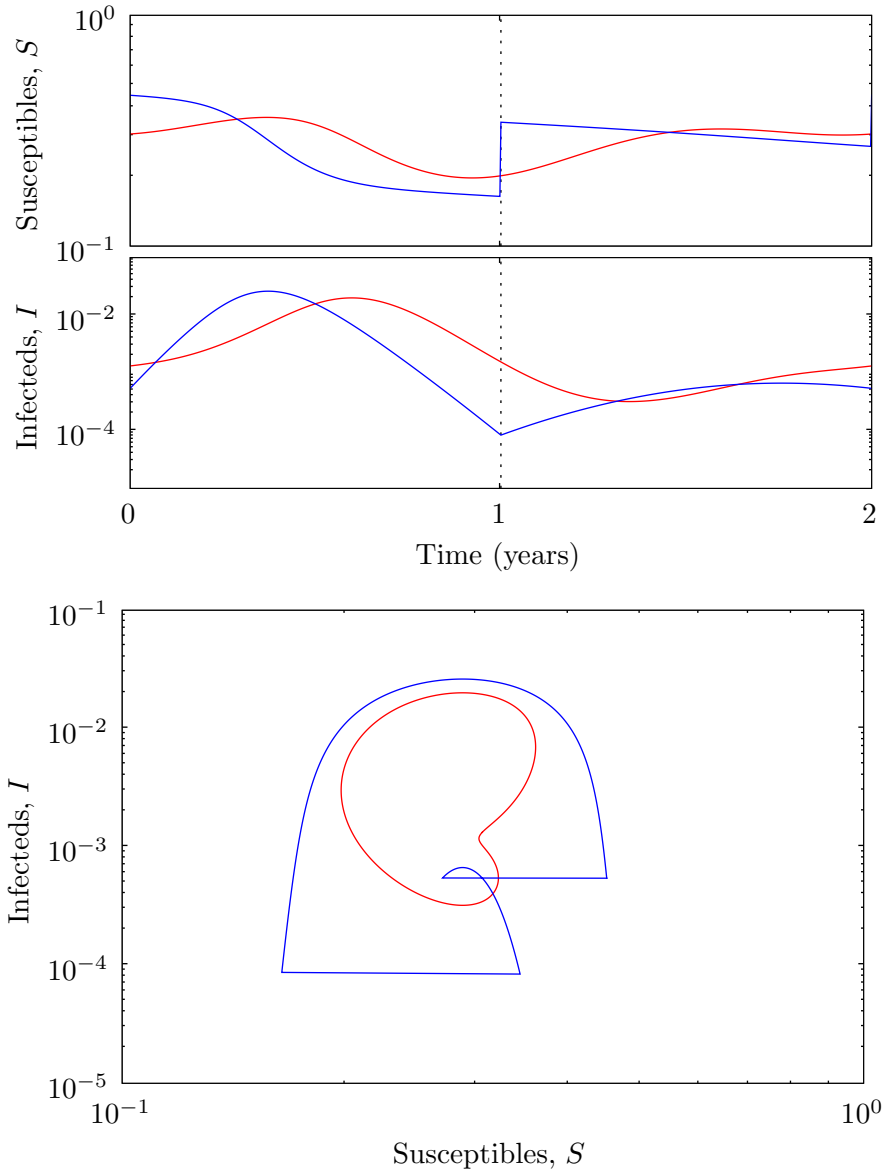

Figure 3.3: A period two attractor of the SIR model with sinusoidal forcing (red line). The period two attractor of the pulsed SIR model (blue line) at the same point in parameter space is also shown for comparison. Parameters: $g = 0.075$, $\beta/g = 3.5$, $x = 0.18$, $d \approx 0.198$, $a = 1$.

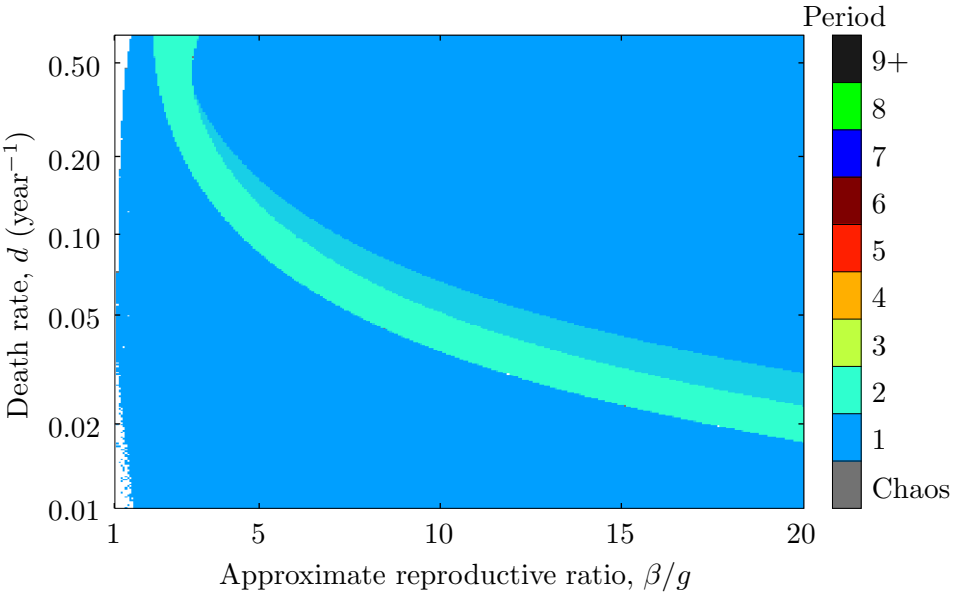

Figure 3.4: Attractors of the SIR system with sinusoidal forcing, $g = 0.075$, $a = 1$.

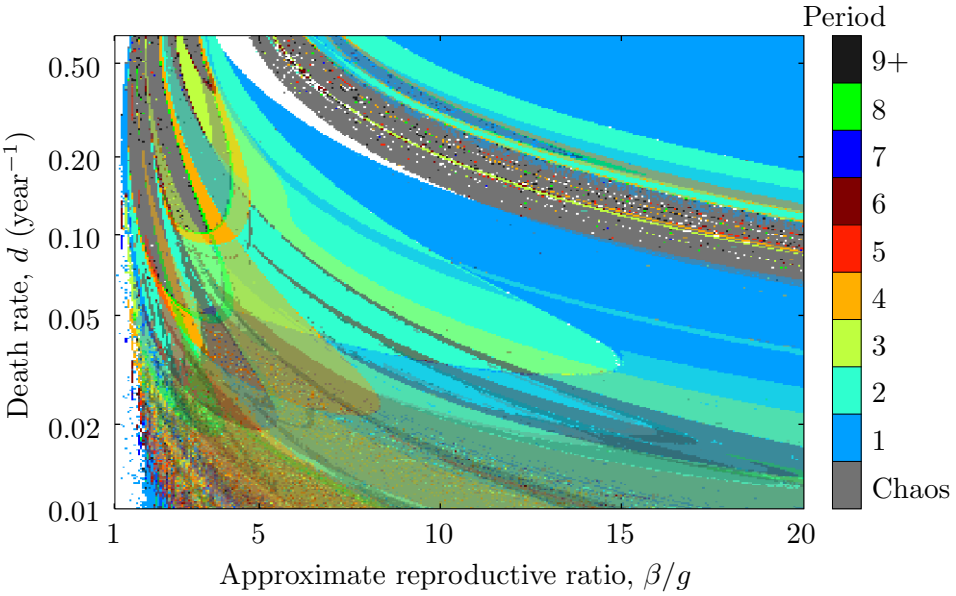

Figure 3.5: Attractors of the SIR system with sinusoidal forcing, $g = 0.5$, $a = 1$.

Figure 3.4 on the previous page shows the periods of attractors found after pushing out (*cf.* Box 2.3 on page 49) for this model. The dynamics seem much simpler than those of the pulsed SIR model of Section 2.1 on page 29. Period one dynamics cover the vast majority of parameter space. There is a thin slice of period two attractors, that has on its upper side a small overlap with the upper period one region. The existence of period two dynamics is in line with the results of Dietz [1976]. Figure 3.5 on the preceding page shows the dynamics for $g = 0.500$. In this case increasing g has made the dynamics much more complex with multiple tongues and high period dynamics becoming apparent.

It seem that for lower values of g, sinusoidal forcing does not provide sufficient impetus to the system for it to exhibit the complex dynamics seen with pulsed births. It is suspected that this is due to the 'smoothness' of the sine function when compared to the instantaneous pulse.

3.2.2 Top hat function

Using a sine function for the forcing significantly changes the behaviour of the system. This subsection considers something much closer to the original birth pulse: a top hat function. This maintains the strong transitions, but extends the temporal extent of the birth pulse over a period of time. Hence $B(t)$ (from Equations 3.1 on page 93) is now given by

$$B(t) = \begin{cases} x/w & \text{for } t > \tau - w \mod 365 \\ 0 & \text{otherwise.} \end{cases} \tag{3.2}$$

This function provides a fixed birth rate for the last w days of the year. The following values of w were chosen to study: 1, 7, 30, 60, 90, 120 and 150. The dynamics of the system with this forcing, for these values of w, is compared to the pulsed SIR model in Figure 3.6 on the following page. It is clear that, at this point in parameter space at least, the limit cycles persist as w is increased, even as high as 150 days. Also, the dynamics during the parts of the year where $B(t) = 0$ seem to be remarkably similar especially during the peak of the major epidemics. It is not surprising that the dynamics are similar, for small w at least, because under discretisation an instantaneous pulse is the same as this top hat function, but with a width, w, of a single time step.

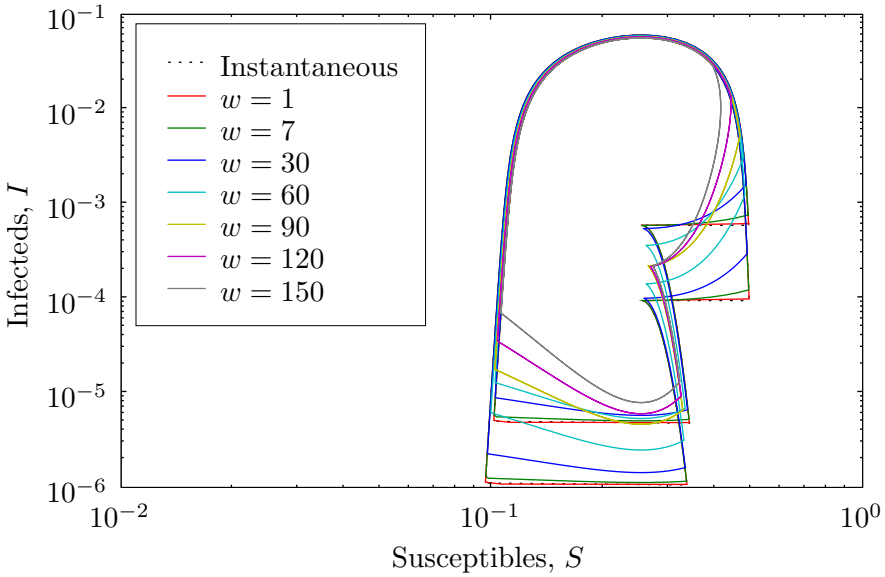

Figure 3.6: Comparison of limit cycles for the standard Pulsed SIR model, with instantaneous birth pulse, and the same system forced with a top hat function having widths of 1, 7, 30, 60, 90, 120 and 150 days. For $R_0 = 4$, $x = 0.24$ and $g = 0.075$. It is clear that even with a pulse as long at 90 days the dynamics show a small variation from the standard pulsed SIR model.

The next step was to see if these observations held over the whole of parameter space. It was decided to only consider $g = 0.075$ as the simpler dynamics in this region would allow an easier comparison. For each value of w, as usual, a fixed initial condition ($S = 0.02$ and $I = 0.0005$) was taken throughout parameter space, and the period calculated. The resultant dataset was then pushed out (*cf.* Box 2.3 on page 49). The data is displayed in Figure 3.7 on page 99 along with the instantaneous pulse data for comparison.

It is quite surprising how little effect varying w has. Even at $w = 90$ the dynamics are little changed, the main difference being in the size of the overlap between period one and two dynamics. At $w = 150$ the general pattern is still similar, although all the period four dynamics are lost from the parameter regime considered. It is interesting to observe that for $w = 150$ the dynamics start to look similar to those obtained with sinusoidal forcing (Figure 3.4 on page 95). This implies that it is not just the 'smoothness' of

the sinusoidal forcing, but also its temporal extent that causes the change in the dynamics. The comparison can be made by thinking of the sinusoidal forcing as a smoothed top hat function $w = \tau/2$.

Interpreting this biologically, it means that the same cycle of epidemics is likely to be seen in populations whether all the births occur on the same day, or are spread over a couple of months. This means that the pulsed SIR model could be applied to model disease in a much wider range of populations (see the introduction to Chapter 2 on page 24 for examples).

3.2.3 Smoothed top hat function

The previous two examples show two extremes, sine is a very smooth function, where as the top hat function has the sharp transients—like the birth pulse. This section examines if the 'smoothness' of the birth function is the factor that causes the change in behaviour. Hence a function with similar shape to that of the top hat function (Equation 3.2 on page 96), but with a parameter to control the smoothing. The birth function is now given by:

$$B(t) = x\left(\frac{1+\tanh\left(\frac{t+w/2}{\rho}\right)}{2} - \frac{1+\tanh\left(\frac{t-w/2}{\rho}\right)}{2}\right) \tag{3.3}$$

where ρ is the smoothing parameter, that controls the shape of the function. For large values, $\rho \approx 50$, $B(t)$ resembles a bell shaped curve, but for small values, $\rho \leq 5$, $B(t)$ looks more like the top hat function of the previous example, although translated so that the births peak in the middle of the year. Figure 3.8 on page 100 shows how the shape of the curve changes with ρ.

A fixed value of $w = 90$ was chosen for the width of the underlying pulse. Looking at Figure 3.7 on the next page, this is the highest values of w for which the dynamics are mostly unchanged. Five values of ρ where considered: 10, 20, 30, 40 and 50. Again a fixed initial condition ($S = 0.02$ and $I = 0.0005$) was taken throughout parameter space, the period calculated and the data pushed out. Figure 3.8 on page 100 shows the periods of attractors across parameter space for each value of ρ and includes a plot of the forcing functions used. The un-smoothed case for the same width (from the previous section) is also included for comparison.

These results are similar to those for varying the width of the top hat

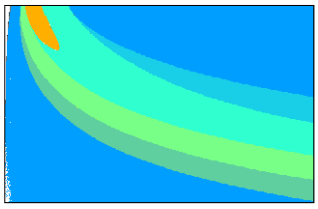

Instantaneous

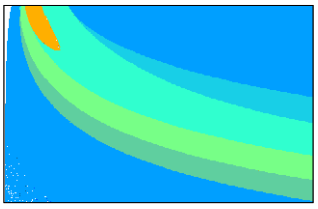

$w = 1$

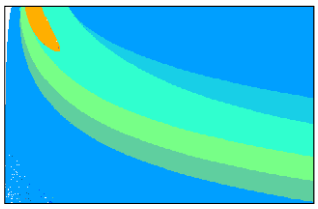

$w = 7$

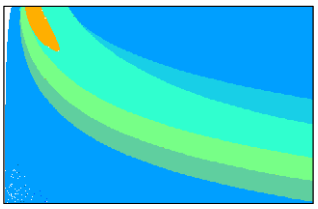

$w = 30$

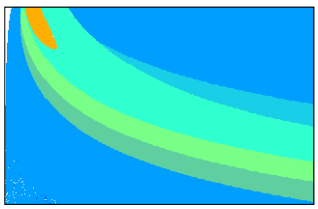

$w = 60$

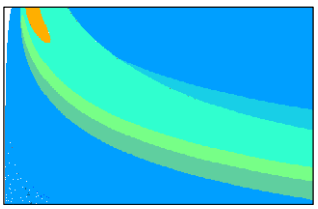

$w = 90$

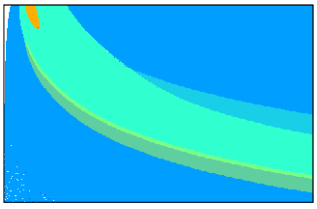

$w = 120$

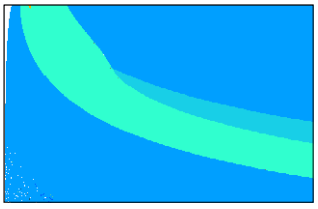

$w = 150$

Figure 3.7: Sequence showing how the period changes across parameter space as the pulse function is varied from an instantaneous pulse to a pulse of width 150 days.

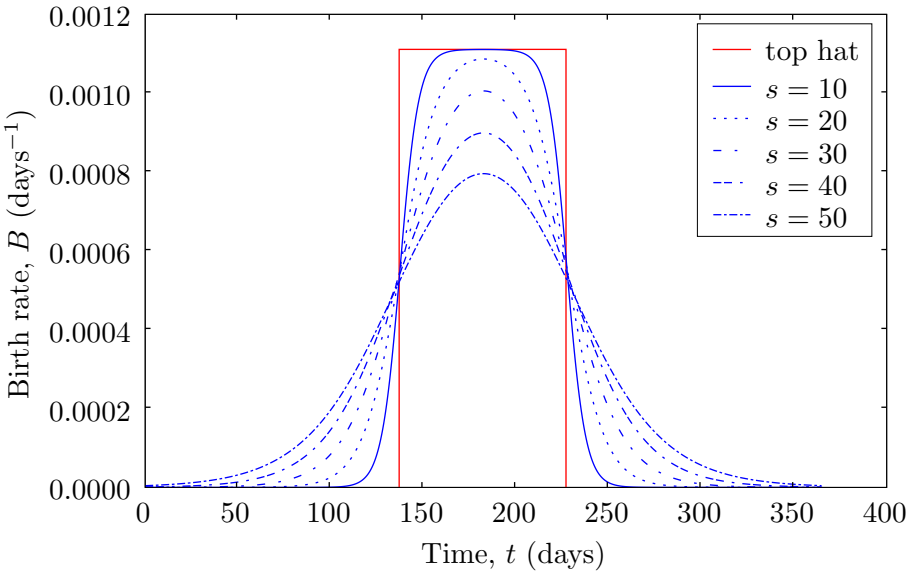

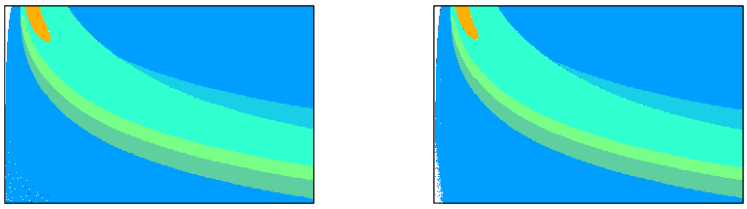

top hat

$s = 10$

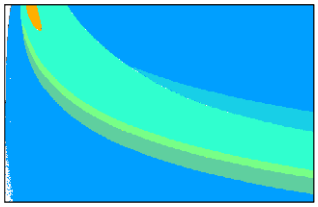

$s = 20$

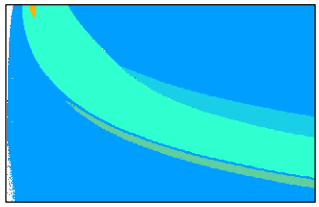

$s = 30$

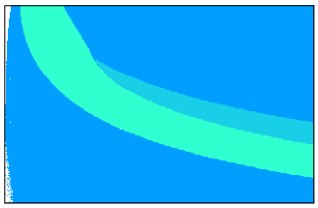

$s = 40$

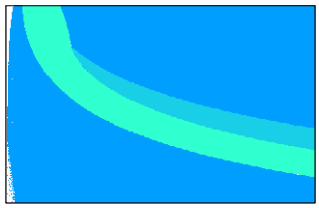

$s = 50$

Figure 3.8: Sequence of plots showing how the period changes across parameter space as increasing amounts of smoothing, s, are applied to a pulse of width, $w = 90$ days.

function. Small amounts of smoothing ($\rho = 10, 20$) show little change in the dynamics compared to the un-smoothed case. With the most smoothing, $\rho = 40, 50$, the results look more like those with sinusoidal forcing (Figure 3.4 on page 95), the period four dynamics retreat and the region of period two thins.

From this it would be fair to conclude that what makes the results for sinusoidal forcing so different, is a combination of smoothness with the long temporal extent. In general the results for the top hat and smoothed top had functions are qualitatively similar to the dynamics of the pulsed SIR model, only when functions with very slow transients or long temporal extents are used do the dynamics become similar to those with sinusoidal forcing. In between the dynamics seem to depend continuously on the forcing function.

A biological interpretation is that for the pulsed SIR model (Equations 2.1 on page 29) to be a good fit the births must be highly seasonal. The birthing period can extend up to several months, but must drop off sharply at either end. Conversely, the model may still be applicable with a less sharp drop off if the birthing period is shorter. Moreover, it is only necessary to have a good knowledge of the total annual births. The exact distribution is less important. This observation is important as it may mean fewer observations are needed when collecting field data.

3.3 Change in model structure

The standard SIR model is in some ways quite a simplistic model. It makes many assumptions about the nature of the disease and the population. A poignant question is whether or not pulsed births lead to the same kinds of dynamics in other related models, where certain assumptions are relaxed or other features are added to the model.

This section considers such changes. This entails making alterations to the structure of the model, adding new terms to the equations, or new equations all together. The following models are considered.

SEIR model This model splits the infected class into two. An exposed class represents those who are infected, but are not yet themselves infectious. These individuals then move into the infectious class.

Simple SIR The simple SIR model is essentially the same as the standard

pulsed SIR model, but without the death terms. This model can be useful in situations where the time-scales on which deaths occur in the population are much longer than those on which infection occurs.

Vaccination pulse Rather than adding a pulse of births this model annually moves a proportion of the population from the susceptible class to the recovered class to represent a pulsed vaccination strategy.

Childhood disease This model attempts to capture the behaviour of childhood diseases within schools. The birth pulse, in this context is new children entering school, is accompanied by a 'death' pulse representing children leaving school.

Frequency dependent transmission This model assumes frequency dependence to the transmission rather than density dependence, making it possibly more suitable for infections in human populations.

Density dependent death In this model the death rate is dependent on the total density of the population, thus taking into account mortality caused by competitions for resources *etc.*

Gamma distributed infectious period Two models are considered in this section, firstly the pulsed SIR model is adapted to have a gamma distributed infectious period. Secondly, the same is applied infectious and latent periods of the SEIR model. This distribution, which is more mean centred than the exponential distribution it replaces, is seen as more realistic.

Imports The final model considered the effect of adding imports, that is a small continuous source of infection preventing the disease from dying out.

3.3.1 SEIR model

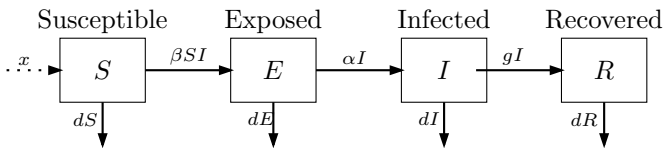

Figure 3.9: Box diagram for the SEIR model.

The SEIR model extends the SIR model by adding an exposed class. Members of this class are infected, but are not infectious and can therefore not pass on the disease to members of the susceptible class. A new parameter α is introduced, which is the inverse of the average latent period—the time where an individual is infected but not infectious. Figure 3.9 on the previous page shows the model structure.

The equations for the forced SEIR model are

$$\begin{aligned} \dot{S} &= -\beta SI - dS \\ \dot{E} &= \beta SI - \alpha E - dE \\ \dot{I} &= \alpha E - gI - dI \\ \dot{R} &= gI - dR. \end{aligned} \tag{3.4}$$

In the same way as with the standard pulsed SIR model a birth pulse is applied to the susceptible class every year:

$$S(t^+) = S(t^-) + x \qquad \text{where } t = n\tau,\ n \in \mathbb{N}.$$

For simplicity the latent period is assumed to be equal to the infectious period, that is to say $\alpha = g$, and g takes the same values as for the SIR model. Fixing this relationship has the benefit of not introducing another parameter, though it is not clear that keeping the infectious rather than the infected period the same as that of the standard pulsed model SIR is the correct assumption to make the results comparable. Of course, this is not always be a biologically realistic assumption depending on the disease in question. For example rubella has an average latent period of 10.5 days and an average infectious period of 11.5 days which supports this assumption. On the other hand, measles has a latent period of 10–12 days and an infectious periods of 3–4 days [Schwartz and Smith, 1983], clearly not in line with this assumption.

A period 6 attractor for this system is shown in Figure 3.10 on the following page. The dynamics are reminiscent of the standard pulsed SIR model.

Figure 3.11 on the next page shows the results for $g = 0.075$ after pushing out (*cf.* Box 2.3 on page 49). The result are much simpler than for the standard pulsed SIR model with the same infectious period (as illustrated

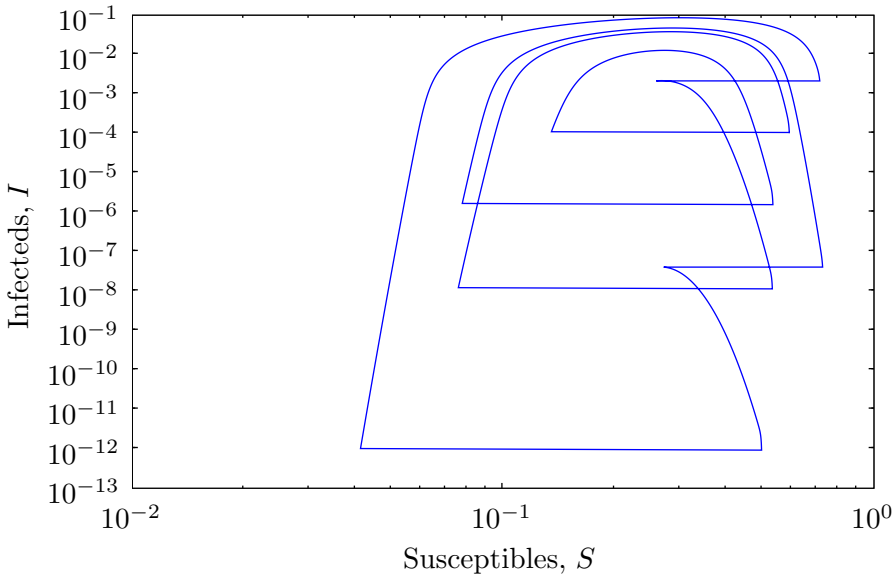

Figure 3.10: A period 6 attractor for the pulsed SEIR model, in this case $\beta/g = 3.86$, $x = 0.456$, $d \approx 0.610$ $g = \alpha = 0.150$.

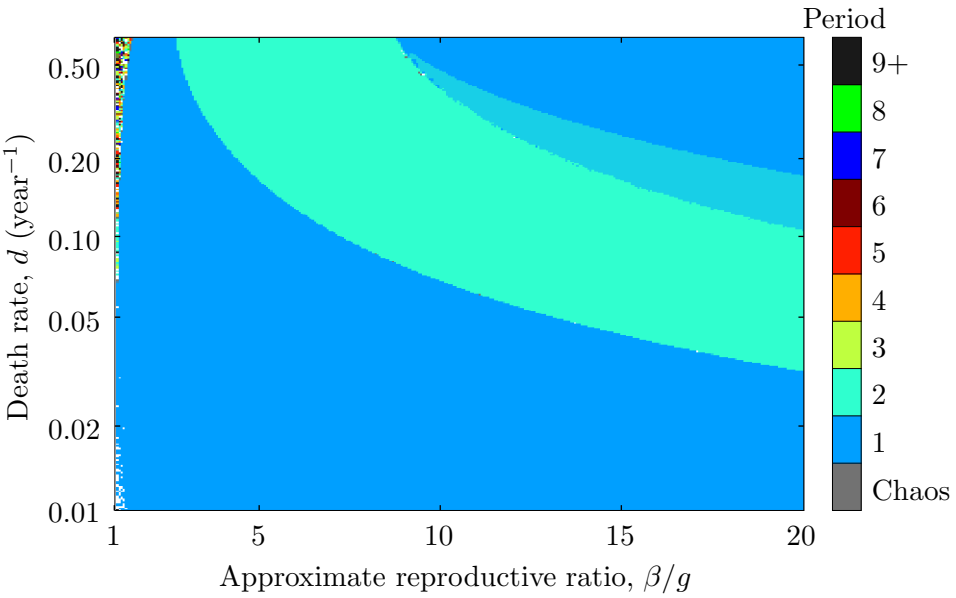

Figure 3.11: Attractors found for the pulsed SEIR model after pushing out for $g = 0.075$.

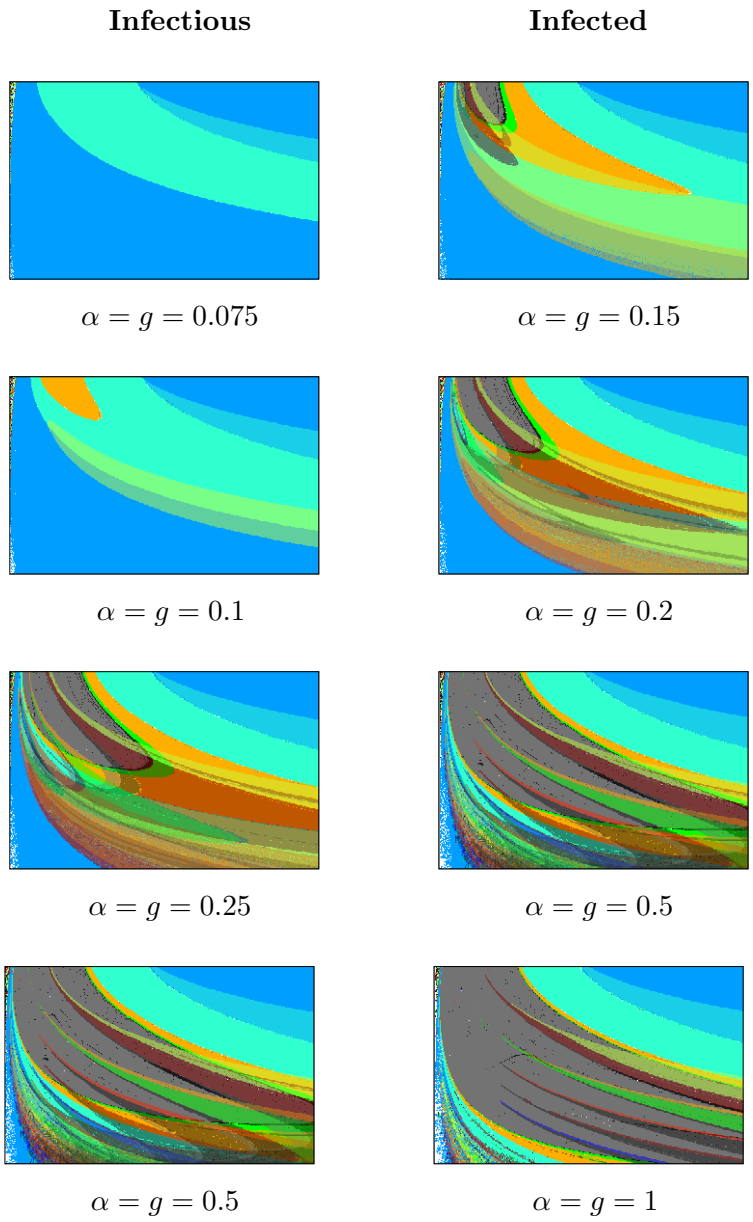

Figure 3.12: Sequence showing how the period of attractors changes across parameter space for the pulsed SEIR model (Equations 3.4 on page 103) as the infected/latent period decreases from ≈ 14–2 days (left column) and the total infected period from ≈ 14–2 days (right column).

in Figure 2.16 on page 55), showing only periods one and two, with an overlap between the period two region and the upper period one region. This may suggest that what really affects the dynamics is not the infectious period, but the infected period.

Figure 3.12 on the preceding page shows how the period exhibited varies as the infectious period varied from $\approx$ 14–2 days in the left hand column and the infected period varied in the same range in the right hand column. Neither column matched well the behaviour of the standard pulsed SIR model. In terms of complexity the results for standard SIR model fit somewhere in between the two columns. There are other differences too, the tongues coming down from the top left are wider than for the standard pulsed SIR model and they seem to bend up more, disappearing to the right hand side rather than the bottom right corner. Thus simply matching the infectious or infected period is not quite enough to compare this model to the standard pulsed SIR model. Having said that the dynamics are still very similar, at different values of g and α. For example $\alpha = g = 0.1$ is the most similar to $g = 0.075$ standard pulsed SIR model (Figure 2.14 on page 54), and $\alpha = g = 0.15$ is similar to $g = 0.100$ standard pulsed SIR model (Figure 2.15 on page 54). This is surprising given a whole new class has been added to the model.

3.3.2 Simple SIR

All of the other models in this section are refinements of the standard SIR model, adding extra terms or equations and a birth pulse to make the model more realistic. This subsection considers a simplification of the standard SIR model: the simple SIR model. This model omits the death terms for each of the classes. This doesn't necessarily make the model more inaccurate it merely assumes that the deaths happen on a much longer time scale to the spread of infection, and thus the change in the numbers of individuals in each class over the time scale considered is negligible. Alternatively it could represent a disease in a population where all individuals become infected before they die, so that death plays no part in the disease dynamics.

The simple SIR (Equations 1.5 on page 15) model is given by:

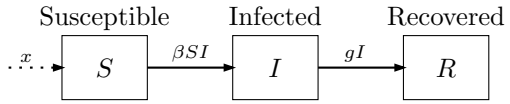

Figure 3.13: Box diagram for the pulsed simple SIR model.

$$\begin{aligned} \dot{S} &= -\beta SI \\ \dot{I} &= +\beta SI - gI \\ \dot{R} &= gI. \end{aligned}$$

The birth pulse is applied in the same way as the pulsed SIR model:

$$S(t^+) = S(t^-) + x \qquad \text{where } t = n\tau,\ n \in \mathbb{N}.$$

Figure 3.14 on the following page shows typical period one, two and three dynamics for this system with the attractors for the standard pulsed SIR system shown for comparison. The period one and two attractors are similar for both systems. The main difference is that the sides are more vertical for the pulsed simple SIR model. This is explained by the death of susceptibles during that phase of the cycle. The difference in the period three attractors is more pronounced, as for the standard model, the sides lean in much more clearly.

Figure 3.15 on page 109 and Figure 3.16 on page 109 show the periods of the attractors obtained throughout parameter space after pushing out for $g = 0.075$ and $g = 0.500$ respectively. For $g = 0.075$ the results are very similar to the standard pulsed SIR model (Figure 2.14 on page 54). The most immediate difference is the disappearance of the period four region seen the top left corner. The bands of period two and three dynamics are also shifted to the left near the top left corner and the region in the top left where extinction occurs has also disappeared. To explain the previous two observations R_0 for this system must be considered.

For the simple SIR model, in the absence of infection, the density of susceptible individuals will grow unbounded. As such in this scenario the basic reproductive ratio is not a well defined concept. So instead the basic reproductive ratio of the un-forced system is considered instead, using caution

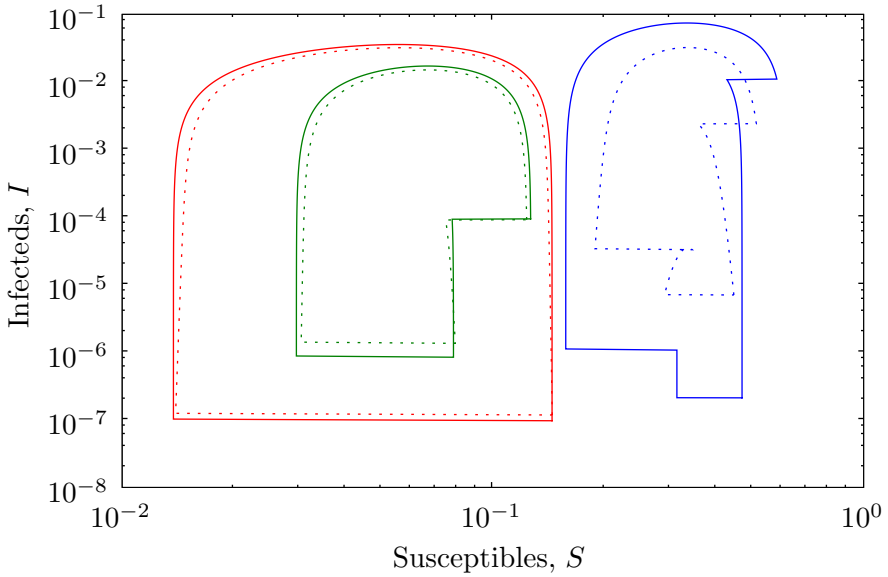

Figure 3.14: Typical dynamics of the pulsed simple SIR model(Equations 1.5 on page 15) . Dashed lines show the an attractor of the same period at the same point in parameter space for the pulsed standard SIR model(Equations 2.1 on page 29). Parameters are given as (R_0, x) and $g = 0.075$ throughout. Red: $(18, 0.131)$ period 1, green: $(15, 0.0488)$ period 2, blue: $(3, 0.156)$ period 3.

in what conclusions are drawn.

For the un-forced simple SIR model $R_0 = \beta/g$, which is measured directly on the x-axis. Thus the R_0 isolines are vertical lines. Compare this with Figure 2.9 on page 45 for the standard pulsed SIR model where the R_0 isolines bend to the right at the top. Thus there is no region where $R_0 < 1$ in the parameter space for the simple SIR model. If the periods for the standard pulses SIR model were to be plotted on an transformed grid, such that the R_0 isolines were vertical then it would not look so dissimilar to the picture for the pulsed simple SIR model.

For $g = 0.500$ the dynamics are very different to the pulsed standard SIR model. There do not appear to be any tongues, but the period seems to increase moving towards the bottom left corner. An approximation to the pulsed simple SIR model that helps explains this observation is studied in Section 4.3 on page 162.

The pulsed simple SIR model shows that deaths within each class do

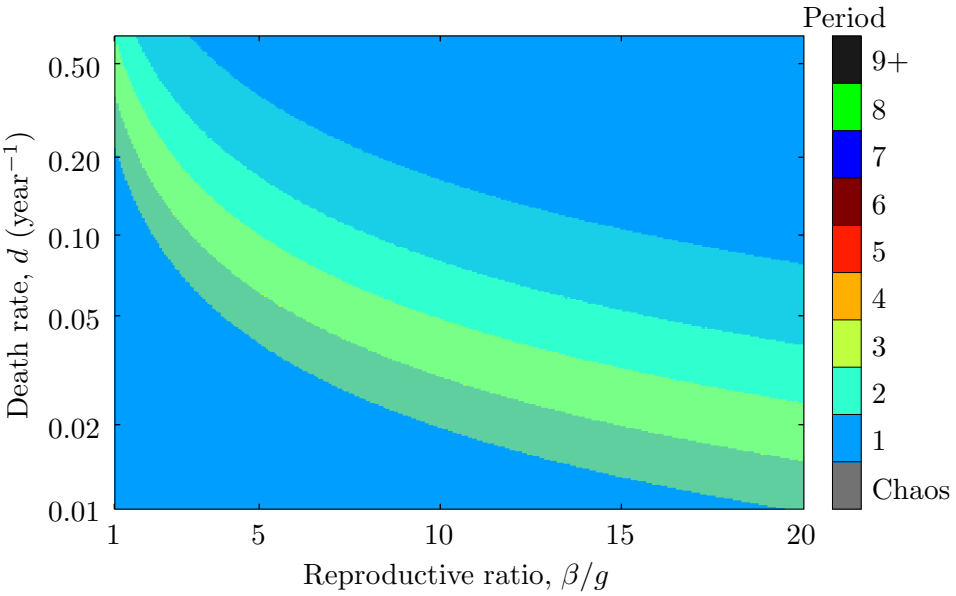

Figure 3.15: Attractors found for the pulsed simple SIR model (Equations 1.5 on page 15) after pushing out for $g = 0.075$.

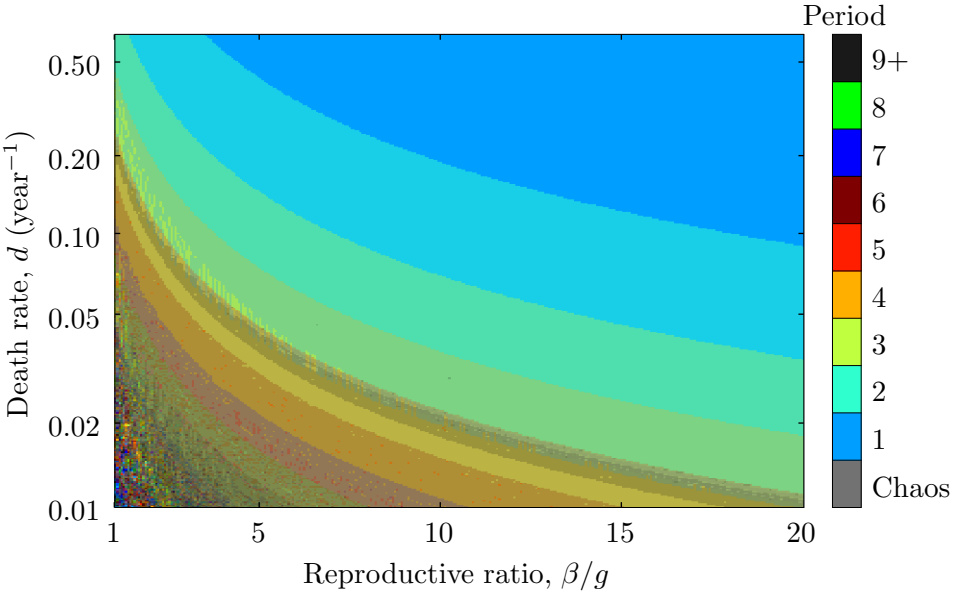

Figure 3.16: Attractors found for the pulsed simple SIR model (Equations 1.5 on page 15) after pushing out for $g = 0.500$.

play an important role in the dynamics of the system especially for short infectious periods. For a long infectious period the dynamics are actually slightly simplified.

3.3.3 Vaccination pulse

This model is somewhat different from the others presented in this section. Rather than modelling the births with a pulse, they are assumed to be continuous and pulse is used to model vaccination. Every year a proportion of susceptibles are moved directly into the recovered class, mimicking a proportion of the population being vaccinated on a single day. This is not unrealistic, large numbers of individuals are in fact frequently vaccinated together. A good example is the mass vaccination of United Kingdom school children against measles (and rubella) in November 1994 [Ramsay et al., 1994]. Modelling had predicted a large epidemic would occur in 1995. The mass pulse vaccination of more than 90% of school children [Shulgin et al., 1998] successfully prevented the epidemic.

Quite a lot of work has been done in the field of pulsed vaccinations as part of the study of vaccination strategies in general driven by the need to make best use of the available resources. In their review Nokes and Swinton [1997] noted how pulsed vaccination was used in America to great success in particular against polio. They highlight the mixed success of pulsed vaccination in other areas of the world and suggest that part of the problem is due to the time intervals and age ranges for vaccination being decided based on "intuitive reasoning rather than quantitative epidemiological understanding".

A slight generalisation of this model is used by Stone et al. [2000], where rather than applying the vaccination pulse every year, it is applied every T years. He examines the model's "infection free" solution. That is a solution where $I \equiv 0$ and S oscillates driven by the pulsing. An explicit expression for this solution is found. The criteria for the stability of this "infection free" equilibrium are determined, and the maximum number of years between pulses for which the stability is sustained is computed. This gives an estimate for the maximum advisable separation between vaccination pulses if the strategy is to be effective in eliminating the disease. This work is continued in D'Onofrio [2002b].

Agur et al. [1993] is the first theoretical treatment of pulsed vaccination.

Using an age structured SIR model, they evaluate pulsed vaccination as a strategy for controlling measles in Israel. They show that pulsed vaccination could be a more effective strategy than the cohort vaccination strategy in place at the time.

D'Onofrio [2002a] applies the same vaccination pulse to an SEIR model. He revisits his work [D'Onofrio, 2004] by adding gamma distributed infectious and latent periods (see Subsection 3.3.7 on page 131) to the basic SEIR model.

Lu et al. [2002] considers another variant of the SIR model. This time adding vertical transmission, that is a proportion of those born to infected parents are themselves infected. Thus births come into both the susceptible and infected classes. Two different vaccination strategies are considered in conjunction with this system: a constant rate and pulsed vaccination. For the pulsed vaccination strategy, the existence of both infection-free and endemic solutions is observed. A similar analysis is performed on the SIS model with both constant rate an pulsed vaccination by Zhou and Liu [2003].

Here, in contrast to much of the work above, only the endemic equilibria are considered so as to be comparable to the results from other systems in this section.

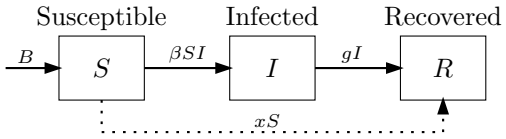

Figure 3.17: Box diagram for the vaccination pulse model.

This model takes the simple SIR model from the previous subsection, but with a constant birth rate:

$$\begin{aligned} \dot{S} &= -\beta SI + B \\ \dot{I} &= +\beta SI - gI \\ \dot{R} &= gI. \end{aligned} \tag{3.5}$$

The system is forced by

$$\left.\begin{aligned} S(t^+) &= S(t^-)(1-x) \\ R(t^+) &= R(t^-) + S(t^-)x \end{aligned}\right\} \qquad \text{for } t = n\tau,\ n \in \mathbb{N}$$

at the start of each year. This simulates the vaccination of a proportion

x of the susceptibles at the start of every year. For comparability with the pulsed SIR model the same range of proportions x is used. Hence $0.01 \leq x \leq 0.5$. For simplicity the birth rate is tied to x so that $B = x/\tau$. Although the frequency of vaccination pulses is fixed to be annual for comparison with other models, it is possible to simulate varying the interval between pulses by rescaling time. This would also rescale the infectious period, hence to consider the effect of a biannual vaccination pulse the value of g would need to be doubled.

Figure 3.18 on the next page shows a selection of attractors for the system. They appear very different from the previous attractors studied. Most strikingly they appear "upside down". The pulses of vaccination lead to a drop in the level of infection, rather than a rise with the birth pulses, this is of course just what a vaccination pulse should achieve. The second feature not seen before is the apparent spiralling to a fixed point in the blue and magenta attractors. It is suspected that this is not seen in the other systems because the perturbations here are smaller because they are a proportion of the value of S, rather than a fixed size. This means that the system is perturbed less from its un-forced fixed point.

The periods of the resulting attractors over the whole of the parameter space, after pushing out, for $g = 0.075$ and $g = 0.500$ are displayed in Figure 3.19 and Figure 3.20 (on pages 113–115) respectively. The dynamics for $g = 0.075$ are very simple. Period one dominates, with only a small region of period two in the top left. Attractors from both regions are shown in Figure 3.18 on the following page. However, when g is raised to 0.500 the dynamics become much more complex. As seen before multiple tongues come down from the top left, although the pattern is subtly different, rather than overlapping the tongues lie next to each other.

Clearly much more work could be done here, and much has been done. Nevertheless, this model provides an interesting comparison to the other models with birth pulses. Showing that similar kinds of complex dynamics do occur and that they are perhaps a general feature of models with where seasonality is modelled though pulsing. Much more work would need to be done to demonstrate this.

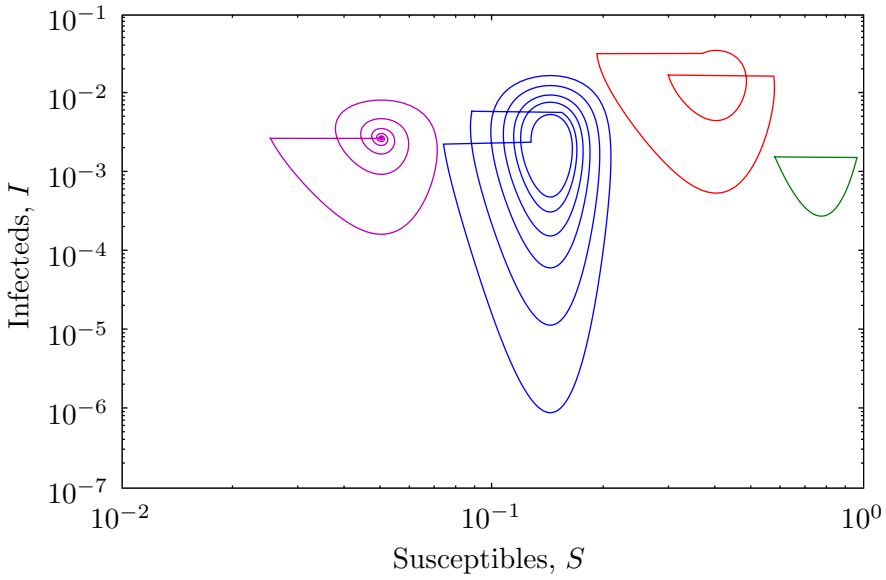

Figure 3.18: A selection of attractors of the vaccination pulse model (Equations 3.5 on page 111). Parameters are given as $(\beta/g, x, g)$. Red: $(2.5, 0.48, 0.075)$ period 2, green: $(1.3, 0.4, 0.075)$ period 1, blue: $(7, 0.42, 0.500)$ period 2, magenta: $(20, 0.5, 0.500)$ period 1.

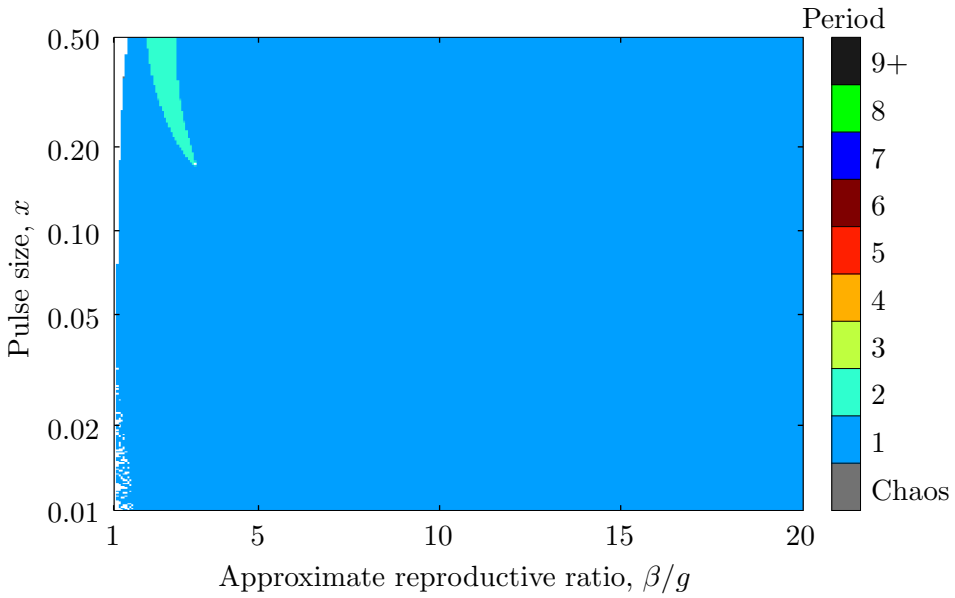

Figure 3.19: Attractors found for the vaccination pulse model (Equations 3.5 on page 111) after pushing out for $g = 0.075$.

3.3.4 Childhood

Much work has been done in modelling the epidemics of childhood diseases such as measles. One of the key factors in the spread of childhood diseases is the aggregation of hosts within schools [Fine and Clarkson, 1982, Keeling et al., 2001]. The model in this subsection uses pulsing, in an attempt to represent the annual throughput of hosts in schools or other similar environments.

In this model x new susceptibles are added each year as before, but a proportion x, of each class is also removed each year. This can be thought of as new (susceptible) children entering school and older children (from all classes) leaving. The model ignores deaths, as they will be negligible due to the short time period. The model is given by:

$$\begin{aligned} \dot{S} &= -\beta SI \\ \dot{I} &= \beta SI - gI \\ \dot{R} &= gI. \end{aligned} \tag{3.6}$$

with the mapping:

$$\left.\begin{aligned} S(t^+) &= S(t^-)(1-x) + x \\ I(t^+) &= I(t^-)(1-x) \\ R(t^+) &= R(t^-)(1-x) \end{aligned}\right\} \quad \text{for } t = n\tau,\ n \in \mathbb{N}.$$

This mapping balances the losses though removal—children leaving school—and the influx of susceptibles—new children starting school—keeping the population size constant.

Figure 3.22 on page 116 shows several attractors for the system in comparison with attractors of the same period and with the same parameter values for the standard pulsed SIR model. The pulse section of the attractors are no longer "horizontal" as both S and I are changed by the pulse. The period one attractors are very similar and the difference in the period three is minimal. The period two attractors show the most difference, which is probably caused by the lower β value allowing the death terms, not present in Equations 3.6, to take a larger part in the dynamics. Here the slope of the pulse section is more pronounced, but most noticeable is the fact that there is only an epidemic every two years rather than alternating small and

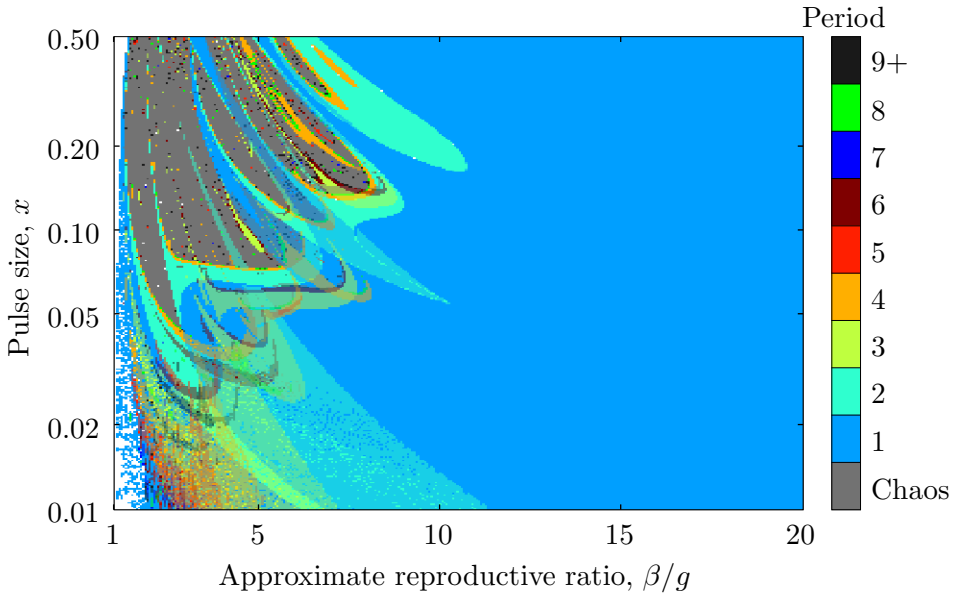

Figure 3.20: Attractors found for the vaccination pulse model (Equations 3.5 on page 111) after pushing out for $g = 0.500$.

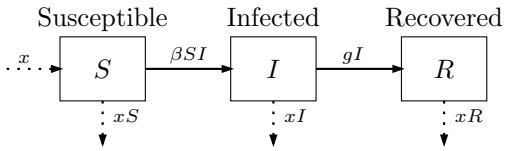

Figure 3.21: Box diagram for the pulsed childhood model.

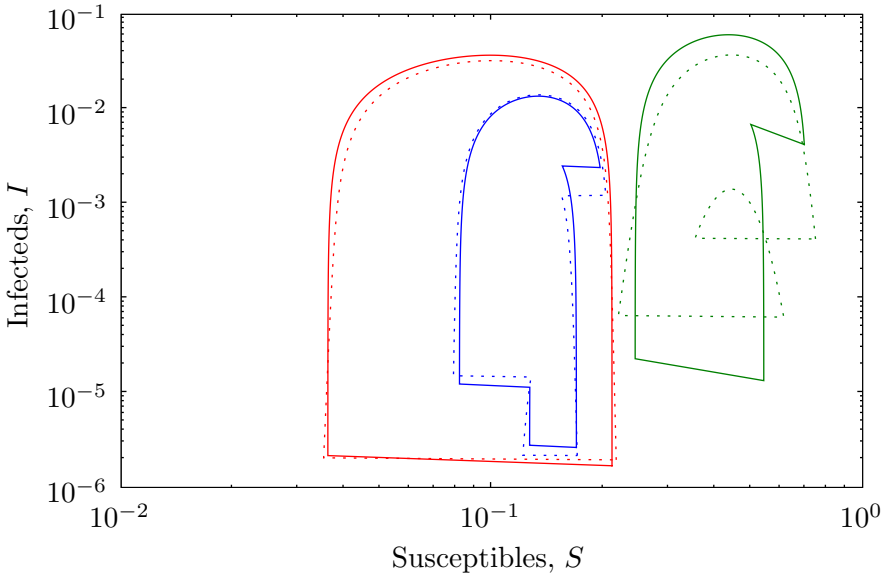

Figure 3.22: Typical dynamics of the pulsed childhood SIR model (Equations 3.6 on page 114). Dashed lines show an attractor of the same period at the same point in parameter space for the standard pulsed SIR model (Equations 2.1 on page 29). The parameters are given as $(\beta/g, x)$ and $g = 0.075$ throughout. Red: $(10.1, 0.181)$ period 1, green: $(2.3, 0.393)$ period 2, blue: $(7.5, 0.0488)$ period 3.

large epidemics with the standard pulsed SIR model.

Figure 3.23 on the next page shows the attractors obtained from a fixed initial condition ($S = 0.02$, $I = 5 \times 10^{-4}$) at each point in parameter space, after pushing out, for $g = 0.075$.

Two things are striking about the results in Figure 3.23 on the following page. There are only period one, two and three dynamics and the period two region is substantially smaller than that for the standard pulsed SIR model (Figure 2.14 on page 54). It is also interesting that the period three "tongue" does not persist in for higher d values as it does with other models. There is also some speckling in the bottom left corner, which is caused by the very slow convergence in that region of the order of 1500 years, some what longer than the standard pulsed SIR model. This is a very long time-scale compared to those normally associated with schools, and it is quite likely that the system would be perturbed before it converges close to the attractor, thus any disease in a population with parameters in that region (low R_0, low

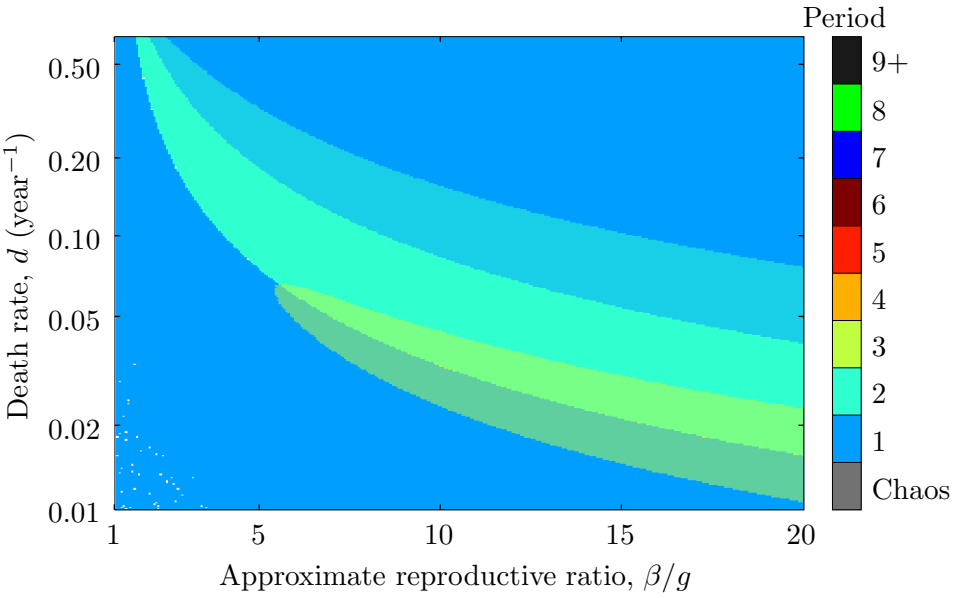

Figure 3.23: Attractors found for the pulsed childhood SIR model (Equations 3.6 on page 114) after pushing out for $g = 0.075$.

birth rate) is unlikely to show the simple period one dynamics predicted.

3.3.5 Frequency dependent transmission

This common variant of the standard SIR model alters that way transmission from infected to susceptible individuals occurs. Rather than assuming that the contact rate is proportional to the total population density, it is assumed that the contact rate is constant. Thus the force of infection increases with the prevalence of infection within the population. The differences between the two types of transmission term are discussed in more detail in Section 1.6 on page 15. The use of frequency dependent transmission make this model more suitable for looking at diseases in human populations. Of course human populations are not generally know to exhibit pulsed births, but it is interesting nevertheless to consider this type of transmission.

This model is given by the following equations:

$$\begin{aligned} \dot{S} &= -\beta SI/N - dS \\ \dot{I} &= +\beta SI/N - gI - dI \\ \dot{R} &= gI - dR. \end{aligned} \tag{3.7}$$

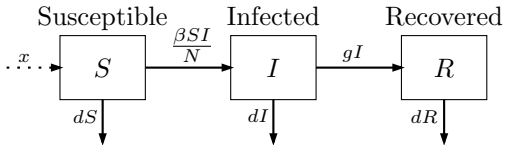

Figure 3.24: Box diagram for the SIR model with density dependent transmission.

The birth pulsing is applied to the susceptible class in the usual way:

$$S(t^+) = S(t^-) + x \qquad \text{where } t = n\tau,\ n \in \mathbb{N}.$$

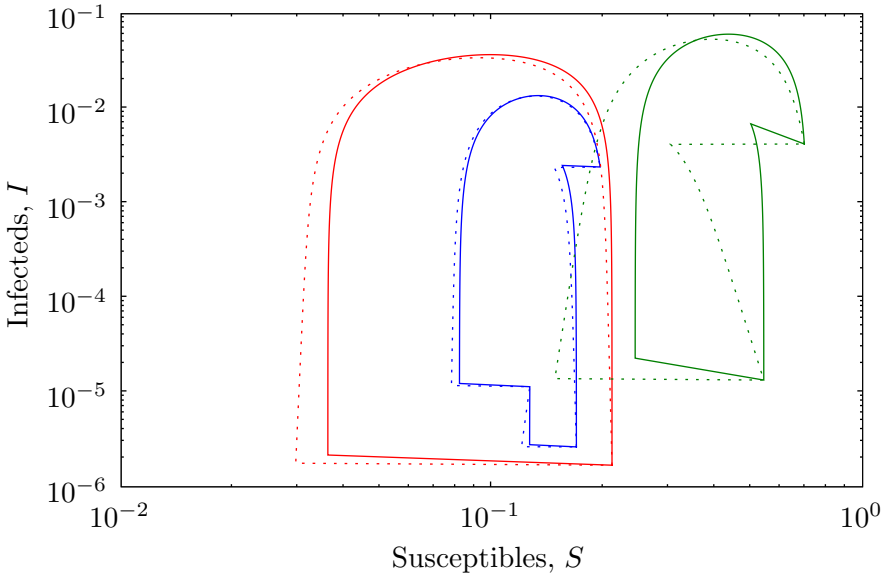

Figure 3.25: Typical dynamics of the pulsed childhood SIR model(Equations 3.6 on page 114) compared with the pulsed SIR model with density dependent transmission. Dashed lines show the an attractor of the same period at the same point in parameter space for the pulsed SIR model with frequency dependent transmission (Equations 3.7 on the preceding page). Parameters are given as $(\beta/g, x)$ and $g = 0.075$ throughout. Red: $(10.1, 0.181)$ period 1, green: $(2.3, 0.393)$ period 2, blue: $(7.5, 0.0488)$.

Figure 3.25 shows a comparison of attractors for the SIR model with frequency dependent transmission presented in this subsection and attractors with the same parameters for the childhood SIR model presented in the

previous subsection. What is striking is that although the trajectories differ throughout the year, they share the same annual fixed points. Moreover, when the period of attractors across parameter space was calculated for the model presented here the results, not shown, were identical to those found in the previous subsection (Figure 3.23 on page 117). It is now shown that there is a transformation between the two models.

Theorem 3.1 *Under the transformation*

$$S \to S/N, \quad I \to I/N, \quad R \to R/N$$

the pulsed SIR model with frequency dependent transmission (Equations 3.7 on page 117) becomes the childhood SIR model (Equations 3.6 on page 114).

Proof: Consider the making the substitution

$$\begin{aligned} s(t) &= S(t)/N(t), \\ i(t) &= I(t)/N(t), \\ r(t) &= R(t)/N(t), \end{aligned}$$

into Equations 3.7 on page 117.

Firstly note that by summing Equations 3.6

$$\dot{N} = -dN,$$

so that

$$N = e^{-dt} \qquad \text{where } t \in [0, \tau)$$

Because $N_0 = 1$ by the same argument used in the proof of Lemma 2.1 on page 29. When the birth pulse is taken into account, recalling that $x = 1 - e^{-d\tau}$, N is periodic with period one year.

Now the new susceptible equation is given by

$$\begin{aligned}\dot{s} &= \frac{\dot{S}N - S\dot{N}}{N^2} \\ &= \frac{-\beta SI - dSN + SdN}{N^2} \\ &= -\beta si.\end{aligned}$$

Similarly for the infected equation:

$$\begin{aligned}\dot{i} &= \frac{\dot{I}N - I\dot{N}}{N^2} \\ &= \frac{-\beta SI - gIN - dIN + IdN}{N^2} \\ &= -\beta si - gi.\end{aligned}$$

Finally the recovered equation:

$$\begin{aligned}\dot{r} &= \frac{\dot{R}N - R\dot{N}}{N^2} \\ &= \frac{gIN - dRN + RdN}{N^2} \\ &= -\beta gi.\end{aligned}$$

All three of which are the same equations as the childhood SIR model. It only remains to show that the forcing functions are the same. Firstly notice that as N is periodic, $N(t^+) = N(0) = 1$, where $= n\tau$, $n \in \mathbb{N}$. The forcing for the susceptibles is given by the impulse equation:

$$S(t^+) = S(t^-) + x \qquad \text{where } t = n\tau,\ n \in \mathbb{N},$$

substituting for S,

$$\begin{aligned}s(t^+)N(t^+) &= s(t^-)N(t^-) + x \\ s(t^+) &= s(t^-)(1-x) + x\end{aligned}$$

as $N(t^-) = 1 - x$. In the pulsed SIR model with frequency dependent transmission the infected equation is not forced, but this can be expressed

as an impulse equation:

$$I(t^+) = I(t^-) \qquad \text{where } t = n\tau,\ n \in \mathbb{N},$$

and substituting for I yields

$$\begin{aligned} i(t^+)N(t^+) &= i(t^-)N(t^-) \\ i(t^+) &= i(t^-)(1-x). \end{aligned}$$

The same argument holds for the removed equation. The result follows by replacing s, i and r by S, I and R respectively. □

The observation that in Figure 3.25 on page 118 the two sets of attractors share fixed points, but differ through the year can now be explained. At the annual fixed points ($t = n\tau$, $n \in \mathbb{N}$) $N = 1$ making the transformation the identity, hence the annual points are the same. Throughout the following year N then decays exponentially and the paths diverge, until after the next pulse, when they come back into line again.

3.3.6 Density dependent death

The model presented in this subsection adds density dependence to the death term. This attempts to incorporate effects such as overcrowding. Assuming there is a fixed finite area where the population resides, if the population size increases, and therefore the density, then there is an increase in competition for resources. Inevitably, this means that some individuals loose out and suffer mortality increasing the death rate. Conversely, if the population is small the death rate becomes smaller due to the reduced levels of competition. The dynamics of wildlife diseases are discussed at length in Hudson et al. [2002].

Greenhalgh [1990] considers a similar model where the death rate is a generalised function of the population size. His model has constant births, and features a term to model mortality due to infection. He derives a threshold parameter and conducts a stability analysis, and concludes that the endemic equilibrium is stable with respect to small perturbations. Some numerical simulations for specific death rate functions are carried out, including the one used in this section.

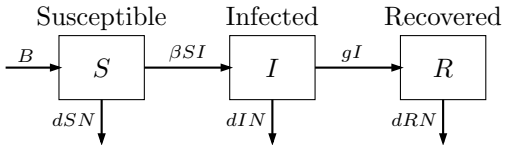

Figure 3.26: Box diagram for the SIR model with density dependent death.

This extra assumption is added to the model by assuming that the death rate is directly proportional to the population density:

$$\begin{aligned} \dot{S} &= -\beta SI - dSN \\ \dot{I} &= +\beta SI - gI - dIN \\ \dot{R} &= gI - dRN. \end{aligned} \tag{3.8}$$

Unlike with most of the other models considered in this section, the standard birth pulse

$$S(t^+) = S(t^-) + x \qquad \text{where } t = n\tau,\ n \in \mathbb{N},$$

where $x = 1 - e^{-d\tau}$, does not preserve the population size from one year to the next. So a different formula for x is required.

Summing Equations 3.8 obtains the following equation for the rate of change of the total population density N:

$$\dot{N} = -dN^2$$

as $S + I + R = N$. This can be solved by separation of variables:

$$\begin{aligned} \int_{N_0}^{N} \frac{\mathrm{d}N}{N^2} &= \int_0^t -d\mathrm{d}t \\ \left[-\frac{1}{N}\right]_{N_0}^{N} &= [-dt]_0^t . \end{aligned}$$

Assuming that $N_0 = 1$

$$N = \frac{1}{1 + dt}. \tag{3.9}$$

For the population density to be preserved over a year x must satisfy

$$x = N(0) - N(\tau)$$
$$x = 1 - \frac{1}{1 + d\tau}.$$

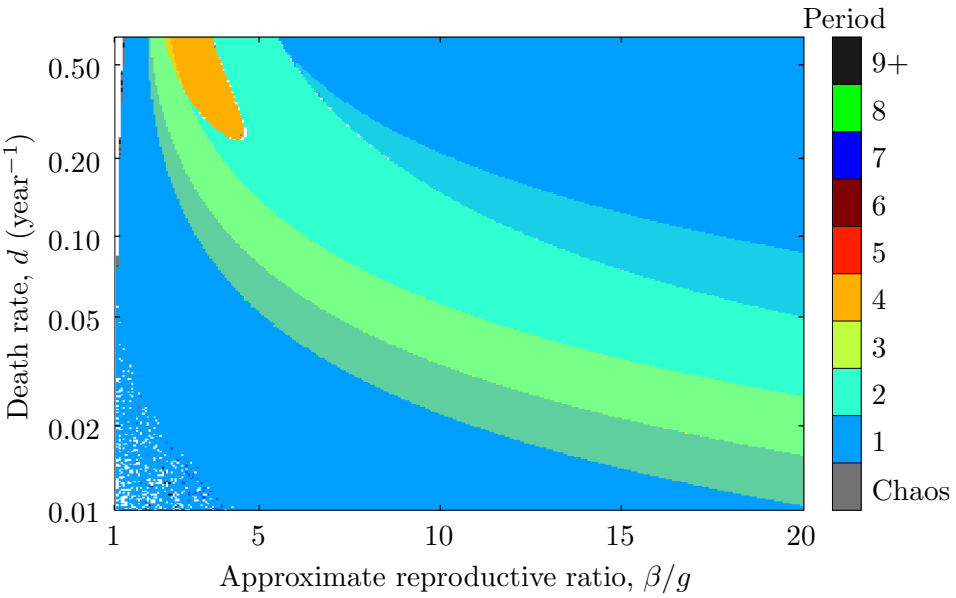

Figure 3.27: Attractors found for the SIR model with density dependent death (Equations 3.8 on the preceding page) after pushing out for $g = 0.075$.

Figure 3.27 shows the results for pulsed SIR model with density dependent death, using the new formula for x. The periodicity of the dynamics are almost identical to those from the standard pulsed SIR model (Figure 2.14 on page 54). The only differences being an apparent slight upward stretching, and the period three region extending to higher β/g so that it overlaps the period four region slightly.

To try and understand these results the R_0 for this system was calculated (cf. Lemma 2.1 on page 29). With $I = 0$ the S equation becomes

$$\begin{aligned} \dot{S} &= -dSN \\ &= \frac{-dS}{1 + dt}. \end{aligned}$$

Again this can be solved by separation of variables

$$\begin{aligned}
\int_{S_0}^{S} \frac{\mathrm{d}S}{S} &= \int_0^t \frac{-d}{1+dt}\mathrm{d}t \\
[\ln S]_{S_0}^{S} &= [-\ln(1+dt)]_0^t \\
\ln\left(\frac{S}{S_0}\right) &= -\ln(1+dt) \\
S &= \frac{S_0}{1+dt}.
\end{aligned}$$

and since, by the definition of R_0, a wholly susceptible population is being considered,

$$S = \frac{1}{1+dt}. \tag{3.10}$$

Notice that this is the same as the expression for N obtained above. This is because a wholly susceptible population is being considered.

R_0 is now given by (*cf.* Section 1.3 on page 9)

$$\begin{aligned}
R_0 &= (\text{infectious period}) \times \begin{pmatrix}\text{average rate at which}\\ \text{secondary cases are produced}\end{pmatrix} \\
&= \frac{\beta}{\tau}\int_0^\tau \frac{1}{g+dN} \times S|_{I=0}\,(t)\mathrm{d}t \\
&= \frac{\beta}{\tau}\int_0^\tau \frac{1}{g+dN}\frac{1}{1+dt}\mathrm{d}t \qquad \text{by Equation 3.10} \\
&= \frac{\beta}{\tau}\int_0^\tau \frac{1}{g+d+gdt}\mathrm{d}t \qquad \text{by Equation 3.9 on page 122} \\
&= \frac{\beta}{\tau}\left[\frac{\ln(g+d+gdt)}{gd}\right]_0^\tau \\
&= \frac{\beta}{gd\tau}\ln\left(\frac{g+d+gd\tau}{g+d}\right)
\end{aligned} \tag{3.11}$$

Figure 3.28 on the next page shows a contour plot of R_0 over parameter space for this model and the standard pulsed SIR model. This shows a shear to the left relative to R_0 for the standard pulsed SIR model, in agreement with the apparent upward stretching seen in the period plot (Figure 3.27 on the preceding page). There is also good correlation between the edge of the period one region and the $R_0 = 1$ contour.

The clear correlation between the shift in the period transitions and R_0 is

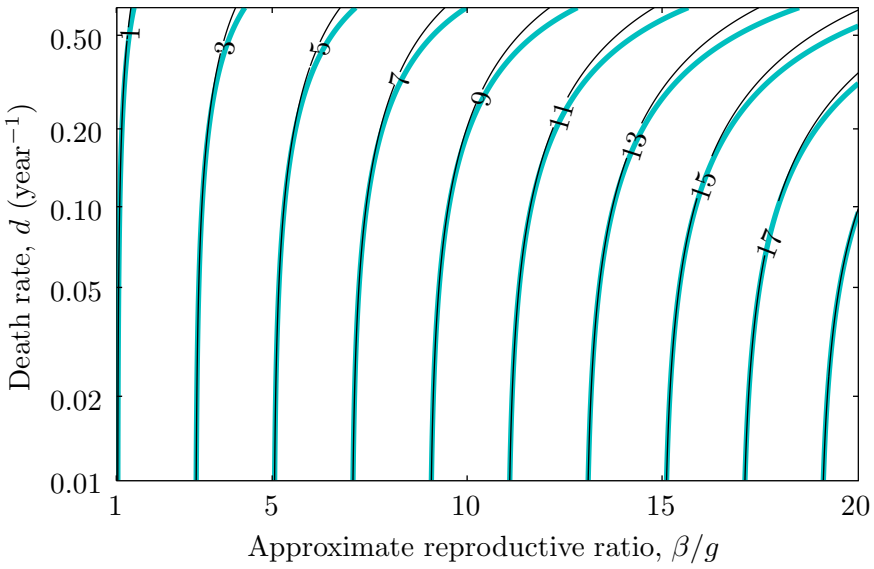

Figure 3.28: R_0 for the SIR model with density dependent death described by Equations 3.8 on page 122 (black lines), compared to that of the standard pulsed SIR model (blue lines).

a strong indicator that the shift in R_0 is the cause of the shift in the period transitions but it cannot offer a complete explanation of the behaviour. This is possibly because R_0, by definition, only describes behaviour of very low levels of infection, so utilising it to predict global behaviour is somewhat flawed. In order to understand the shift in the transitions between periods it is first necessary to understand what causes these transitions in the first place. This is not currently well understood, so it is impossible to draw conclusions directly relating the shift to parameters such as R_0.

3.3.7 Distribution of infectious and latent periods

The standard SIR model assumes that the infectious periods of individuals are distributed exponentially meaning that, for example, the probability of recovery is independent from the time since infection [D'Onofrio, 2004, Lloyd, 2001b]. The realism of this assumption has been questioned and alternative distributions tested [Anderson and Watson, 1980, Bailey, 1964]. Statistical analysis of infected populations has shown that the infectious and latent periods, for measles and infectious hepatitis at least, have a well defined mean

and small standard deviation [Bailey and Alff-Steinberger, 1970], in other words the infectious, or latent periods are likely to be close to their mean, and unlikely to be shorter or longer. The incorporation of non-exponential distributions for the infectious and latent periods can lead to models with complex integro-differential or partial differential equations [Lloyd, 2001b].

However, a simple method exists to incorporate non-exponential distributions into the compartmental models studied here. The method of stages as used by Anderson and Watson [1980], Bailey [1964] involves replacing the single infected (or exposed) class with a series of n classes or stages. Infected individuals pass though each stage in turn and finally into the recovered class (or the infected in the case of exposed individuals). The time spent in each stage is identically exponentially distributed and the total time spent in the infectious class is then gamma distributed [Lloyd, 2001b]. The individual stages have no biological meaning [D'Onofrio, 2004]. The probability density function for this distribution is given by

$$f_{gn,n}(t) = \frac{(gn)^n}{\Gamma(n)} t^{n-1} e^{-gnt}, \tag{3.12}$$

where $\Gamma(n)$ is the gamma function. The mean of this distribution is $1/g$ and it has standard deviation $1/(gn)$. Notice that for $n = 1$ Equation 3.12 becomes

$$f'_g(t) = ge^{-gt} \tag{3.13}$$

the exponential distribution. Figure 3.29 on the following page shows the gamma distribution for various values of n including the special case $n = 1$.

Pulsed SIR model with gamma distributed infectious period

The pulsed SIR model (Equations 2.1 on page 29) can be made more realistic by using the method of stages described above so that the infectious period is gamma distributed. This model is studied by Lloyd [2001a,b].

The SIR model with n infectious stages is given by the following equations:

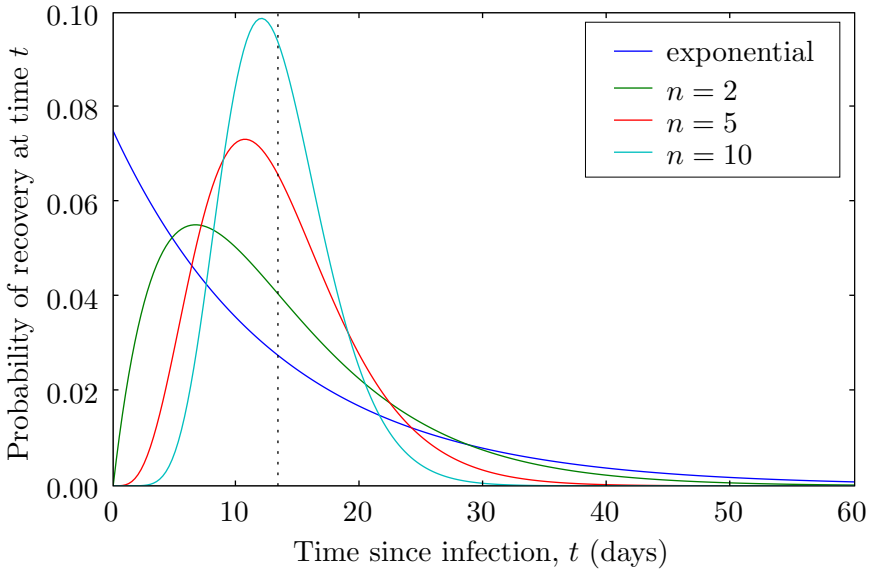

Figure 3.29: The probability density function of the gamma distribution (Equation 3.12 on the preceding page) for $n = 1, 2, 5, 10$ and $g = 0.075$. In the special case $n = 1$ the exponential distribution. is obtained. The dashed line shows the mean, $1/g \approx 13.3$ days.

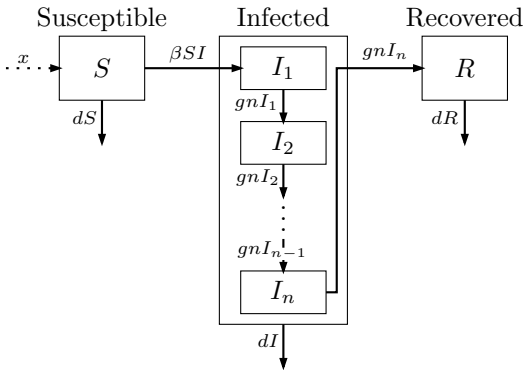

Figure 3.30: Box diagram for the SIR model with gamma distributed infectious period.

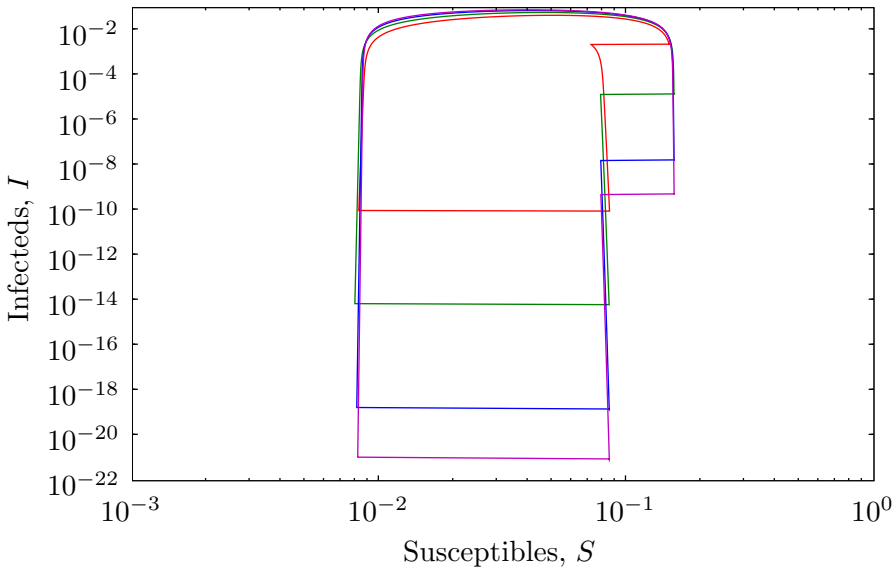

Figure 3.31: Phase plot for the the SIR model with gamma distributed infectious period, showing how the dynamics vary as the number of infected classes changes. Parameters: $\beta/g = 20$, $x = 0.077$, $g = 0.075$ throughout, all attractors are period 2. Red: 1 I class (*i.e.* the standard pulsed SIR model), green: 2 I classes, blue: 5 I classes, magenta: 10 I classes.

$$\begin{aligned} \dot{S} &= -\beta SI - dS \\ \dot{I}_1 &= \beta SI - gnI_1 - dI_1 \\ \dot{I}_2 &= gnI_1 - gnI_2 - dI_2 \\ &\vdots \\ \dot{I}_n &= gnI_{n-1} - gnI_n - dI_n \\ \dot{R} &= gnI_n - dR. \end{aligned} \tag{3.14}$$

Where $I = \sum_{j=1}^{n} I_j$. The birth pulse is applied as usual to the susceptibles class every year:

$$S(t^+) = S(t^-) + x \qquad \text{where } t = n\tau,\ n \in \mathbb{N}.$$

Figure 3.31 shows how a typical period two attractor for the pulsed SIR model with gamma distributed infectious period changes as the number of infectious classes n increases from 1 (the standard pulsed SIR model with

a exponentially distributed infectious period) to 10. The increase in the number of classes seems to mainly change the how low the level of infection drops between epidemics. For $n = 1$ the level of infection drops to around 10^{-10} after a major epidemic, and reaches 10^{-3} when the second pulse is applied, triggering the major epidemic. Contrast this with the $n = 10$ case there the level of infection drops to 10^{-23} after a major epidemic and reaches 10^{-9} at the time the second pulse is applied. Larger n also leads to a slightly increased maximum level of infection. The lower values of I may mean that in a real population the infection has a higher chance of becoming extinct due to stochastic variations.

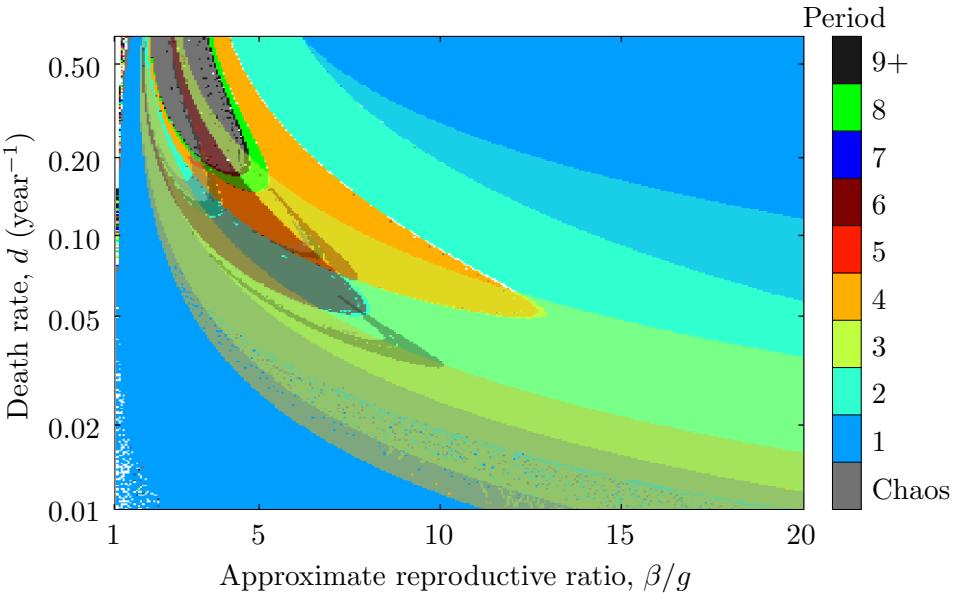

Figure 3.32: Attractors found for the SIR model with 2 I classes (Equations 3.14 on page 126) after pushing out for $g = 0.075$.

Figure 3.32 to Figure 3.34 on pages 129–130 show the periods of attractors found for $n = 2, 5$ and 10, all with $g = 0.075$. The main point to notice about these results is their greater complexity than their exponential counterpart (Figure 2.14 on page 54). In fact the complexity for $n = 2$, compares roughly to the level achieved by increasing g to 0.100 (Figure 2.15 on page 54) in the exponential case. As n increases so does the complexity and a large region of chaotic dynamics opens up in the upper left quadrant of parameter space. The data in all three of these plots is not as clean as for previous

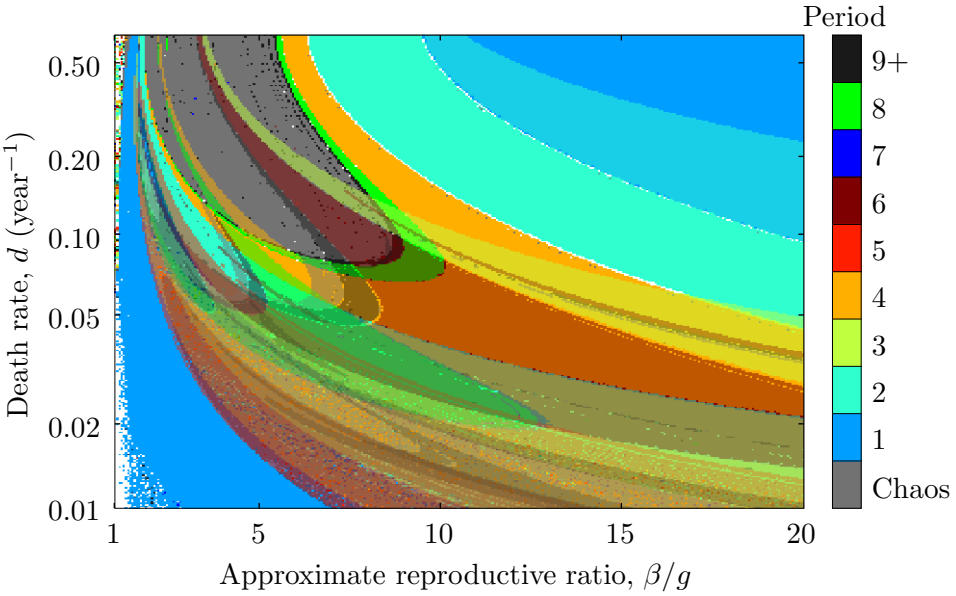

Figure 3.33: Attractors found for the SIR model with 5 I classes (Equations 3.14 on page 126) after pushing out for $g = 0.075$.

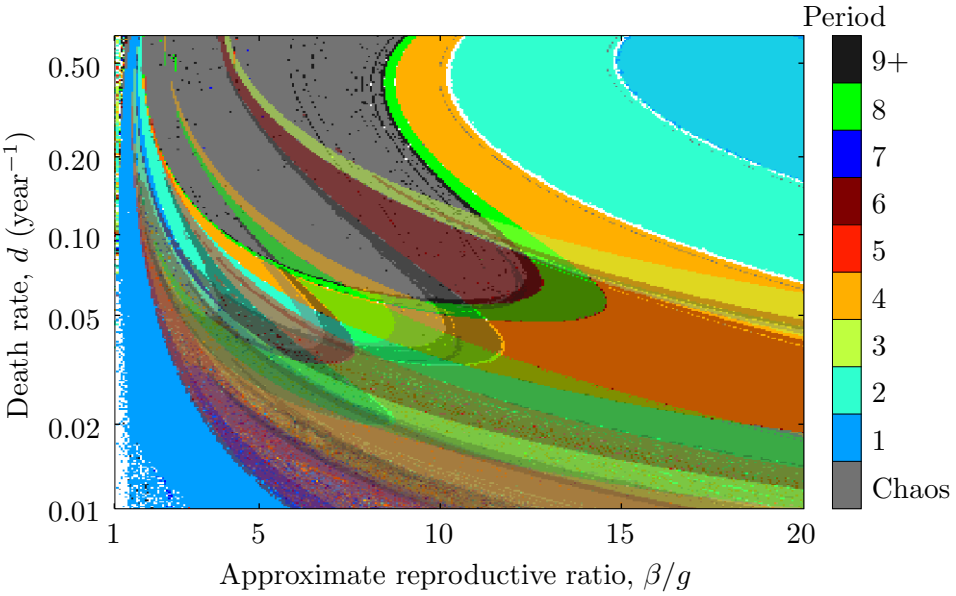

Figure 3.34: Attractors found for the SIR model with 10 I classes (Equations 3.14 on page 126) after pushing out for $g = 0.075$.

models. This is because this model is much more computationally intensive to run. Refining the data, removing speckling would have required too much computational effort. The results broadly agree with those of Lloyd [2001b] in that as n increases the dynamics become more complex, with the appearance of more higher period dynamics and a more complicated bifurcations structure. Further comparison are hard because Lloyd only considered a one dimensional parameter space.

Pulsed SEIR model with gamma distributed infectious and latent periods

Taking this one step further the method of stages is now applied to the pulsed SEIR model so that both the infectious and latent periods are gamma distributed. This system was first seen in Anderson and Watson [1980], though without any forcing. A further generalisation of the un-forced model is given in Andersson and Britton [2000] where the life expectancy follows a gamma distribution as well. Also D'Onofrio [2004] uses an SEIR model with gamma distributed infectious and latent periods combined with a pulsed vaccination strategy (see Subsection 3.3.3 on page 110 for a more detailed discussion for pulse vaccination models).

After applying the method of stages with n infectious stages and m latent stages to the SEIR model the equations become:

$$\begin{aligned}
\dot{S} &= -\beta SI - dS \\
\dot{E}_1 &= \beta SI - \alpha m E_1 - dE_1 \\
\dot{E}_2 &= \alpha m E_1 - \alpha m E_2 - dE_2 \\
&\vdots \\
\dot{E}_m &= \alpha m E_{m-1} - \alpha m E_m - dE_m \\
\dot{I}_1 &= \alpha m E_m - gnI_1 - dI_1 \\
\dot{I}_2 &= gnI_1 - gnI_2 - dI_2 \\
&\vdots \\
\dot{I}_n &= gnI_{n-1} - gnI_n - dI_n \\
\dot{R} &= gnI_n - dR.
\end{aligned} \tag{3.15}$$

Here $I = \sum_{j=1}^{n} I_j$ and $E = \sum_{j=1}^{m} E_j$. Again a birth pulse is applied to the susceptibles class in the normal way.

Figure 3.36 on the following page shows typical period two dynamics for

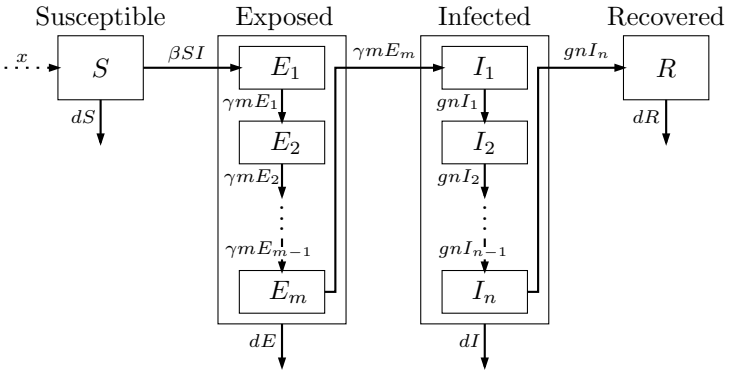

Figure 3.35: Box diagram for the SEIR model with gamma distributed infectious and latent periods.

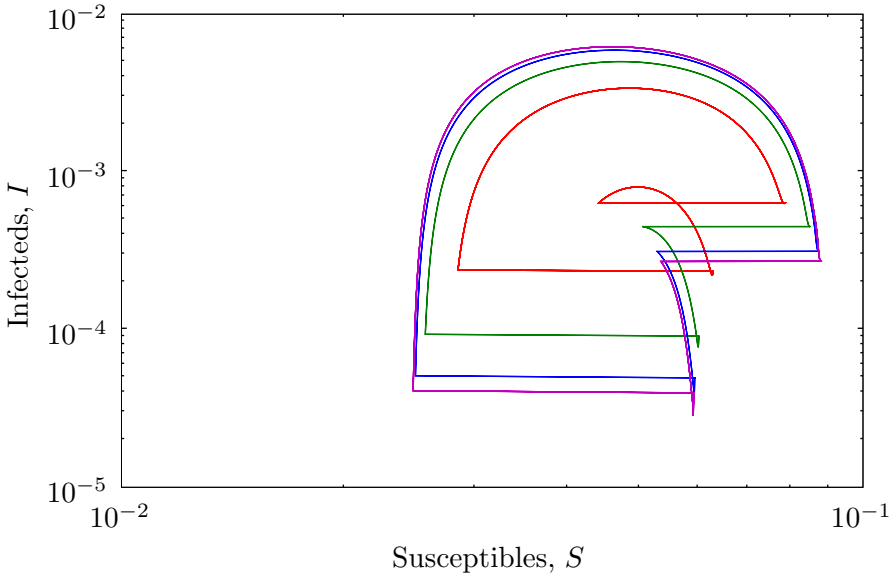

Figure 3.36: Phase plot for the the SEIR model with gamma distributed infectious and latent periods, showing how the dynamics vary as the number of infected and latent classes increases. Parameters: $\beta/g = 20$, $x = 0.034$, $g = 0.075$ throughout, all attractors are period 2. Red: 1 E class and 1 I class (*i.e.* the pulsed SEIR model), green: 2 E and 2 I classes, blue: 5 E and 5 I classes, magenta: 10 E and 10 I classes.

the pulsed SEIR model with gamma distributed infectious and latent periods as the number of infections and latent classes is increased. The general trend as m and n are increased from $m = n = 1$ (representing the pulsed SEIR model with exponential infectious and latent periods), to $m = n = 10$, is that the range of both S and I expands, leading to an increased peak level of infection as well as a decreased minimum level between epidemics. For the case $n = m = 1$, there is a smaller minor epidemic in years between the major ones, however this is not present in for larger values of m and n, it appears that it does not have time to build up sufficient infection before the next pulse is applied. Another feature not seen before is the small "tail" after pulse following the major epidemic. It appears that the level of infection and the level of susceptibles continues to fall for a short time even after the pulse is applied, the effect is more pronounced for larger numbers of classes. This effect is due to the change in latent period distribution. In the pulsed SEIR model with exponentially distributed infectious period the probability of an individual having a zero or very small latent period is high (see Figure 3.29 on page 127). However, as the number if latent classes increases this probability decreases rapidly, and individuals are most likely to have a latent period close to the mean, $1/\alpha$. Thus there is a now a delay, approximately equal to the latent period before any of the newly born susceptibles become infected. During this time the level of infection continues to drop as infected individuals recover or die.

Figure 3.37 to Figure 3.39 on pages 134–135 show the periods of attractors found for $m = n = 2, 5$ and 10. For the case $m = n = 2$ the qualitative structure of tongues is similar to that seen in the standard pulsed model and the pulsed SEIR model. The main difference in this case is that they appear wider and there is no upper region of period one dynamics. It is almost as though smaller parameter space has been considered. For the cases $m = n = 5$ and $m = n = 10$ there is a very large region of chaotic dynamics, as wall as some higher period dynamics. Again only the lower regions area of period one dynamics is present.

It has been verified that in the cases $m = n = 2$ and $m = n = 5$ the speckling in the lower left quadrant of parameter space is because the period finding algorithm (described in Box 2.1 on page 40) has not allowed enough time for the they system to converge to the period one attractor. The length of time allowed is a trade off between accuracy and computational effort

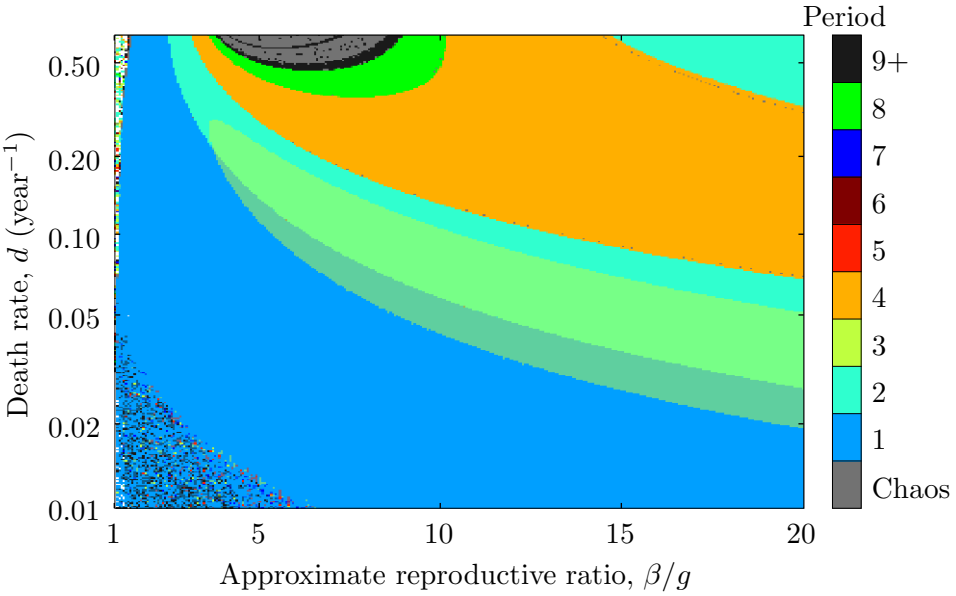

Figure 3.37: Attractors found for the pulsed SEIR model with 2 I and 2 E classes (Equations 3.15 on page 131) after pushing out for $g = 0.075$.

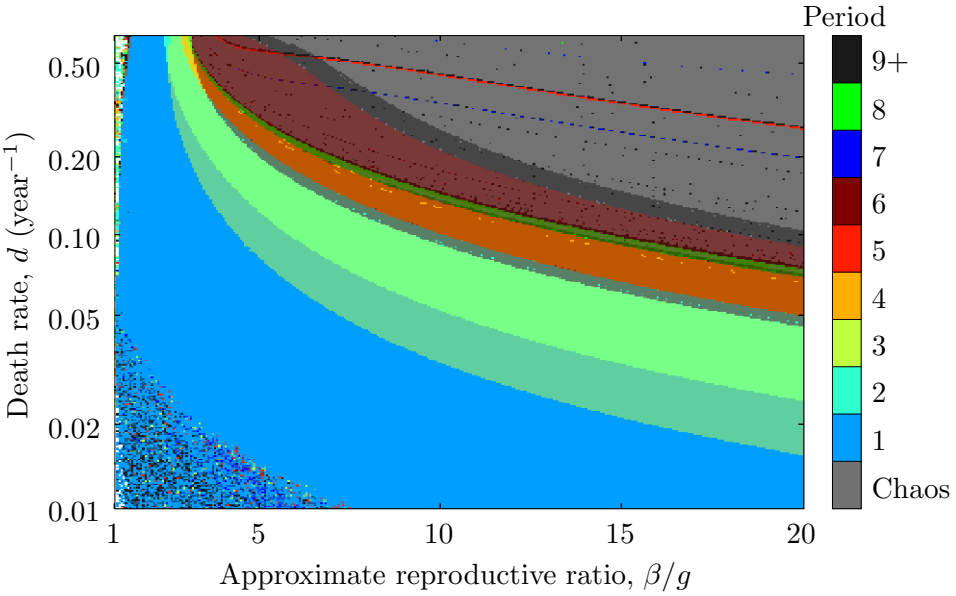

Figure 3.38: Attractors found for the pulsed SEIR model with 5 I and 5 E classes (Equations 3.15 on page 131) after pushing out for $g = 0.075$.

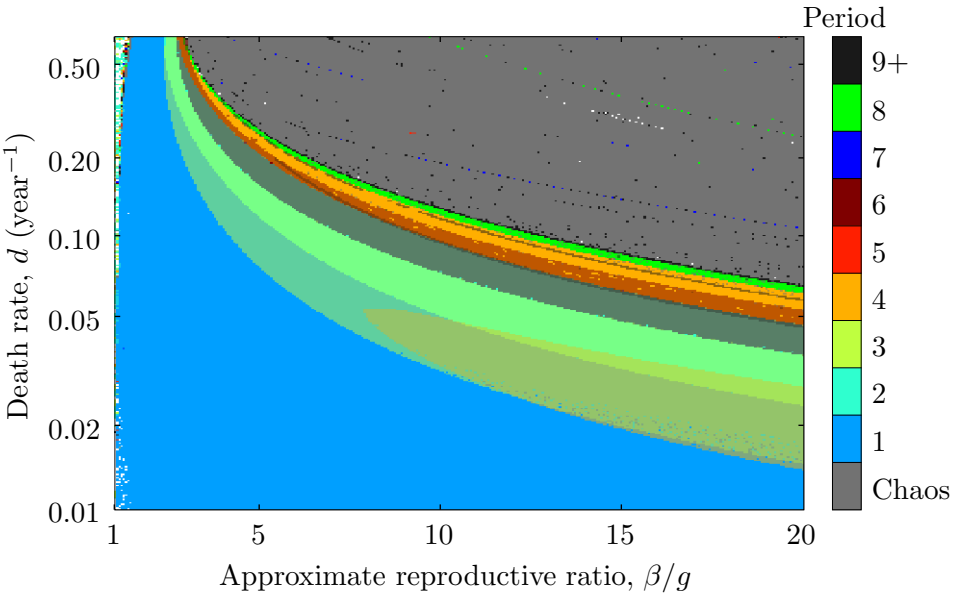

Figure 3.39: Attractors found for the pulsed SEIR model with 10 I and 10 E classes (Equations 3.15 on page 131) after pushing out for $g = 0.075$.

expended.

In summary the introduction of gamma distributed infectious and latent periods introduces much greater complexity. It is conjectured that because the standard deviation of the gamma is so much smaller than that of the exponential it replaces, there is much less damping of the birth pulse so that rapid transitions also occur in the exposed and infected classes. This is discussed at length in Section 3.4 on page 138.

3.3.8 Imports

This case considers what happens when a small number of infectious imports ϵ is added [Bartlett, 1956, 1957]. This can be considered as an external source of infection, this maybe a reservoir of infection within a population of a different species. In this case ϵ is chosen to be constant, but it could vary to model the size of an external population, or the amount of mixing between the two populations.

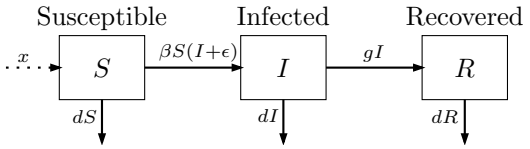

Figure 3.40: Box diagram for the SIR model with imports.

The model is described by the following equations:

$$\begin{aligned} \dot{S} &= -\beta S(I+\epsilon) - dS \\ \dot{I} &= +\beta S(I+\epsilon) - gI - dI \\ \dot{R} &= gI - dR. \end{aligned} \tag{3.16}$$

Here ϵ is the size of the imports. The annual birth pulse is applied to the susceptible class in the usual way:

$$S(t^+) = S(t^-) + x \qquad \text{where } t = n\tau,\ n \in \mathbb{N}.$$

Note that strictly speaking the death rate or pulse size should be adjusted to balance the imports and ensure comparability with other models. However, as ϵ is assumed small, this can be safely omitted for simplicity.

The periods obtained across parameter space are shown in Figure 3.41 on the following page, for $\epsilon = 10^{-5}$, and Figure 3.42 on the next page, for $\epsilon = 10^{-10}$. It is clear that very small levels of imports, $\epsilon = 10^{-10}$, have little effect on the dynamics. The only real difference is that extinction does not occur along the left hand edge where for the standard pulsed SIR model $R_0 < 1$. This is what is to be expected as the imports are a mechanism to prevent extinction. It is in fact not possible to calculate R_0 for this system because the imports ensure that a infection free state cannot persist.

Figure 3.44 on page 139 shows the minimal I attained on the attractor, or attractors, at each point in parameter space for $\epsilon = 10^{-10}$. Comparing this to Figure 2.20 on page 57 the only noticeable difference is in the extinction region, where the minimum is now around 10^{-10}, which is less than the level of imports in some regions.

For a larger level of imports, $\epsilon = 10^{-5}$ the dynamics, illustrated in Figure 3.41 on the following page, differ more dramatically from those of the standard pulsed SIR model. Firstly, there are no period three and four dynamics, and secondly, there is no overlap between the upper period one

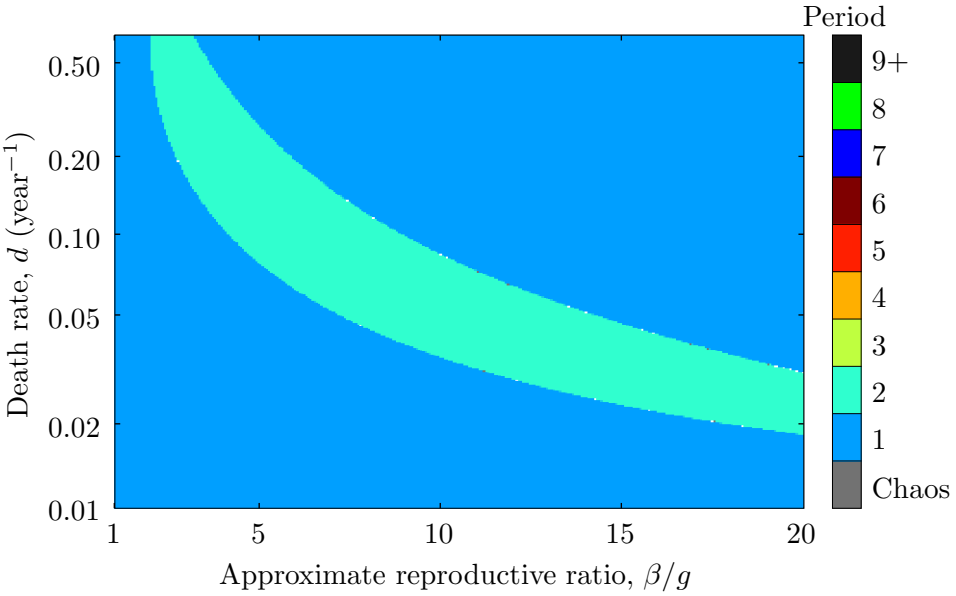

Figure 3.41: Period of attractors found for the SIR model with imports (Equations 3.16 on the previous page) after pushing out for $g = 0.075$ and $\epsilon = 10^{-5}$.

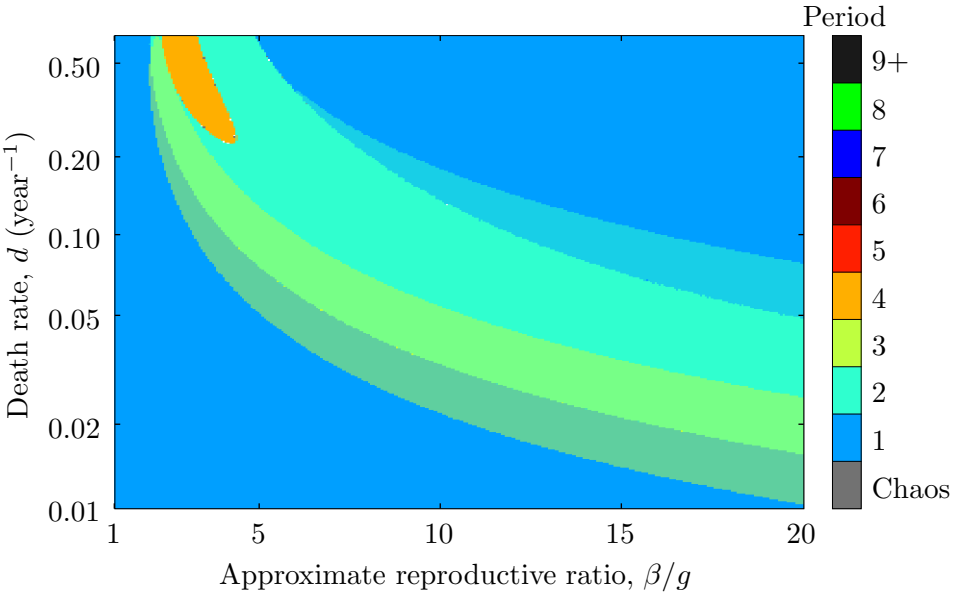

Figure 3.42: Period of attractors found for the SIR model with imports (Equations 3.16 on the previous page) after pushing out for $g = 0.075$ and $\epsilon = 10^{-10}$.

and period two regions. As with $\epsilon = 10^{-10}$ the is no extinction down the left edge. Also the minimum I around the attractors (Figure 3.43 on the next page) has increased, the minimum now being around 10^{-8} compared to around 10^{-11} for $\epsilon = 10^{-10}$ and the standard pulsed SIR model.

In summary the inclusion of imports into the standard pulsed SIR model in an effective tool for limiting the minimum values attained by I on the attractors of the system. This is important when applying these models to real, discrete populations, where due to stochastic effects, the density only need approach the inverse of the populations size for extinction to be a possibility. However, countering this by applying too higher level of imports significantly changes the behaviour of the system, eliminating higher period dynamics.

3.4 Conclusions

Broadly speaking the results of the previous chapter have been shown to be robust to a wide range of perturbations, with only the most extreme causing significant qualitative differences in the results.

For the majority of parameter space the attractors exhibited in Figure 2.14 on page 54 were shown to be stable to small perturbations in S and I. Only in the both small d and small β/g region of parameter space showed any instability. This is illustrated by the slow convergence to the attractors in that region. However the dynamics still show period one like behaviour while converging to the attractor as is seen in Figure 3.2 on page 92. Consequently, the pulsed SIR model is likely to predict the possible periods of a real biological system accurately, wherever in parameter space it falls.

An instantaneous pulse of births is realistic for some animal populations (*e.g.* Saiga antelope), but for others may still be highly seasonal, but have a larger temporal spread. The second section in this chapter (Section 3.2 on page 92) shows that the qualitative dynamics of the pulsed SIR model persist when a different seasonal birth patterns are used. Only those functions that have very smooth transitions from high to low birth rates, or have a high birth rate for most of the year, significantly change the periodicity of the dynamics. Perhaps the most surprising result is that when the births are modelled by a top hat function (Subsection 3.2.2 on page 96) the periodicity

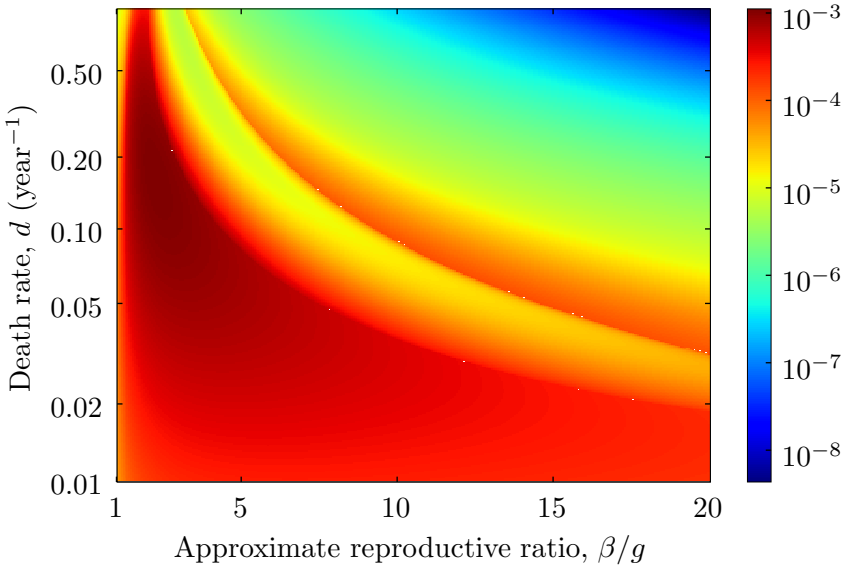

Figure 3.43: The minimum value of I attained on each attractor, or attractors, in Figure 3.41 on page 137. Parameters: $\epsilon = 10^{-5}$, $g = 0.075$.

.

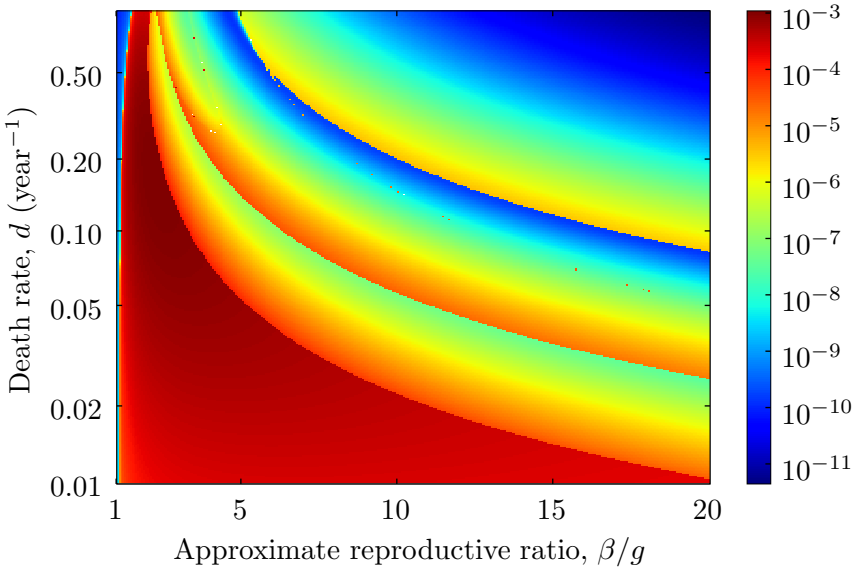

Figure 3.44: The minimum value of I attained on each attractor, or attractors, in Figure 3.42 on page 137. Parameters: $\epsilon = 10^{-10}$, $g = 0.075$.

of the dynamics remains virtually unchanged, even when the width of the pulse is 90 days—a quarter of a year!

These results are very important, because it means that the pulsed SIR model could be applied to a much larger range of populations. It even suggests that when fitting the seasonal births of a real population, it may not be necessary to have a detailed knowledge of distribution of births throughout the year, only a good idea of the total number of births occurring.

Further work on the birth function could include the use of functions designed to fit with observed birth rates showing different patterns of seasonality, rather than annual peaks already considered. For example, using a combination of a constant birth rate, and top hat functions to represent the pattern of biannual peaks above the mean observed in the UK cattle population (Figure 2.3 on page 28).

The changes to the structure of the model, effectively changing the underlying assumptions made in formulating the model, investigated in Section 3.3 on page 101 also seem not to affect the qualitative dynamics of the pulsed SIR model.

Perhaps the lower levels of complexity for the pulsed SEIR model, when the infectious period is compared to that of the pulse SIR model can be explained by thinking of the exposed class as adding damping in between the susceptible and infectious classes. When the birth pulse increases the number of susceptibles the transmission can not increase until more individuals become infectious, and they must pass though the exposed class first. The exponentially distributed latent period damps the birth pulse, preventing a sharp rise in infection and reducing the complexity of the dynamics.

The situation is slightly different when the pulsed SIR/SEIR models with gamma distributed infectious and latent periods are considered. Here, because the gamma distribution has a much smaller standard deviation, the exposed class mainly acts to delay, rather than damp, the sudden increase in the level of susceptibles being transmitted to the exposed and infectious classes. This served to actually increase the level of complexity for given infectious period.

Another change in model structure not considered here is adding age structure to the model by partitioning the S, I, and R classes into separate classes for different age groups. This technique is used extensively in the modelling of childhood infectious diseases such as measles (See Agur et al.

[1993], Bolker and Grenfell [1993], Hethcote [2000]). Also perhaps some spatial structure could be added by having separate S, I, and R classes for, for example, neighbouring cities.

Also worth considering is whether the dynamics illustrated here are a feature just a feature of models with pulsed births, or do they generalise to models where pulsed forcing is use to model other seasonal influences. The childhood model (Subsection 3.3.4 on page 114), which shifts the focus slightly by modelling deaths (departures) by a pulse as well as births (arrivals), shares many of the qualitative features with the pulsed SIR model. The vaccination pulse model (Subsection 3.3.3 on page 110) also shares many similarities with the pulsed SIR.

Another direction this work could be taken would be to introduce stochasticity into the model and see how robust the dynamics are to random perturbations. Randomness could be integrated into the model in several different ways. Adding some kind of randomness to the transmission terms would make the model more suitable for modelling smaller populations, or very low levels of infection. Another possibility would be to introduce a random element into the size, or timing of the birth pulse. One issue with stochastic models is how to deal with extinction when it occurs and one possible way to circumvent this is to use the imports model (Subsection 3.3.8 on page 135) as a base.

In conclusion the pulsed SIR model shows a great deal of robustness to several classes of perturbation, most of which leave the qualitative periodic dynamics unchanged. In general as the infectious period is increases, the complexity increases too, more higher period dynamics are seen, leading to substantial areas of parameter space showing chaotic behaviour.

Chapter 4

Analytical methods

The previous two chapters focused almost exclusively on the use of numerical methods to understand the dynamics of pulsed SIR models. This chapter tries to redress the balance, by using analytical techniques to verify some of the results from previous chapters.

Numerical methods were chosen in the first place because the pulsed SIR model is hard to treat analytically. The nonlinear transmission terms make it impossible to directly integrate the ODEs, and the pulsing terms prevent the use of some of the standard tools for analysing systems of ODEs.

As discussed in Section 2.2 on page 34, within the chosen parameter space there are regions where the numerics can be more computationally demanding, and less reliable. There are two such areas, small x; representing hosts with a long life expectancy, and R_0 close to 1; considering pathogens that can not easily invade their target population. It is, however, possible to do some analytical work in these areas.

This chapter presents three analytical approximations to the standard pulsed SIR model and the pulsed simple SIR model. Progress is made by considering only specific areas of parameter space, sometimes coinciding with areas of parameter space where the numerics are either inaccurate, or take a long time to converge.

The first approximation uses multi-scale techniques to approximate the dynamics of the pulsed SIR model for small x, the limiting case of which is the un-forced simple epidemic model. The approximation affirms the presence of annual dynamics in the small x region of parameter space, confirming the numerical results of Chapter 2 on page 24 (see Figure 4.2 on page 154). An

error analysis is performed, and the errors are verified to be of the correct order. It is noted that the same approximation could be performed for R_0 close to unity.

By assuming a large infectious period it is possible to split the dynamics of an attractor of the pulsed simple SIR model into four distinct phases: growth, epidemic, decay and birth pulse. The second approximation exploits this giving equations for the S and I in each phase. The epidemic and pulse phases are assumed to be instantaneous. Determining the time spent in the growth phase is complex and, has to be done numerically. If the time spent in the growth phase is determined to be a year or more, then no epidemic occurs that year. It is noted that the same approximation could be carried out for the standard pulsed SIR model, but it would inevitably be more complex.

The final approximation is a simplification of the previous large g approximations. By assuming that, at the peak of the epidemic, the density of infecteds is $\mathcal{O}(1)$ it is possible to obtain an expression for the time spent in the growth phase directly. A transformation normalising S with respect to R_0 and considering the logarithm of I leads to a simple discrete model with only a single parameter. The discrete model still shows complex multi-annual dynamics, and it is in close agreement with the pulsed simple SIR model. Finally, the results are related back to the pulsed simple SIR model.

4.1 Multi-scale analysis for small x

One significant difficulty with calculating the dynamics of the pulsed SIR model is that the numerics can break down (because the magnitude of the pulsing approaches the numerical error) and convergence times can be very long when the magnitude of pulsing is small. Fortunately, this limit is one that can be investigated analytically. A multi-scale analysis of the system is performed in the small x region of parameter space and the results are compared to those obtained by numerical integration. The aim of this analysis is to provide an insight into the possible dynamics of this region of parameter space.

To ease the analysis, a slightly modified version of the standard pulsed

SIR model (Equations 2.1 on page 29) system is considered:

$$\begin{aligned} \dot{S} &= -\beta SI - dS + B'(t) \\ \dot{I} &= \beta SI - aI \end{aligned} \tag{4.1}$$

Here the new parameter a represents the loss of infection due to both natural mortality and recovery and can be related to the original parameters as $g + d$, noting that d is small. As before, $B'(t)$ gives the instantaneous birth rate, and the cumulative birth rate since $t = 0$ is given by

$$B(t) = \left\lfloor \frac{t}{\tau} \right\rfloor x. \tag{4.2}$$

For this analysis the pulse size x is set to be a small parameter. Recall that

$$\begin{aligned} x &= 1 - e^{-d\tau} \\ &= d\tau + \frac{d^2\tau^2}{2} + \mathcal{O}(d^3), \end{aligned} \tag{4.3}$$

so that the corresponding natural death rate d is also small. Thus the multi-scale analysis proceeds by analysing the dynamics at different orders of d.

The state variables S and I are expressed as Taylor series in d:

$$S = S_0 + dS_1 + d^2S_2 + \mathcal{O}(d^3) \tag{4.4}$$

$$I = I_0 + dI_1 + d^2I_2 + \mathcal{O}(d^3). \tag{4.5}$$

Similarly, the birth pulse function is expanded as:

$$B(t) = B'_0(t) + dB'_1(t) + d^2B'_2(t) + \mathcal{O}(d^3). \tag{4.6}$$

The multi-scale analysis attempts to find closed forms for the coefficients of the above Taylor series (Equation 4.4 to Equation 4.6 on the current page), the values of which are given with the following theorem.

Theorem 4.2 *Where a periodic orbit exists of the pulsed SIR model (as defined in Equations 4.1) for small x, and hence small d, then it is well approximated by the second order approximation given in Equation 4.4 and Equa-*

tion 4.5 on the previous page with:

$$\begin{aligned} S_0(t) &= \frac{a}{\beta} \\ S_1(t) &= \frac{\tau}{2} - t \\ S_2(t) &= \textit{An annual function} \\ I_0(t) &= 0 \\ I_1(t) &= \frac{1}{a} - \frac{1}{\beta} \\ I_2(t) &= \frac{1}{2}\left(\frac{\beta}{a} - 1\right)(\tau t - t^2) + \frac{(a-\beta)\tau^2 - 6\tau}{12a} \end{aligned}$$

for $0 \leq t < \tau$*. The dynamics are, to order* d^2*, annual.*

Notice how the point $(S_0(t), dI_1(t)) = (\frac{g+d}{\beta}, \frac{d}{g+d} - \frac{d}{\beta})$, about which the trajectories predicted by this approximation oscillate is the endemic fixed point of the un-forced SIR model with continuous births (see Section 1.4 on page 11).

Corollary 4.1 *The dynamics of an annual periodic orbit where one exists can be bounded within a ball of* $\mathcal{O}(d)$*.*

Proof: The result follows directly from Theorem 4.2 by the fact that $S_0(t)$ and $I_0(t)$ are constant, so S and I can only vary by a maximum of $\mathcal{O}(d)$. □

The proof of Theorem 4.2 on the previous page is tackled as a series of lemmas, deriving closed forms for each of the coefficients S_0, S_1, S_2 and I_0, I_1, I_2 and various other intermediate results. The explicit calculation of S_2 is omitted because the algebra is complex and the result uninformative.

Before proceeding with the proof it is informative to make a few observations. Firstly, the ODEs for coefficients of the Taylor series for S and I are derived. Substituting into the $\dot{S}$ equation of Equations 4.1 on the preceding page and collecting terms by their order of d yields:

$$\mathcal{O}(d^0): \quad \dot{S}_0 = -\beta S_0 I_0 + B_0'(t) \tag{4.7}$$

$$\mathcal{O}(d^1): \quad \dot{S}_1 = -\beta(S_0 I_1 + I_0 S_1) - S_0 + B_1'(t) \tag{4.8}$$

$$\mathcal{O}(d^2): \quad \dot{S}_2 = -\beta(I_2 S_0 + I_1 S_1 + I_0 S_2) - S_1 + B_2'(t). \tag{4.9}$$

Following the same procedure with the $\dot{I}$ equation gives:

$$\mathcal{O}(d^0): \quad \dot{I}_0 = \beta S_0 I_0 - a I_0 \tag{4.10}$$

$$\mathcal{O}(d^1): \quad \dot{I}_1 = \beta(S_0 I_1 + I_0 S_1) - a I_1 \tag{4.11}$$

$$\mathcal{O}(d^2): \quad \dot{I}_2 = \beta(I_2 S_0 + I_1 S_1 + I_0 S_2) - a I_2. \tag{4.12}$$

Lemma 4.4 *The $\mathcal{O}(1)$, $\mathcal{O}(d)$ and $\mathcal{O}(d^2)$ components of the cumulative birth function B are given by:*

$$\begin{aligned} B_0(t) &= 0 \\ B_1(t) &= \left\lfloor \frac{t}{\tau} \right\rfloor \tau \\ B_2(t) &= -\left\lfloor \frac{t}{\tau} \right\rfloor \frac{\tau^2}{2}. \end{aligned}$$

Proof: To expand the cumulative birth function B (Equation 4.2 on page 144) note that only x depends on d, so the expansion of x, as given in Equation 4.3 on page 144, is substituted into Equation 4.2 yielding

$$B(t) = \left\lfloor \frac{t}{\tau} \right\rfloor \left(d\tau - \frac{d^2\tau^2}{2} + \mathcal{O}(d^3) \right).$$

The result follows by using Equation 4.6 on page 144 to substitute for $B(t)$ and equating terms of the same order of d. □

Observation 4.1 *I_0 the $\mathcal{O}(1)$ component of I is zero.*

Proof: Consider

$$\int_0^{n\tau} I \qquad \text{as} \quad n \to \infty.$$

It is clear that the total number of recoveries is less than the total births, because there are losses due to death, so

$$\int_0^{n\tau} gI < nx \qquad \text{as} \quad n \to \infty$$

Given that

$$x = 1 - e^{-d\tau} \approx d\tau + \mathcal{O}(d^2),$$

so $x = \mathcal{O}(d)$ and hence $I = \mathcal{O}(d)$. Thus $I_0 = 0$.

□

Lemma 4.5 *The average of S, over one year is a/β, i.e. $\bar{S} = \frac{a}{\beta}$. Moreover, S_0 is constant and $S_0(t) = a/\beta$.*

Proof: The $\dot{I}$ equation of Equations 4.1 on page 144 states that

$$\dot{I} = (\beta S - a)I.$$

Now integrating this with respect to t

$$\begin{aligned} I &= I_0(0) \exp\left(\int_0^t (\beta S - a)\mathrm{d}t\right) && (4.13) \\ &= I_0(0) \exp\left(\beta \int_0^t S\mathrm{d}t - at\right). && (4.14) \end{aligned}$$

A key premise of Theorem 4.2 on page 144 is that the dynamics being considered lie on a periodic orbit, so it is clear that I is bounded, that is, there exists ϵ with $0 < \epsilon \leq I_0 < 1$ such that

$$\epsilon \leq I(t) < 1 \quad \forall t \in \mathbb{R}^+.$$

In fact I can be shown to be more generally bounded by some of the results of Chapter 2 on page 24. By assuming that $R_0 > 1$, the disease can never die out, so I must be bounded above zero. Equally I is bounded above by 1 since N, the total population density, has a sawtooth behaviour achieving a maximum of 1.

Returning to the proof, the above inequality becomes

$$\begin{aligned} \epsilon \leq I_0(0) \exp\left(\beta \int_0^t S\mathrm{d}t - at\right) < 1 \\ \frac{\epsilon}{I_0(0)} \leq \exp\left(\beta \int_0^t S\mathrm{d}t - at\right) < \frac{1}{I_0(0)}. \end{aligned}$$

Now this inequality must hold for all $I_0(0)$, so the upper bound can be replaced with 1. Taking logs:

$$\log\left(\frac{\epsilon}{I_0(0)}\right) \leq \beta \int_0^t S\mathrm{d}t - at \leq 0.$$

Rearranging this to isolate the integral gives:

$$\frac{1}{\beta}\log\left(\frac{\epsilon}{I_0(0)}\right)+\frac{at}{\beta}\leq\int_0^t S\mathrm{d}t\leq\frac{at}{\beta}.$$

Now dividing though by t and taking the limit as $t\to\infty$ gives:

$$\lim_{t\to\infty}\left(\frac{1}{\beta t}\log\left(\frac{\epsilon}{I_0(0)}\right)+\frac{a}{\beta}\right)\leq\lim_{t\to\infty}\left(\frac{1}{t}\int_0^t S\mathrm{d}t\right)\leq\lim_{t\to\infty}\frac{a}{\beta}$$

Both the left and right hand sides evaluate to a/β, and hence

$$\bar{S}=\frac{a}{\beta}.$$

Now as

$$\bar{S}=\bar{S_0}+d\bar{S_1}+d^2\bar{S_2},$$

by the linearity of the averaging operator $\bar{\cdot}$,[1] and as here $a/\beta=\mathcal{O}(1)$ it is clear that

$$\bar{S_0}=\frac{a}{\beta}\quad\text{and}\quad\bar{S_1},\bar{S_2}=0.$$

Finally, by Observation 4.1 on page 146 and Equation 4.7 on page 145

$$\dot{S_0}=0,$$

it is possible to conclude that

$$S_0(t)=S_0(0)=\frac{a}{\beta}.$$

□

Lemma 4.6 *I_1 is constant.*

Proof: By Observation 4.1 on page 146 and Lemma 4.5 it is possible to

[1] This is only guaranteed if the system possesses a periodic attractor that is uniformly hyperbolic.

solve Equation 4.11 on page 146 for I_1, to find that:

$$\begin{aligned}\dot{I}_1 &= \beta S_0 I_1 - aI_1 \\ &= aI_1 - aI_1 \\ &= 0.\end{aligned}$$

Hence I_1 is constant so

$$I_1(t) = I_1(0). \tag{4.15}$$

The value of $I_1(0)$ is derived as part of the proof of the next lemma. □

Lemma 4.7 *S_1 is annual and given by*

$$S_1(t) = \frac{\tau}{2} - t + B_1(t), \tag{4.16}$$

and therefore has a sawtooth type behaviour.

Proof: Solving Equation 4.8 on page 145 for S_1, using Observation 4.1 on page 146 and Lemma 4.5 on page 147 and Equation 4.15 gives

$$\begin{aligned}\dot{S}_1 &= -\beta\frac{a}{\beta}I_1(0) - \frac{a}{\beta} + B_1'(t) \\ &= aI_1(0) - \frac{a}{\beta} + B_1'(t).\end{aligned}$$

Integrating this with respect to t it becomes apparent that

$$S_1(t) = S_1(0) - \left(aI_1(0) + \frac{a}{\beta}\right)t + B_1(t).$$

To complete the proof it remains to obtain values for the constants $S_1(0)$ and $I_1(0)$. Lemma 4.5 on page 147 states that $\bar{S}_1 = 0$, so by definition

$$\lim_{t\to\infty} \frac{1}{t}\int_0^t S_1(s)\mathrm{d}s = 0.$$

This implies

$$\lim_{n\to\infty} \frac{1}{n\tau}\int_0^{n\tau} S_1(t)\mathrm{d}t = 0.$$

Substituting for S_1 in the above:

$$\begin{aligned}
0 &= \lim_{n\to\infty} \frac{1}{n\tau} \int_0^{n\tau} S_1(0) - \left(aI_1(0) + \frac{a}{\beta}\right) t + B_1(t))\mathrm{d}t \\
&= \lim_{n\to\infty} \frac{1}{n\tau} \left[S_1(0)t - \left(aI_1(0) + \frac{a}{\beta}\right) \frac{t^2}{2}\right]_{t=0}^{n\tau} + \frac{1}{n\tau} \frac{n(n-1)}{2} \tau^2 \\
&= \lim_{n\to\infty} S_1(0) - \left(aI_1(0) + \frac{a}{\beta}\right) \frac{n\tau}{2} + \frac{n-1}{2}\tau \\
&= \lim_{n\to\infty} \left(S_1(0) - \frac{\tau}{2}\right) + \frac{n\tau}{2} \left(1 - \left(aI_1(0) + \frac{a}{\beta}\right)\right).
\end{aligned}$$

For the limit to be zero the following must hold

$$S_1(0) = \frac{\tau}{2} \quad \text{and} \tag{4.17}$$

$$I_1(0) = \frac{1}{a} - \frac{1}{\beta}. \tag{4.18}$$

Substituting these two expressions into Section 4.1 on the preceding page gives the result. □

Lemma 4.8 *I_2 is annual and given by*

$$I_2(t) = I_2(0) + \beta I_1(0) \left(\frac{t\tau}{2} - \frac{t^2}{2}\right)$$

for $0 \leq t < \tau$.

Proof: To solve Equation 4.12 on page 146 for I_2, first substitute values for I_0 from Observation 4.1 on page 146, S_0 from Lemma 4.5 on page 147 and I_1 from Equation 4.15 on the preceding page, the equation then simplifies to

$$\begin{aligned}
\dot{I_2} &= \beta \left(I_2 \frac{a}{\beta} + I_1(0)S_1\right) - aI_2 \\
&= \beta I_1(0) S_1 \\
&= \beta I_1(0) \left(\frac{\tau}{2} - t\right) + \beta I_1(0) B_1(t).
\end{aligned}$$

Integrating with respect to t gives

$$I_2(t) = I_2(0) + \beta I_1(0) \left(\frac{t\tau}{2} - \frac{t^2}{2}\right) + \beta I_1(0) \int_0^t B_1(s)\mathrm{d}s. \tag{4.19}$$

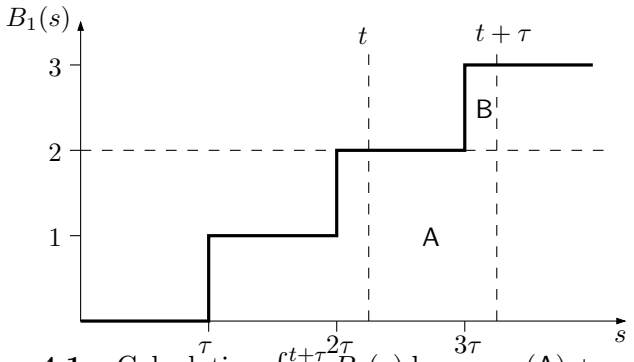

Figure 4.1: Calculating $\int_t^{t+\tau} B_1(s)\mathrm{d}s = \text{area}(\mathsf{A}) + \text{area}(\mathsf{B})$.

It is straightforward to show that I_2 is annual. Consider

$$\begin{aligned} I_2(t+\tau) &= I_2(0) + \beta I_1(0)\left(\frac{\tau(t+\tau)}{2} - \frac{t^2+2\tau t+\tau^2}{2}\right) \\ &\quad +\beta I_1(0)\int_0^{t+\tau} B_1(s)\mathrm{d}s \\ &= \underbrace{I_2(0) + \beta I_1(0)\left(\frac{t\tau}{2} - \frac{t^2}{2}\right) + \beta I_1(0)\int_0^{t} B_1(s)\mathrm{d}s}_{I_2(t)} \\ &\quad -\beta I_1(0)t\tau + \beta I_1(0)\int_t^{t+\tau} B_1(s)\mathrm{d}s. \end{aligned}$$

To show I_2 is annual it suffices to show that

$$\int_t^{t+\tau} B_1(s)\mathrm{d}s = t\tau.$$

Looking at Figure 4.1 it is clear that the integral is given by the sum of area(A) and area(B). Now

$$\text{area}(\mathsf{A}) = \left\lfloor \frac{t}{\tau} \right\rfloor \tau \times \tau \tag{4.20}$$

and

$$\begin{aligned} \text{area}(\mathsf{B}) &= \left((t+\tau) - \left\lfloor \frac{t+\tau}{\tau} \right\rfloor \tau\right) \times \tau & (4.21) \\ &= t\tau = \left\lfloor \frac{t}{\tau} \right\rfloor \tau^2 & (4.22) \end{aligned}$$

which proves I_2 is annual. Since $B_1(t) = 0$ for $0 \leq t < \tau$ the the integral

in Equation 4.19 on page 150 is zero so that

$$I_2(t) = I_2(0) + \beta I_1(0)\left(\frac{t\tau}{2} - \frac{t^2}{2}\right). \tag{4.23}$$

for $0 \leq t < \tau$. As I_2 is annual I_2 can be expressed for all t as

$$I_2(t) = I_2(0) + \beta I_1(0)\left(\frac{\hat{t}\tau}{2} - \frac{\hat{t}^2}{2}\right)$$

where

$$\hat{t} = t - \tau\left\lfloor\frac{t}{\tau}\right\rfloor,$$

is the phase of t, that is the remainder when t is divided by τ. The value of $I_2(0)$ is given in Equation 4.24 on the next page, as it is derived in the proof of the next lemma. □

Lemma 4.9 *The integral of the order d^2 component of I over a year can be expressed as*

$$\int_0^\tau I_2 = \left(\frac{\beta}{a} - 1\right)\frac{\tau^3}{12} + I_2(0)\tau.$$

Proof: Taking the expression for I_2 from Equation 4.23 in the proof of Lemma 4.8, which is valid for $0 \leq t < \tau$, and integrating with respect to t gives the result. □

Lemma 4.10 *S_2 is annual.*

Proof: By Observation 4.1 on page 146, Lemma 4.5 on page 147 and Lemma 4.7 on page 149 the $\dot{S}_2$ equation (Equation 4.9 on page 145) simplifies to

$$\begin{aligned}
\dot{S}_2 &= -aI_2 + \beta I_1(0)S_1 - S_1 + B_2'(t) \\
&= -aI_2 - S_1(1 + \beta I_1(0)) + B_2'(t) \\
&= -aI_2 - \frac{\beta}{a}\left(\frac{\tau}{2} - t + B_1(t)\right) + B_2'(t).
\end{aligned}$$

Now integrating this with respect to t gives

$$S_2(t) = -a\int_0^t I_2(s)\mathrm{d}s - \frac{\beta t(\tau - t)}{2a} - \frac{\beta}{a}\int_0^t B_1(s)\mathrm{d}s + B_2(t).$$

Considering the long time behaviour of S_2

$$\begin{aligned}
S_2(n\tau) &= -a\int_0^{n\tau} I_2(s)\mathrm{d}s + \frac{\beta\tau^2}{2a}n(n-1) - \frac{\beta}{a}\int_0^{n\tau} B_1(s)\mathrm{d}s + B_2(n\tau) \\
&= n\left((a-\beta)\frac{\tau^3}{12} - aI_2(0)\tau\right) \quad \text{by Lemma 4.9 and } \because I_2 \text{ is annual} \\
&\quad + \frac{\beta\tau^2}{2a}n(n-1) - \frac{\beta\tau^2}{2a}n(n-1) - \frac{\tau^2}{2}n \\
&= n\left(-\frac{\tau^2}{2} - (\beta-a)\frac{\tau^3}{12} - aI_2(0)\tau\right).
\end{aligned}$$

As S_2 is bounded (because S is bounded) the parentheses must be zero so

$$\begin{aligned}
-aI_2(0)\tau &= \frac{\tau^2}{2} + (\beta-a)\frac{\tau^3}{12} \\
I_2(0) &= \frac{(a-\beta)\tau^2 - 6\tau}{12a}. \qquad (4.24)
\end{aligned}$$

Now S_2 is annual because

$$\begin{aligned}
S_2(t+\tau) =& -a\int_0^{t+\tau} I_2(s)\mathrm{d}s - \frac{\beta(t+\tau)(\tau-(t+\tau))}{2a} \\
&- \frac{\beta}{a}\int_0^{t+\tau} B_1(s)\mathrm{d}s + B_2(t+\tau) \\
=& \underbrace{-a\int_0^{t} I_2(s)\mathrm{d}s - \frac{\beta t(\tau-t)}{2a} - \frac{\beta}{a}\int_0^{t} B_1(s)\mathrm{d}s + B_2(t)}_{S_2(t)} \\
&- a\int_t^{t+\tau} I_2(s)\mathrm{d}s - \frac{\beta}{a}\int_t^{t+\tau} B_1(s)\mathrm{d}s - \frac{\tau^2}{2} + \frac{\beta\tau t}{2a} + \frac{\beta\tau t}{2a} \\
=& S_2(t) - a\int_o^{t} I_2(s)\mathrm{d}s - \frac{\beta}{a}\int_t^{t+\tau} B_1(s)\mathrm{d}s - \frac{\tau^2}{2} + \frac{\beta\tau t}{a} \\
=& S_2(t) - \frac{(\beta-a)\tau^3}{12} - aI_2(0)\tau - \frac{\beta\tau t}{a} - \frac{\tau^2}{2} + \frac{\beta t\tau}{a} \quad \text{by Lemma 4.9} \\
=& S_2(t) - aI_2(0)\tau - \frac{(\beta-a)\tau^3}{12} - \frac{\tau^2}{2} \\
=& S_2(t) \qquad \text{by Equation 4.24.}
\end{aligned}$$

□

Most of the work is now done and the above results can now be brought

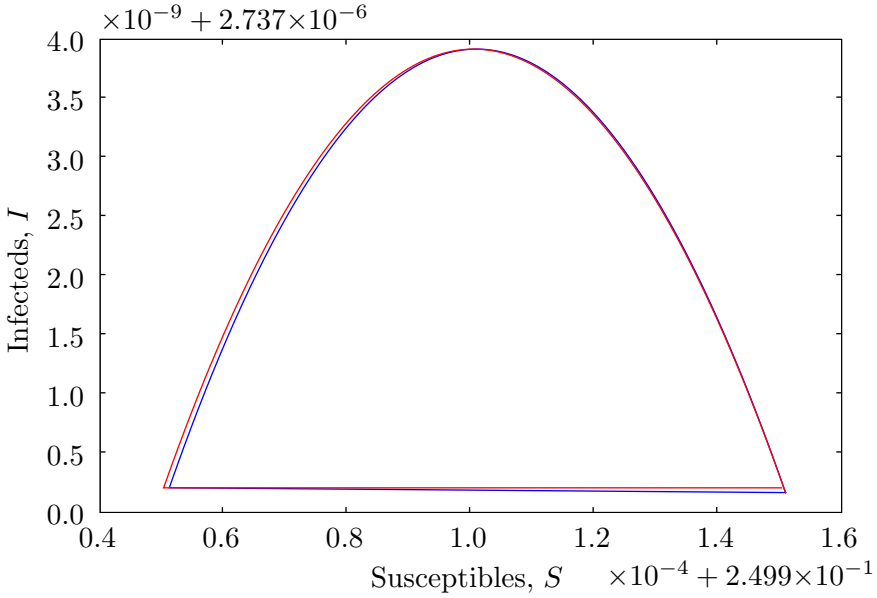

Figure 4.2: A period one attractor (blue line) for the pulsed SIR system compared with the trajectory predicted by the small x approximation (red line). Parameters: $g = 0.075$, $R_0 = 4$ and $x = 10^{-4}$.

together to prove Theorem 4.2 on page 144.

Proof: Firstly, considering the coefficients of the expansion of S, the result for S_0 is given directly by Lemma 4.5 on page 147. Similarly the equation for S_1 follows from Lemma 4.7 on page 149, noting that $B_1(t) = 0$ for $0 \leq t < \tau$ and by substituting the value of $S_1(0)$ from Equation 4.17 on page 150 calculated in the proof of Lemma 4.7 . The explicit calculation of S_2 is omitted, but Lemma 4.10 on page 152 shows it is an annual function.

Secondly, in the case of I, Observation 4.1 on page 146 shows that I_0 is zero. Lemma 4.7 on page 149 shows that I_1 is constant and this value is derived in the proof of Lemma 4.7, specifically in Equation 4.18 on page 150. In this case it is necessary to explicitly calculate the $\mathcal{O}(d^2)$ coefficient I_2 because the lower order terms where found to be constant. This is done in Lemma 4.8 on page 150, and by the substituting of values for $I_1(0)$, from Equation 4.18 on page 150 in the proof of Lemma 4.7, and $I_2(0)$, from Equation 4.24 on the previous page in the proof of Lemma 4.10. □

Utilising Theorem 4.2 the approximation is compared to the results from

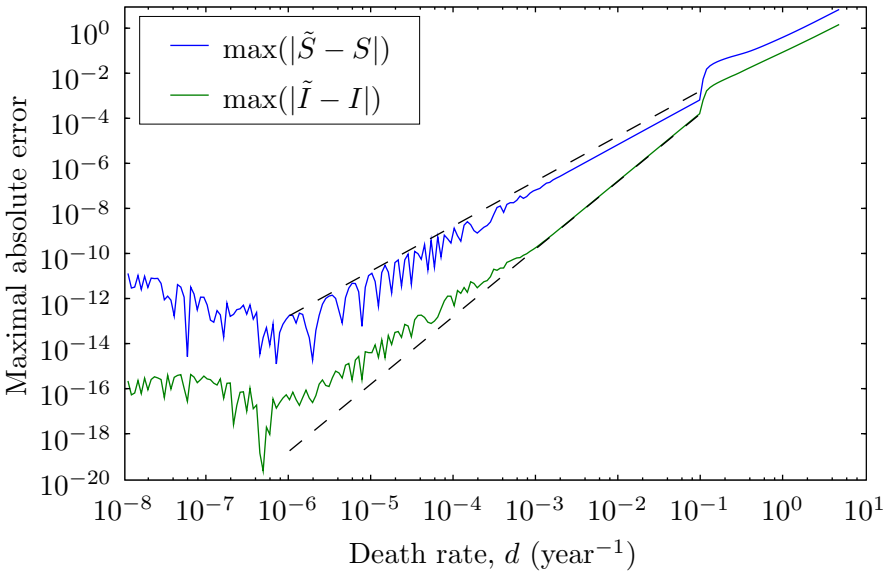

Figure 4.3: Results of an error analysis of the small x approximation. The maximum absolute error around the attractor measured between the numerically integrated pulsed SIR model, (S, I) and the trajectory predicted by the small x approximation $(\tilde{S}, \tilde{I})$ (Theorem 4.2 on page 144). Where $\tilde{S} = S_0 + dS_1$ and $\tilde{I} = I_0 + dI_1 + d^2 I_2$ Parameters: $g = 0.075$, $R_0 = 4$.

numerically integrating the original system. A period one attractor for $x = 10^{-4}$ is compared to its approximation in Figure 4.2 on the preceding page. A very close agreement can be seen between the two, showing that the approximation is valid for these parameter values.

An error analysis of this approximation is now undertaken and the results are shown in Figure 4.3. The graph shows the maximal absolute error between (S, I), the "exact" path calculated by numerical integration and $(\tilde{S}, \tilde{I})$, the approximation predicated by the small x approximation presented here, that is

$$\tilde{S} = S_0 + dS_1$$
$$\tilde{I} = I_0 + dI_1 + d^2 I_2.$$

The graph can be split into 3 parts: left, centre and right. In the central region, roughly between $d = 10^{-6}$ and $d = 10^{-1}$, the error in I is clearly

$\mathcal{O}(d^3)$ (the upper dashed line shows the curve $f(d) = d^2$), and S is clearly $\mathcal{O}(d^2)$ (again the lower dashed line shows $f(d) = d^3$). This is exactly what is expected because the approximation $\tilde{S}$ has been evaluated up to order one in d and $\tilde{I}$ up to order two. This shows that the approximation is valid in this region. In the right hand region where $d > 10^{-1}$ the error behaviour changes and the approximation starts to break up because d is too large. Finally, in the left region, where $d < 10^{-6}$, the error behaviour changes due to numerical errors in the integration. Using a smaller time step does decrease the value of d where breakup occurs, but not significantly.

There may be scope for generalising this result, to show that only period one attractors can exist for small x. The results for S_0, I_0 and I_1 do not depend on the dynamics lying on an attractor of period specifically one. Thus, as the oscillations in S and I are small, $\mathcal{O}(d)$ and $\mathcal{O}(d^2)$ respectively, it may be possible to show, using a linearity argument similar to that used by Keeling et al. [2001], that only period one attractors exist.

It is possible to carry out a similar multi-scale analysis for R_0 close to one, by setting $R_0 = 1 + \epsilon$. However, the analysis is much more complex and not considered here.

4.2 Large g approximations

This section considers an approximation to the pulsed simple SIR model with a short infectious period ($g > 0.5$). Having a short infectious period means that epidemics occur rapidly and also decay rapidly. Diseases with an infectious period in this range include Norwalk-like viral gastroenteritis, which has a infectious period of 2–3 days [Kaplan et al., 1982], so that an epidemic in a closed population, such as on a cruise ship, can take place in as little as five days [Gunn et al., 1980]. Similarly influenza has a latent period of only 1–3 days and an infectious period of only 2–3 days, meaning that an epidemic can sweep though a city in less than six weeks [Hethcote, 2000].

The rapid occurrence and decay of epidemics allows assumptions to be made about the dynamics, that lead to the formulation of a discrete approximation to the standard pulsed SIR model in this region of parameter

space. The system is given by the following set of equations:

$$\begin{aligned} \dot{S} &= -\beta SI \\ \dot{I} &= \beta SI - gI \\ \dot{R} &= gI. \end{aligned} \tag{4.25}$$

In the same way as with the standard pulsed SIR model, described in Chapter 2 on page 24, a birth pulse is applied to the susceptible class every year:

$$S(t^+) = S(t^-) + x \qquad \text{where } t = n\tau,\ n \in \mathbb{N}.$$

The use of the simple SIR model, without deaths, simplifies the analysis.

Figure 4.4 on the next page shows a typical period one attractor of the pulsed simple SIR model with a short infectious period, $g = 0.500$. It is clear that the trajectory is split into four distinct phases: growth; during which the level of infection increases but the level of susceptibles remains constant, epidemic; where level of susceptibles is reduced but the level of infecteds is constant, decay; as the level of infection decreases after the epidemic, pulse; where the susceptibles are replenished. Clearly the pulse phase is instantaneous, and the epidemic phase is extremely short, so most of the year is spent in the growth and decay phases.

A simplified model of four stages is constructed by assuming, amongst other things, that the epidemic phase is instantaneous, so that all the time is split between the growth and decay phases. The time spent in the growth phase is denoted by t_1, so that a time of $\tau - t_1$ is spent in the decay phase. If it is found that $t_1 \geq \tau$, then no epidemic takes place that year and birth pulse is followed by another growth phase. The equations for each phase are derived as follows, where initially $(S, I) = (S_0, I_0)$.

Growth: This phase describes the growth of infection building to an epidemic, during which it is assumed S is constant. Using this assumption it is possible to solve the $\dot{I}$ equation to obtain an explicit expression for I during this phase of the cycle, whence

$$\left.\begin{aligned} S &= S_0 \\ I &= I_0 e^{(\beta S_0 - g)t} \end{aligned}\right\} \text{for} \quad 0 \leq t < t_1.$$

Note that if $\beta S_0 < g$ then this phase would describe decay, rather than

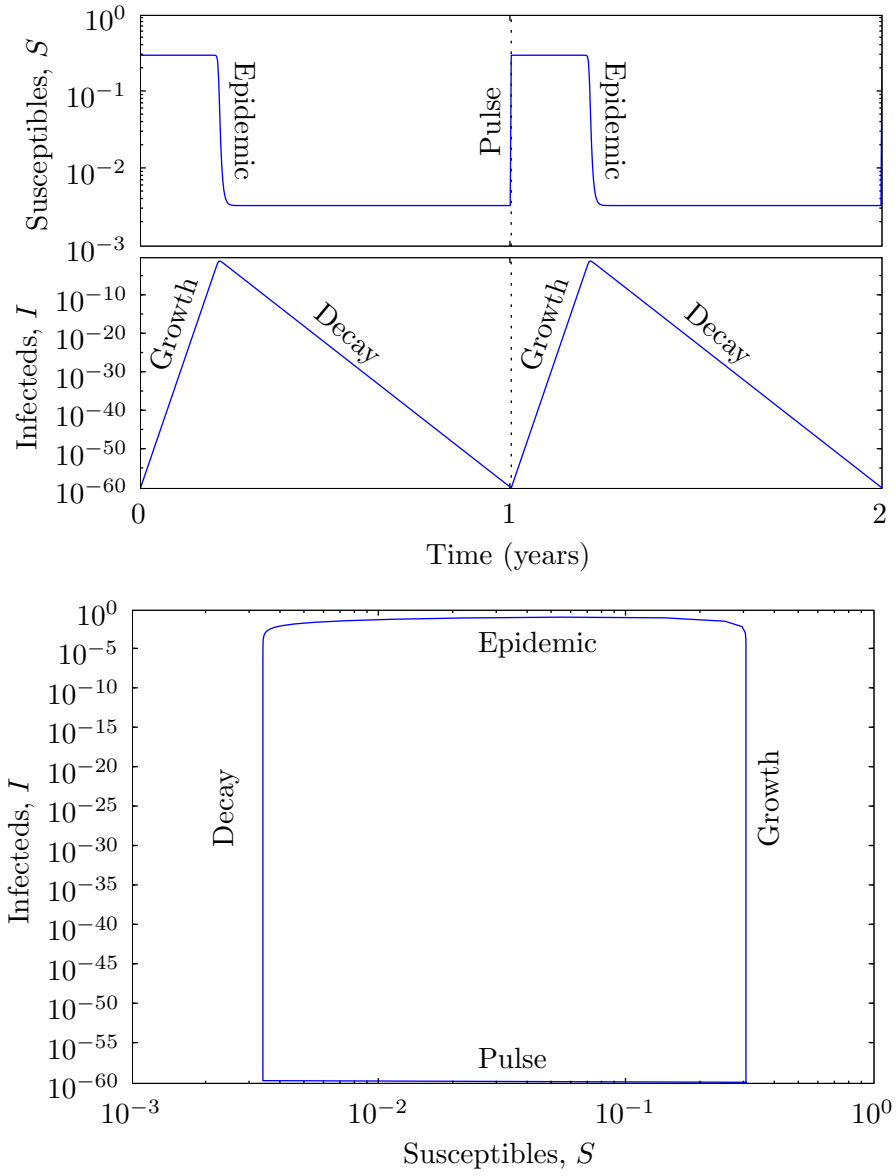

Figure 4.4: A period one attractor of the pulsed simple SIR model showing how, when g is large, the dynamics can be split into four distinct phases: growth, epidemic, decay and pulse. Parameters: $\beta/g = 15$,$x = 0.3$,$g = 0.500$.

growth, in the level of infecteds. This occurs in the case where S was greatly reduced by a previous large epidemic, and it may take several birth pulses before the level of infection starts to grow again.

Epidemic: During this phase I remains constant and S jumps to S_∞. Here S_∞ is defined as the value S would attain in the un-forced simple SIR model as $t \to \infty$. This assumption requires a short infections period causing the epidemic to be sufficiently quick so that this limit is approached. Hence

$$\left.\begin{array}{rcl} S & = & S_\infty(S_0, I_0) \\ I & = & I_1 = I_0 e^{(\beta S_0 - g)t_1} \end{array}\right\} \text{at} \quad t = t_1.$$

Decay: For this phase, similar to the growth phase, S is again constant and I evolves in the same way as in the growth phase. Here, however, $\beta S_\infty < g$ so the exponent is negative and I is decreasing during this phase. The duration of this phase it $\tau - t_1$, assuming it is non zero, that is this phase continues until the next pulse. The equations are

$$\left.\begin{array}{rcl} S & = & = S_\infty(S_0, I_0) \\ I & = & I_1 e^{(\beta S_\infty - g)(t - t_1)} \end{array}\right\} \text{for} \quad t_1 < t < \tau.$$

Birth Pulse: This phase is instantaneous and represents the now familiar birth pulse, introduced in Chapter 2. Hence S is incremented by the constant value x while I remains constant:

$$\left.\begin{array}{rcl} S & = & S_\infty + x \\ I & = & I_1 e^{(\beta S_\infty - g)(\tau - t_1)} \end{array}\right\} \text{at} \quad t = \tau.$$

In the case that $t_1 \geq \tau$ the epidemic and decay phases are omitted and the system proceeds straight to the pulse phase before starting the next cycle with another growth phase. In order to determine the time spent in the growth and decay phases, the change in S over the epidemic $S_0 - S_\infty$, is assumed to match the total number of infecteds that recover over a year. This again requires the assumption that the infections period be short and thus that g is large, so that one year is sufficient time for all the infecteds to recover. Hence the change in S over the epidemic is given by integrating the

recovery rate over a year:

$$S_0 - S_\infty = \int_0^\tau gI(t)\mathrm{d}t. \tag{4.26}$$

It is now necessary to derive an expression for S_∞.

Lemma 4.11 *For the simple SIR model the proportion of susceptibles remaining after the epidemic, that is, the limit* $\lim_{t\to\infty} S(t)$*, is given by*

$$S_\infty(S_0, I_0) = \frac{-W(-R_0 S_0 e^{-R_0 S_0 - R_0 I_0})}{R_0}. \tag{4.27}$$

Where W is the Lambert W function, the inverse of $f(W) = We^W$.

Proof: The proof proceeds by calculating the final size of the epidemic R_∞, then uses the fact that

$$R_\infty = 1 - S_\infty.$$

Dividing the susceptible equation by the recovered equation (a trick developed by Kermack and McKendrick [1927]) shows that

$$\frac{\mathrm{d}S}{\mathrm{d}R} = -R_0 S$$

Which has the solution

$$S = S(0)e^{R(0)R_0}e^{-R_0 R}.$$

Since $S + I + R = 1$ and $I(\infty) = 0$,

$$R_\infty = 1 - S(0)e^{R(0)R_0}e^{-R_0 R_\infty}.$$

Hence

$$S_\infty = S_0 e^{(S_\infty - S_0 - I_0)R_0}.$$

There is no closed form for S_∞, but the form using the Lambert W function was found using Maple$^{\mathrm{TM}}$. This makes it possible to directly evaluate S_∞ numerically. □

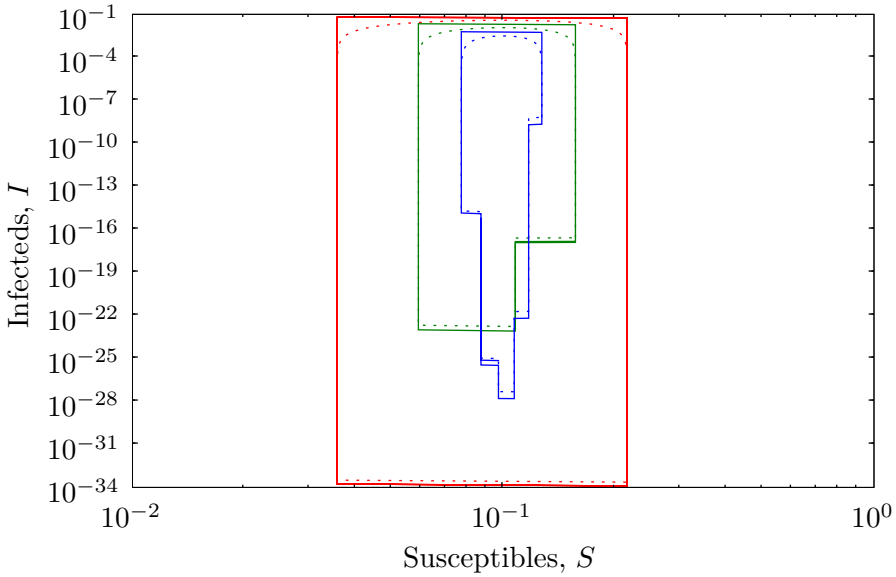

Figure 4.5: A comparison of several attractor from the pulsed simple SIR model (dashed lines), with their approximations predicted by the large g model (solid lines). Parameters: $\beta/g = 10$ and $g = 0.500$ throughout. Red: $x = 0.18$ period 1, green: $x = 0.049$ period 2, blue: $x = 0.01$ period 5.

Now all that remains is to determine t_1. By Equation 4.26

$$\begin{aligned} S_0 - S_\infty(S_0, I_0) &= gI_0 \int_0^{t_1} e^{(\beta S_0 - g)t} \mathrm{d}t + gI_1 \int_{t_1}^{\tau} e^{(\beta S_\infty - g)t} \mathrm{d}t \\ &= \frac{I_0}{\beta S_0 - g} \left(e^{(\beta S_0 - g)t_1} - 1 \right) \\ &\quad + \frac{I_0 e^{(\beta S_0 - g)t_1}}{\beta S_\infty(S_0, I_0) - g} \left(e^{(\beta S_\infty(S_0, I_0) - g)(\tau - t_1)} - 1 \right) \end{aligned}$$

Again no closed form for t_1 exists, even involving S_∞, thus numerical methods must be used. A simple bisection method is used to find the value of t_1 that solves this equation for the given values of S_0 and I_0. A library function is utilised to evaluate the Lambert W function.

The above calculations now give a framework to approximate the trajectory that any initial point (S_0, I_0) will take during the next year. The process can be repeated to approximate the multi-annual attractors seen in Chapter 2. Figure 4.5 shows the trajectories predicted by this approximation for starting points on attractors of the pulsed simple SIR model as discussed

in Subsection 3.3.2 on page 106. The approximation shows good correlation with the numerical results. It slightly over estimates the peak level of infection, and fails to capture start and end of the epidemic phase very accurately, but this is to be expected as the epidemic is being modelled as a pulse. The value of $g = 0.5$ used is not very big, a larger g would improve the fit at the start and end epidemic phase. The level of infection at which the birth pulse occurs is slightly under predicted. This again would improve with a larger g.

This approximation shows how even the complex dynamics of multi-annual attractors can be well approximated by simple combinations of exponential growth/decay and pulses representing epidemics as well as births.

The same techniques can be applied to the standard pulsed SIR model, but lead to a significantly more complex approximation where S, as well as I varies exponentially during the growth and decay phases. Given the complexity of the approximation for the simple SIR model, it was felt that nothing would be gained from the analysis.

4.3 The Q-L large g approximation

Although the first large g approximation presented in the previous section is a good fit to the dynamics, the approximation itself is quite complicated to compute. In particular, the calculation of t_1 is particularly unintuitive. A simpler approximation would be a more useful tool to help understand the dynamics. This sections shows how making one extra assumption greatly simplifies the previous approximation.

Looking again at the time-series plot of Figure 4.4 on page 158, it is clear that at the peak of the epidemic I is $O(1)$. If it is assumed that $I_1 = 1$, the value of t_1, here denoted by T, can be calculated directly from the I equation during the growth phase. Hence, under this assumption

$$1 = I_0 e^{(\beta S_0 - g)T}$$

so,

$$T = \frac{1}{\beta S_0 - g} \log\left(\frac{1}{I_0}\right).$$

Using this approximate the system is transformed into a discrete annual map,

where S_t and I_t denote the values of S and I at the start of the year.

Given T is known, the growth, epidemic, decay and pulse stages of the previous model can be compressed into one process, obtaining expressions for S_{t+1} and I_{t+1}—the values of S and I at the start of the next year. There are two possibilities, if $0 < T < \tau$ then an epidemic occurs so

$$S_{t+1} = S_\infty(S_t, I_t) + x \tag{4.28}$$
$$I_{t+1} = I_t e^{(\beta S_t - g)T} e^{(\beta S_{t+1} - g)(\tau - T)} \tag{4.29}$$

otherwise no epidemic occurs and

$$S_{t+1} = S_t + x \tag{4.30}$$
$$I_{t+1} = I_t e^{(\beta S_t - g)\tau}. \tag{4.31}$$

In both cases the birth pulse is applied.

Now consider the transformation

$$Q_t = \beta S_t / g = R_0 S_t$$
$$L_t = \frac{log(I_t)}{g}.$$

Under this transformation the time spent in the growth phase is given by

$$T = \frac{-L_t}{Q_t - 1}. \tag{4.32}$$

Next the equations for S_{t+1} and I_{t+1} are transformed into Q_t and L_t. Firstly the case $0 < T < \tau$ when an epidemic occurs is calculated. To obtain an expression for Q_{t+1} the expression for S_∞ (Equation 4.27 on page 160) is substituted into Equation 4.28, so that

$$R_0 S_{t+1} = -W\left(-R_0 S_t e^{-R_0 S_t - R_0 I_t}\right) + R_0 x$$

and by assuming that the I_t, is small in relation to S_t, so that the $R_0 I_t$ term can be neglected,

$$Q_{t+1} = -W\left(-Q_t e^{-Q_t}\right) + R_0 x,$$

where, as before, W is the Lambert W function.

An expression for L_{t+1} is gained from Equation 4.29 by substituting $I_t = e^{gL_t}$ and $S_t = Q_t/R_0$, then taking logs, so

$$gL_{t+1} = gL_t + g(Q_t - 1)T + g(Q_{t+1} - 1)(\tau - T),$$

by Equation 4.32

$$L_{t+1} = (Q_{t+1} - 1)(\tau - T).$$

In the case $0 > T > \tau$, where no epidemic occurs that year, the equations are simpler. By Equation 4.30

$$Q_{t+1} = Q_t + R_0 x,$$

then substituting into Equation 4.31, taking logs and dividing though by g yields

$$L_{t+1} = L_t + (Q_t - 1)\tau.$$

Thus the new discrete approximation can be summarised as

$$\text{Epidemic: } \left.\begin{array}{l} Q_{t+1} = -W\left(-Q_t e^{-Q_t}\right) + R_0 x \\ L_{t+1} = (Q_{t+1} - 1)(\tau - T) \end{array}\right\} \text{ when } 0 < T = \frac{-L_t}{Q_t - 1} < \tau$$

$$\text{No Epidemic: } \left.\begin{array}{l} Q_{t+1} = Q_t + R_0 x \\ L_{t+1} = L_t + (Q_t - 1)\tau \end{array}\right\} \text{ otherwise.}$$

Notice how this discrete approximation only has a single parameter. Also note that in order to evaluate the Q_{t+1} equation in the epidemic case, a library function must be used for the Lambert W function.

Figure 4.6 on the following page shows a bifurcation plot for this approximation. Notice how simple period one dynamics as well as complex high period dynamics are present. The dynamics closely resemble those of the pulsed simple SIR model (Figure 3.16 on page 109). It is striking how such a simple approximation can yield such complex dynamics.

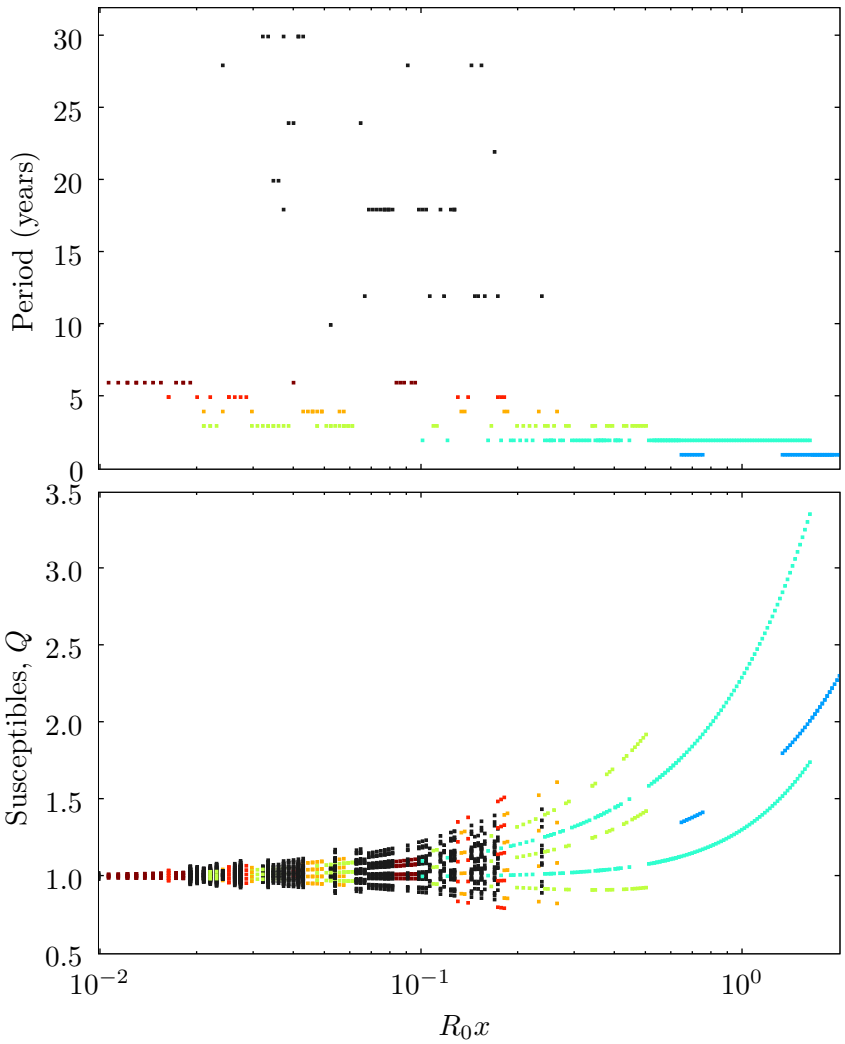

Figure 4.6: A bifurcation plot for the second large g approximation. The single variable R_0x varies from 0.0098–2.50. This corresponds to the product of x, varying logarithmically from 0.01–0.18, and R_0, varying linearly from 0.98–14.18.The top plot shows the periods of attractor found for each value of R_0x, and the bottom shows the values of Q_t at the fixed points.

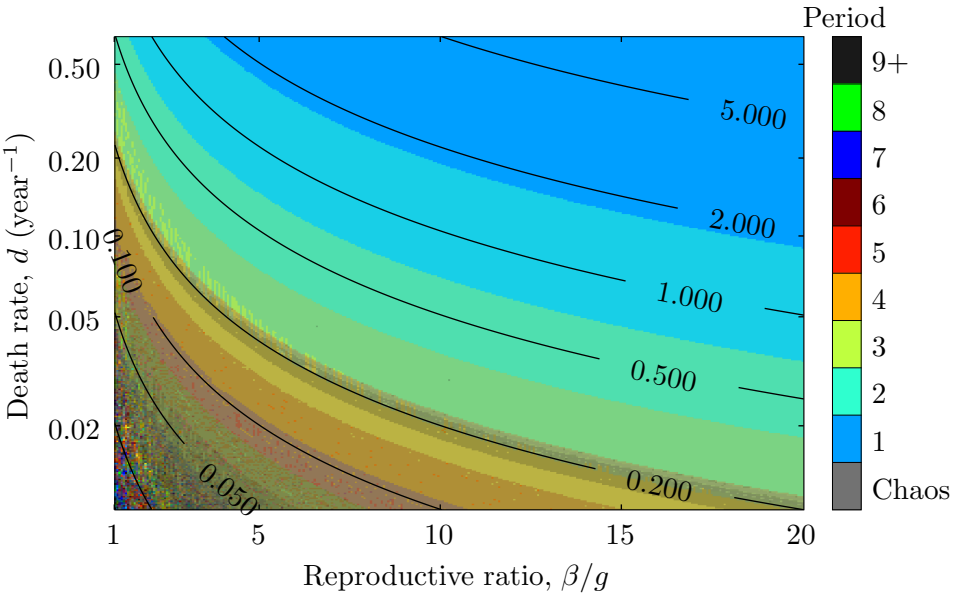

Figure 4.7: The periods exhibited by the pulsed simple SIR model, for $g = 0.500$, overlaid with contours of constant R_0x.

For this approximation the dynamics are controlled by the single parameter R_0x. A poignant question is whether or not this relates back to the pulse simple SIR model which is being approximated. Figure 4.7 shows contours of constant R_0x overlaid on the periodicity data from Figure 3.16. It is immediately apparent that the contours run parallel to the boundaries between regions of different periods. This suggests that the single parameter R_0x does indeed control the behaviour of the pulsed simple SIR model, or at least their periodicity, and that there exist threshold values of R_0x at which the period of the attractors change. This result greatly simplifies the study of this model.

4.4 Conclusions

The three approximations presented in this chapter all show excellent agreement with the models they represent. They give insight into causes of the dynamics of both the standard and simple SIR model.

The multi-scale approach used for the small x region of parameter space, is useful because it is a region where the numerical solutions can be inaccurate due to the very slow convergence times experienced in that region. The

results also help to explain what happens to the attractors in the limit when the forcing goes to zero, helping to understand the transition from an annual attractor to a fixed point.

Further work could include performing the same analysis in the case R_0 is close to unity. Though this is more complicated than the small x case it may lead to some insight into how the dynamics become unstable as R_0 approaches 1.

The two large g approximations to the pulsed simple SIR model are a useful tool. They provide accurate results within their remit and are much less computationally intensive than numerically integrating the ODE models which they approximate.

The first large g approximation does involve carrying out the bisection algorithm on a complex expression in order to determine the time spent in the growth phase, a calculation that is quite unintuitive.

This problem is solved with the second approximation, in which the time spent in growth is a simple function of the state variables and parameters. The number of parameters is also reduced to a single one: R_0x, which controls the dynamics of the system. It is astonishing that the simple discrete model provided by this approximation so accurately describes the high period dynamics exhibited by the pulsed simple SIR model. It turns out that for the pulsed simple SIR model changes in the single parameter R_0x also coincide accurately with changes in its attractors periodicity. This will greatly simplify the study of this model.

It should be possible to formulate a similar approximation for pulsed SIR model. This would be more complicated because the level of susceptibles will vary, due to deaths, during the growth and decay stages. It might then be possible to come up with an discrete system similar to the Q-L approximation, though it will have more than a single parameter.

An alternative analytic approach that could be considered would be to find a system of ODEs that have similar behaviours to the SIR model, but are integrable. This would open up the door to many other analytical techniques. For example if an explicit annual map could be written down, the addition of pulsing becomes trivial. This work could then be used to aid understanding of the behaviours of the pulsed SIR model and its variants.

The analytical work done in this chapter greatly enhances the understand-

ing of the at times very complex dynamics of pulsed SIR systems. Much more work could be done in this field to give further insights into the dynamics of pulsed SIR models.

Chapter 5

Conclusions

There has been little work in investigating the role that seasonal birth rates play in disease dynamics, whereas there is a very large body of work focusing on the effects of seasonal transmission rates, in particular measles and other childhood diseases. This thesis attempts to redress the balance.

After considering the various seasonal birth patterns observed in animal and human populations it was decided to focus on populations with a highly seasonal birth rate. Observing that for species such as Saiga antelope reproduction is synchronised to the extent where all births occur in a period of 3–8 days, it was concluded that an instantaneous pulse of births applied to the population would be a simple way to model these phenomena.

Chapter 2 introduced the pulsed SIR modelEquations 2.1 on page 29. An annual birth pulse was applied to the susceptible class, the size of which was tied to the death rate so that, on average over a year, the population size remained constant. A biologically reasonable parameter space was chosen (which was used throughout the later chapters) and the model was found to exhibit periodic attractors in all areas of parameter space where $R_0 > 1$. After reviewing the numerical techniques used in the literature, suitable methods where chosen and refined to determine periodicity of the dynamics. This proved to be nontrivial, due to long convergence times and higher period oscillations about the attractors fixed points. It was discovered that, in some regions of parameter space multiple attractors coexisted. A method dubbed "pushing out" was developed to determine their extent (see Box 2.3 on page 49). However, this method only distinguished attractors of different period. Figure 2.19 on page 56 shows the existence of a region where two

period six attractors coexist. The figure was produced by manually separating the two areas and pushing out again. The problem of how to automatically distinguish coexisting attractors of the same period remains to be tackled. Perhaps a solution to this is the use of some of the more sophisticated, yet less robust numerical methods, such as minimisation techniques for the location of periodic orbits as discussed in Subsection 2.2.2 on page 37. Similar techniques could be used to improve the predictor-corrector algorithm used in pushing out. The data sets for the coexisting attractors were calculated for several different infectious periods. The general trend was that as the infectious period decreased (g increasing, but also β increasing so that R_0 is kept approximately constant) the complexity of the dynamics increases. More higher period dynamics appeared and even chaos.

Later sections of Chapter 2 considered other properties of the attractors. Their modal frequency was calculated, and the minimal level of infection in some areas of parameter space was seen to show a possible risk of extinction, due to stochastic variations, because of the very low levels reached in between epidemics. A way to deal with this problem is to use a small level imports of infection from an external source to keep the levels form dropping to low. This solution is considered in Subsection 3.3.8 on page 135.

Resonant effects are examined in Section 2.5 on page 62. By considering the transition from low amplitude forcing to the pulsed births the onset of nonlinear resonance is observed. This is seen to be typical behaviour across parameter space. The existence of coexisting attractors is explained by the overlapping of the breaking waves characteristic of nonlinear resonance. This further advances the understanding of the multi-annual dynamics and coexisting attractors observed here.

The bifurcation structure was briefly analysed, and period doubling bifurcations, leading to chaos where observed. Finally, the presence of unstable period one attractors was discovered, and the level of their instability, as measured by their Floquet multipliers, was shown to generally increase with the periodicity of the stable attractors, with which they coexist.

Chapter 3 aimed to show the robustness of the results of Chapter 2 to a wide range of perturbations. Broadly speaking this was shown to be the case.

Small perturbations in phase space were the first to be considered. Using

the modulus of the largest Floquet multiplier as a measure of linear stability it was shown that most regions of parameter space were stable with respect to small perturbations. The main region where the stability was not very strong was the small d, small β/g region of parameter space. This provided an explanation for the slow convergence observed in that region.

Although an instantaneous pulse of births is a realistic assumption for certain animal populations (*e.g.* Saiga antelope) it may not be so realistic for some populations that still have highly seasonal births, but show greater temporal spread. Section 3.2 on page 92 investigated the effects of using other functions to model seasonal births. An obvious choice was to use sinusoidal forcing, which has been used successfully to model seasonal variations in the transmission rate. However, the qualitative dynamics of the pulsed SIR model did not persist under sinusoidal forcing. A top hat functions was also considered and dynamics showed good qualitative agreement with the pulsed SIR model. One surprising fact, shown in Figure 3.7 on page 99 is that the periodicity of the dynamics remains almost unchanged when the width of the top hat functions is as large as 90 days, a quarter of a year. A smoothed top hat function was also considered, and only when large levels of smoothing were applied did the qualitative dynamics depart from those of the pulsed SIR model. Thus it was concluded that the results where stable to changes in the birth pulse, and that only the most smoothed functions, or those with where the births where present for most of the year caused qualitative changes in the dynamics.

This is a very important result, because it makes the pulsed SIR model applicable to many more populations. It even suggests that if fitting seasonal birth patterns to the model, it may not be necessary to have a detailed knowledge of the distribution of births throughout the year, only their total number. One other type of seasonal birth pattern that should possibly be considered is the combination of a birth pulse with a constant underlying average birth rate. This is the kind of pattern of births that is observed in cattle (Figure 2.3 on page 28).

The final test of the robustness of the results of the pulsed SIR model was to look at changing the structure of the underlying model, effectively changing the assumptions on which the model was based. Numerous variants of the SIR model were tested. In general most qualitative features of the dynamics of the pulsed SIR model were preserved. One of the most significant changes

made was the addition of an exposed class, to form the well know SEIR model. This highlights the difference between the infected and infectious periods. This was followed up by changing the distribution of infected and latent periods from the exponential assumed by the standard SIR/SEIR models, to a gamma distribution. This change caused a marked increase in the complexity of the dynamics. This was explained by the fact that the gamma distribution has a much smaller standard deviation, thus the latent and infectious periods are much more tightly grouped. This means that rather than the strong variations in the level of susceptibles, caused by the birth pulse, being damped as they travel though the exposed and infectious classes, they are in fact merely delayed. It is hypothesised that the now much more rapid changes in these classes causes the increased complexity seen in the dynamics for the gamma models with gamma distributed infectious and or latent periods.

Another model studied is the vaccination pulse model (Subsection 3.3.3 on page 110). This differs from all the other models studied in Chapter 3 in that the births are at a constant rate and a pulse is used to model vaccination. Much work has been carried out in the examination of vaccination strategies and pulsed vaccination is a tried and tested strategy [Nokes and Swinton, 1997]. The vaccination pulse model was shown to share many qualitative features with the pulsed SIR model. Many of the methods developed for the pulsed SIR model could be applied to the vaccination pulse model and this is an area for future work.

The similarities between the vaccination pulse model and the pulsed SIR model raise a poignant question: are the dynamics exhibited by the pulsed SIR model a general feature of models where strong seasonality is modelled using pulses? Much more work would need to be done to fully answer this question. There are many examples in nature where strong seasonality is present and a pulse could be an appropriate modelling tool.

A major modelling tool not considered in this thesis is stochasticity. Much further work could be done to test the robustness of the results of the pulsed SIR model with respect to small random perturbations. This could be in the transmission of infection, or in the timing and size of the birth pulse. One issue that would need to be addressed is the problem of extinction. One answer is the use of imports (Subsection 3.3.8 on page 135).

Chapter 2 and Chapter 3 focused primarily on the use of numerical methods. Chapter 4 attempts to redress the balance and focused on analytical methods. Three approximations to the pulsed models discussed in earlier chapters are presented. They complement the numerics by focusing on specific areas in parameter space where the numerics are computationally costly or inaccurate.

The first approximation looks at the behaviour of the pulsed SIR model for small birth pulse. A multi-scale analysis yields a second order approximation and shows that annual dynamics exist in this region. An error analysis shows good agreement with the numerics. A second multi-scale analysis could be conducted for the region R_0 close to one.

The second two approximations consider what happens for very short infectious periods, large g, for the pulsed simple SIR model. The second of these is a simplification of the first, obtained by making further assumptions. It provides a simple discrete model of single variable that captures all the behaviour of the pulsed simple SIR model including high period dynamics and chaos. The results are related back to the original pulsed SIR model where it is found that the single parameter $R_0 x$ also controls the periodicity of the dynamics. A possible avenue for further work would be to try and repeat this analysis for the standard pulsed SIR model, *i.e.* with deaths.

The main stumbling block to the use of analytic tools on the pulsed SIR model is that there is no closed solution to the system of ODEs: they are not integrable. If an integrable system with similar behaviour to the SIR model could be found it would be much easier to treat analytically, and perhaps some of the results gained could be transfered back to the pulse SIR model.

In conclusion adding pulsed births to standard epidemiological models gives rise to complex dynamics. These are shown to be robust in the broadest of senses. This makes the pulses SIR model a good choice for modelling the spread of disease in populations exhibiting highly seasonal birth patterns.

Bibliography

Z. Agur, L. Cojocaru, G. Mazor, R. M. Anderson, and Y. L. Danon. Pulse mass measles vaccination across age cohorts. *Proceedings of the National Academy of Sciences of the United States of America*, 90(24):11698–11702, 1993.

E. L. Allgower and K. Georg. Piecewise linear methods for nonlinear equations and optimization. *Journal of Computational and Applied Mathematics*, 124(Amsterdam, Netherlands):245–261, 2000.

S. Altizer, A. Dobson, P. Hosseini, P. Hudson, M. Pascual, and P. Rohani. Seasonality and the dynamics of infectious diseases. *Ecology Letters*, 9(4): 467–484, 2006.

D. Anderson and R. Watson. On the spread of a disease with gamma distributed latent and infectious periods. *Biometrika*, 67(1):191–198, 1980.

R. M. Anderson and R. M. May. Directly transmitted infectious diseases: Control by vaccination. *Science*, 215(4536):1053–1060, 1982.

R. M. Anderson and R. M. May. *Infectious Diseases of Humans: Dynamics and Control*. Oxford University Press, London, United Kingdom, 1991.

R. M. Anderson, G. F. Medley, R. M. May, and A. M. Johnson. A preliminary study of the transmission dynamics of the human immunodeficiency virus (HIV), the causative agent of AIDS. *IMA Journal of Mathematics Applied in Medicine and Biology*, 3(4):229–263, 1986.

H. Andersson and T. Britton. Stochastic epidemics in dynamic populations: quasi-stationarity and extinction. *Journal of Mathematical Biology*, 41(6): 559–580, 2000.

H. R. Babad, D. J. Nokes, N. J. Gay, E. Miller, P. Morgan-Capner, and R. M. Anderson. Predicting the impact of measles vaccination in England and Wales: Model validation and analysis of policy options. *Epidemiology and Infection*, 114(2):319–344, 1995.

N. T. J. Bailey. Some stochastic models for small epidemics in large populations. *Applied Statistics*, 13:9–19, 1964.

N. T. J. Bailey. *The mathematical theory of infectious diseases and its applications*. Charles Griffin and Company Ltd, London and High Wycombe, United Kingdom, 1975.

N. T. J. Bailey and C. Alff-Steinberger. Improvements in the estimation of the latent and infectious periods of a contagious disease. *Biometrika*, 57 (1):141–153, 1970.

N. D. Barlow. A model for the spread of bovine TB in New Zealand possum populations. *Journal of Applied Ecology*, 30(1):156–164, 1993.

N. D. Barlow and M. C. Barron. Modelling the dynamics and control of stoats in New Zealand forests. *Science for Conservation*, (252):5–40, 2005.

N. Barquet and P. Domingo. Smallpox: the triumph over the most terrible of the ministers of death. *Annals of internal medicine*, 127(8 Pt 1):635–642, 1997.

M. S. Bartlett. Deterministic and stochastic models for recurrent epidemics. *Proceedings of the Third Berkeley Symposium on Mathematical Statistics and Probability*, 4:81–109, 1956.

M. S. Bartlett. Measles periodicity and community size. *Journal of the Royal Statistical Society A*, 120:48–70, 1957.

D. Beazley. `SWIG`: a simplified wrapper and interface generator, 2007. URL `http://www.swig.org`.

M. Begon, M. Bennett, R. G. Bowers, N. P. French, S. M. Hazel, and J. Turner. A clarification of transmission terms in host-microparasite models: Numbers, densities and areas. *Epidemiology and Infection*, 129 (1):147–153, 2002.

J. Berger and S. L. Cain. Reproductive synchrony in brucellosis-exposed bison in the southern Greater Yellowstone Ecosystem and in noninfected populations. *Conservation Biology*, 13(2):357–366, 1999.

D. Bernoulli. Essai d'une nouvelle analyse de la mortalité causée par la petite vérole. *Mémoires de Mathématique et de Physique L'Imprimerie Royale, Paris*, page 1, 1766.

O. N. Bjørnstad, B. F. Finkenstädt, and B. T. Grenfell. Dynamics of measles epidemics: Estimating scaling of transmission rates using a Time series SIR model. *Ecological Monographs*, 72(2):169–184, 2002.

B. M. Bolker and B. T. Grenfell. Chaos and biological complexity in measles dynamics. *Proceedings of the Royal Society of London - B Biological Sciences*, 251(1330):75–81, 1993.

D. J. Boness, W. D. Bowen, and S. J. Iverson. Does male harassment of females contribute to reproductive synchrony in the grey seal by affecting maternal performance? *Behavioral Ecology and Sociobiology*, 36(1):1–10, 1995.

S. A. Bozzette, R. Boer, V. Bhatnagar, J. L. Brower, E. B. Keeler, S. C. Morton, and M. A. Stoto. A model for a smallpox-vaccination policy. *New England Journal of Medicine*, 348(5):416–425, 2003.

C. E. Brassil. Can environmental variation generate positive indirect effects in a model of shared predation? *American Naturalist*, 167(1):43–54, 2006.

A. Brewis, J. Laycock, and J. Huntsman. Birth non-seasonality on the pacific equator. *Current Anthropology*, 37(5):842–851, 1996.

R. Brookmeyer and J. Liao. Statistical modelling of the AIDS epidemic for forecasting health care needs. *Biometrics*, 46(4):1151–1163, 1990.

G. L. Campbell, A. A. Marfin, R. S. Lanciotti, and D. J. Gubler. West Nile virus. *Lancet Infectious Diseases*, 2(9):519–529, 2002.

U. Chatterjee and R. Acharya. Seasonal variation of births in rural West Bengal: Magnitude, direction and correlates. *Journal of Biosocial Science*, 32(4):443–458, 2000.

M. Choisy, J-F Guégan, and P. Rohani. Dynamics of infectious diseases and pulse vaccination: Teasing apart the embedded resonance effects. *Physica D: Nonlinear Phenomena*, 223(1):26–35, 2006.

G. Chowell, N. W. Hengartner, C. Castillo-Chavez, P. W. Fenimore, and J. M. Hyman. The basic reproductive number of Ebola and the effects of public health measures: The cases of Congo and Uganda. *Journal of Theoretical Biology*, 229(1):119–126, 2004.

R. Clewley. `PyDSTool`: a integrated simulation, modeling and analysis package for dynamical systems, 2007. URL `http://pydstool.sourceforge.net`.

M. Clinchy. *Does immigration 'rescue' populations from extinction?* PhD thesis, The University of Bristish Columbia, 1999.

M. Clinchy, A. C. Taylor, L. Y. Zanette, C. J. Krebs, and P. J. Jarman. Body size, age and paternity in common brushtail possums (*Trichosurus vulpecula*). *Molecular Ecology*, 13(1):195–202, 2004.

F. Cooke, Robert F. Rockwell, and David B. Lank. *The Snow Geese of La Perouse Bay*. Oxford University Press, London, United Kingdom, 1995.

F. Courchamp, D. Pontier, M. Langlais, and M. Artois. Population dynamics of feline immunodeficiency virus within cat populations. *Journal of Theoretical Biology*, 175(4):553–560, 1995.

O. Diekmann, J. A. Heesterbeek, and J. A. Metz. On the definition and the computation of the basic reproduction ratio R_0 in models for infectious diseases in heterogeneous populations. *Journal of Mathematical Biology*, 28(4):365–382, 1990.

O. Diekmann, J. A. P. Heesterbeek, and J. A. J. Metz. The legacy of Kermack and McKendrick. In *Epidemic Models: Their Structure and Relation to Data*, pages 95–115. Cambridge University Press, London, United Kingdom, 1995.

K. Dietz. The incidence of infectious diseases under the influence of seasonal fluctuations. *Lecture Notes in Biomathematics*, 11:1–15, 1976.

K. Dietz and J. A. P. Heesterbeek. Bernoulli was ahead of modern epidemiology [3]. *Nature*, 408(6812):513–514, 2000.

K. Dietz and J. A. P. Heesterbeek. Daniel Bernoulli's epidemiological model revisited. *Mathematical Biosciences*, 180:1–21, 2002.

E. Doedel. `AUTO`: software for continuation and bifurcation problems in ordinary differential equations, 2007. URL `http://indy.cs.concordia.ca/auto/`.

E. Doedel. Nonlinear numerics. *International Journal of Bifurcation and Chaos in Applied Sciences and Engineering*, 7(9):2127–2143, 1997.

L. Z. Dong and L. S. Chen. Positive periodic solution and numerical optimization in the harvesting effort for a single-species stage-structured system with birth pulses. *Computational Mathematics and Modeling*, 16 (2):179–192, 2005.

A. D'Onofrio. Stability properties of pulse vaccination strategy in SEIR epidemic model. *Mathematical Biosciences*, 179(1):57–72, 2002a.

A. D'Onofrio. Pulse vaccination strategy in the SIR epidemic model: Global asymptotic stable eradication in presence of vaccine failures. *Mathematical and Computer Modelling*, 36(4-5):473–489, 2002b.

A. D'Onofrio. Mixed pulse vaccination strategy in epidemic model with realistically distributed infectious and latent times. *Applied Mathematics and Computation (New York)*, 151(1):181–187, 2004.

S. F. Dowell. Seasonal variation in host susceptibility and cycles of certain infectious diseases. *Emerging infectious diseases*, 7(3):369–374, 2001.

M. L. East, H. Hofer, J. H. Cox, U. Wulle, H. Wiik, and C. Pitra. Regular exposure to rabies virus and lack of symptomatic disease in Serengeti spotted hyenas. *Proceedings of the National Academy of Sciences of the United States of America*, 98(26):15026–15031, 2001.

M. Eichner and K. Dietz. Transmission potential of smallpox: Estimates based on detailed data from an outbreak. *American Journal of Epidemiology*, 158(2):110–117, 2003.

F. Fenner, D. A. Henderson, I. Arita, Z. Jezek, and I. D. Ladnyi. *Smallpox and its eradication*. World Health Organization, Geneva, Switzerland, 1988.

N. M. Ferguson, C. A. Donnelly, and R. M. Anderson. Transmission intensity and impact of control policies on the foot and mouth epidemic in Great Britain. *Nature*, 413(6855):542–548, 2001.

N. M. Ferguson, D. A. T. Cummings, C. Fraser, J. C. Cajka, P. C. Cooley, and D. S. Burke. Strategies for mitigating an influenza pandemic. *Nature*, 442(7101):448–452, 2006.

C. S. Findlay and F. Cooke. Breeding Synchrony in the Lesser Snow Goose (*Anser caerulescens caerulescens*). I. Genetic and Environmental Components of Hatch Date Variability and their Effects on Hatch Synchrony. *Evolution*, 36(2):342–351, 1982a.

C. S. Findlay and F. Cooke. Synchrony in the Lesser Snow Goose (*Anser caerulescens caerulescens*). II the Adaptive Value of Reproductive Synchrony. *Evolution*, 36(4):786–799, 1982b.

P. E. M. Fine and J. A. Clarkson. Measles in England and Wales -I: An analysis of factors underlying seasonal patterns. *International Journal of Epidemiology*, 11(1):5–14, 1982.

R. Gani and S. Leach. Transmission potential of smallpox in contemporary populations. *Nature*, 414(6865):748–751, 2001.

R. Gani and S. Leach. Erratum: Transmission potential of smallpox in contemporary populations (Nature (2001) 414 (748-751)). *Nature*, 415 (6875):1056, 2002.

S. Gao and L. Chen. The effect of seasonal harvesting on a single-species discrete population model with stage structure and birth pulses. *Chaos, Solitons and Fractals*, 24(4):1013–1023, 2005.

S. Gao, L. Chen, and L. Su N. Dynamic complexities in a seasonal prevention epidemic model with birth pulses. *Chaos, Solitons and Fractals*, 26(4): 1171–1181, 2005.

A. V. Goodchild and R. S. Clifton-Hadley. Cattle-to-cattle transmission of Mycobacterium bovis. *Tuberculosis*, 81(1-2):23–41, 2001.

W. Govaerts and Y. A. Kuznetsov. `MATCONT`: continuation software in `MATLAB`, 2007. URL `http://www.matcont.ugent.be/`.

N. C. Grassly and C. Fraser. Seasonal infectious disease epidemiology. *Proceedings of the Royal Society - Biological Sciences (Series B)*, 273 (1600):2541–2550, 2006.

D. Greenhalgh. An epidemic model with a density-dependent death rate. *IMA Journal of Mathematics Applied in Medicine and Biology*, 7(1):1–26, 1990.

J. Greenman, M. Kamo, and M. Boots. External forcing of ecological and epidemiological systems: A resonance approach. *Physica D: Nonlinear Phenomena*, 190(1-2):136–151, 2004.

C. Gremillion-Smith and A. Woolf. Epizootiology of skunk rabies in North America. *Journal of wildlife diseases*, 24(4):620–626, 1988.

J. Guckenheimer. `DsTool`: a computer program for the interactive investigation of dynamical systems on computers using unix and the X window system, 2004. URL `http://www.cam.cornell.edu/guckenheimer/dstool.html`.

R. A. Gunn, W. A. Terranova, and H. B. Greenberg. Norwalk virus gastroenteritis aboard a cruise ship: An outbreak on five consecutive cruises. *American Journal of Epidemiology*, 112(6):820–827, 1980.

E. Hairer, S. P. Norsett, and G. Wanner. *Solving Ordinary Differential Equations 1: Nonstiff Problems*. Springer, New York, United states of America, 2002.

W. H. Hamer. The Milroy Lectures on epidemic disease in England–the evidence of variability and of persistency of type. *The Lancet*, 167(4305): 569–574, 1906a.

W. H. Hamer. The Milroy Lectures on epidemic disease in England–the evidence of variability and of persistency of type. *The Lancet*, 167(4306): 655–662, 1906b.

W. H. Hamer. The Milroy Lectures On epidemic disease in England–the evidence of variability and of persistency of type. *The Lancet*, 167(4307): 733–739, 1906c.

D. A. Henderson. The looming threat of bioterrorism. *Science*, 283(5406): 1279–1282, 1999.

M. E. Henderson. Multiple parameter continuation: Computing implicitly defined k-manifolds. *International Journal of Bifurcation and Chaos in Applied Sciences and Engineering*, 12(3):451–476, 2002.

H. W. Hethcote. Qualitative analyses of communicable disease models. *Mathematical Biosciences*, 28(3-4):335–356, 1976.

H. W. Hethcote. Mathematics of infectious diseases. *SIAM Review*, 42(4): 599–653, 2000.

Donald L. Hitzl and Frank Zele. Exploration of the Henon quadratic map. *Physica D: Nonlinear Phenomena*, 14 D(3):305–326, 1985.

M. B. Hoshen and A. P. Morse. A weather-driven model of malaria transmission. *Malaria journal [electronic resource]*, 3(1):32, 2004.

P. J. Hudson, A. Rizzoli, B. T. Grenfell, H. Heesterbeek, A. P. Dobson, and David B. Lank. *The Ecology of Wildlife Diseases*. Oxford University Press, United Kingdom, 2002.

J. Hunter. `matplotlib`: a `python` 2D plotting library which produces publication quality figures in a variety of hardcopy formats, 2007. URL `http://matplotlib.sourceforge.net/`.

R. A. Ims. The ecology and evolution of reproductive synchrony. *Trends in Ecology and Evolution*, 5(5):135–140, 1990.

J. M. Ireland, R. A. Norman, and J. V. Greenman. The effect of seasonal host birth rates on population dynamics: The importance of resonance. *Journal of Theoretical Biology*, 231(2):229–238, 2004.

J. M. Ireland, B. D. Mestel, and R. A. Norman. The effect of seasonal host birth rates on disease persistence. *Mathematical Biosciences*, 206(1):31–45, 2007.

E. H. Kaplan, D. L. Craft, and L. M. Wein. Analyzing bioterror response logistics: The case of smallpox. *Mathematical Biosciences*, 185(1):33–72, 2003.

J. E. Kaplan, R. Feldman, D. S. Campbell, C. Lookabaugh, and G. W. Gary. The frequency of a Norwalk-like pattern of illness in outbreaks of acute gastroenteritis. *American Journal of Public Health*, 72(12):1329–1332, 1982.

M. J. Keeling. Models of foot-and-mouth disease. *Proceedings of the Royal Society - Biological Sciences (Series B)*, 272(1569):1195–1202, 2005.

M. J. Keeling and P. Rohani. *Modeling infectious diseases in humans and animals*. Princeton University Press, New Jersey, United states of America, 2007.

M. J. Keeling, P. Rohani, and B. T. Grenfell. Seasonally forced disease dynamics explored as switching between attractors. *Physica D: Nonlinear Phenomena*, 148(3-4):317–335, 2001.

M. J. Keeling, M. E. J. Woolhouse, R. M. May, G. Davies, and B. T. Grenfell. Modelling vaccination strategies against foot-and-mouth disease. *Nature*, 421(6919):136–142, 2003.

W. O. Kermack and A. G. McKendrick. A contribution to the mathematical theory of epidemics. *Proceedings of the Royal Society, London A*, 115: 700–721, 1927.

Y. Kuznetsov. `CONTENT`: an integrated environment for analysis of dynamical systems, 2001. URL `ftp://ftp.cwi.nl/pub/CONTENT`.

Y. A. Kuznetsov and C. Piccardi. Bifurcation analysis of periodic SEIR and SIR epidemic models. *Journal of Mathematical Biology*, 32(2):109–121, 1994.

D. A. Lam, J. A. Miron, and A. Riley. Modeling seasonality in fecundability, conceptions, and births. *Demography*, 31(2):321–346, 1994.

A. L. Lloyd. Realistic distributions of infectious periods in epidemic models: Changing patterns of persistence and dynamics. *Theoretical Population Biology*, 60(1):59–71, 2001a.

A. L. Lloyd. Destabilization of epidemic models with the inclusion of realistic distributions of infectious periods. *Proceedings of the Royal Society - Biological Sciences (Series B)*, 268(1470):985–993, 2001b.

Z. Lu, X. Chi, and L. Chen. The effect of constant and pulse vaccination on SIR epidemic model with horizontal and vertical transmission. *Mathematical and Computer Modelling*, 36(9-10):1039–1057, 2002.

G. Macdonald. *The Epidemiology and Control of Malaria*. Oxford University Press London, United Kingdom, 1957.

B. B. Mandelbrot. *Fractals: Form, Chance, and Dimension*. W. H. Freeman and company, San Francisco, United states of America, 1977.

The MathWorks. `MATLAB`: a high-level technical computing language and interactive environment for algorithm development, data visualization, data analysis, and numeric computation, 2007. URL `http://www.mathworks.com/products/matlab/`.

E. J. Milner-Gulland. A dynamic game model for the decision to join an aggregation. *Ecological Modelling*, 145(1):85–99, 2001.

E. J. Milner-Gulland and B. Lhagvasuren. Population dynamics of the Mongolian gazelle (*Procapra gutturosa*): An historical analysis. *Journal of Applied Ecology*, 35(2):240–251, 1998.

A. Mitchell, D. Bourn, J. Mawdsley, W. Wint, R. Clifton-Hadley, and M. Gilbert. Characteristics of cattle movements in Britain - An analysis of records from the Cattle Tracing System. *Animal Science*, 80(3):265–273, 2005.

J. D. Murray. *Mathematical Biology*. Springer-Verlag New York, United states of America, 1989.

J. Nocedal and S. J. Wright. *Numerical Optimization*. Springer-Verlag New York, Inc. New York, NY, United states of America, 1999.

D. J. Nokes and J. Swinton. Vaccination in pulses: A strategy for global eradication of measles and polio? *Trends in Microbiology*, 5(1):14–19, 1997.

E. Ott. *Chaos in Dynamical Systems*. Cambridge University Press London, United Kingdon, 2002.

T. S. Parker and L. O. Chua. *Practical numerical algorithms for chaotic systems*. Springer-Verlag New York, Inc. New York, NY, USA, 1989.

I. J. Patterson. Timing and spacing of broods in the black-headed gull. *Ibis*, 107:433–459, 1965.

F. Perez. `IPython`: an enhanced `python` shell designed for efficient interactive work., 2007. URL `http://ipython.scipy.org/`.

J. E. Pinzon, J. M. Wilson, C. J. Tucker, R. Arthur, P. B. Jahrling, and P. Formenty. Trigger events: Enviroclimatic coupling of Ebola hemorrhagic fever outbreaks. *American Journal of Tropical Medicine and Hygiene*, 71 (5):664–674, 2004.

M. Ramsay, N. Gay, E. Miller, M. Rush, J. White, P. Morgan-Capner, and D. Brown. The epidemiology of measles in England and Wales: rationale for the 1994 national vaccination campaign. *Communicable disease report CDR review*, 4(12), 1994.

S. E. Randolph, R. M. Green, M. F. Peacey, and D. J. Rogers. Seasonal synchrony: The key to tick-borne encephalitis foci identified by satellite data. *Parasitology*, 121(1):15–23, 2000.

T. C. Reluga. Analysis of periodic growth-disturbance models. *Theoretical Population Biology*, 66(2):151–161, 2004.

M. Roberts and H. Heesterbeek. Bluff your way in epidemic models. *Trends in Microbiology*, 1(9):343–348, 1993.

M. G. Roberts and R. R. Kao. The dynamics of an infectious disease in a population with birth pulses. *Mathematical Biosciences*, 149(1):23–36, 1998.

S. E. Robinson and R. M. Christley. Identifying temporal variation in reported births, deaths and movements of cattle in Britain. *BMC Veterinary Research*, 2:1–14, 2006.

N. Rojansky, A. Brzezinski, and J. G. Schenker. Seasonality in human reproduction: An update. *Human Reproduction*, 7(6):735–745, 1992.

G. D. Ruxton. The effects of stochasticity and seasonality on model dynamics: Bovine tuberculosis in badgers. *Journal of Animal Ecology*, 65(4):495–500, 1996.

W. M. Schaffer and T. V. Bronnikova. Parametric dependence in model epidemics. I: Contact-related parameters. *Journal of Biological Dynamics*, 1(2):183–195, 2007.

I. B. Schwartz and H. L. Smith. Infinite subharmonic bifurcation in an SEIR epidemic model. *Journal of Mathematical Biology*, 18(3):233–253, 1983.

B. Shulgin, L. Stone, and Z. Agur. Pulse vaccination strategy in the SIR epidemic model. *Bulletin of Mathematical Biology*, 60(6):1123–1148, 1998.

H. L. Smith. Subharmonic bifurcation in an S-I-R epidemic model. *Journal of Mathematical Biology*, 17(2):163–177, 1983.

H. E. Soper. The interpretation of periodicity in disease prevalence. *Journal of the Royal Statistical Society*, 92:34–73, 1929.

L. Stone, B. Shulgin, and Z. Agur. Theoretical examination of the pulse vaccination policy in the SIR epidemic model. *Mathematical and Computer Modelling*, 31(4-5):207–215, 2000.

B. Stroustrup. *The `C++` Programming Language: Special Edition*. Addison-Wesley Reading, Massachusetts, United States of America, 2000.

J. Swinton, C. A. Gilligan, J. Harwood, and B. T. Grenfell. Persistence thresholds for phocine distemper virus infection in harbour seal Phoca vitulina metapopulations. *Journal of Animal Ecology*, 67(1):54–68, 1998.

S. Tang and L. Chen. Multiple attractors in stage-structured population models with birth pulses. *Bulletin of Mathematical Biology*, 65(3):479–495, 2003.

G. van Rossum. `python`: a dynamic object-oriented programming language, 2007. URL `http://www.python.org`.

D. M. Watts, D. S. Burke, and B. A. Harrison. Effect of temperature on the vector efficiency of *aedes aegypti* for dengue 2 virus. *American Journal of Tropical Medicine and Hygiene*, 36(1):143–152, 1987.

P. R. Wheeler. *Linear stability computations of spiral and scroll waves*. PhD thesis, The University of Warwick, Coventry, United Kingdom, 2006.

Y. Zhou and H. Liu. Stability of periodic solutions for an SIS model with pulse vaccination. *Mathematical and Computer Modelling*, 38(3-4):299–308, 2003.